

**HIGH-THROUGHPUT ORGANIC REACTION SCREENING USING
DESORPTION ELECTROSPRAY IONIZATION MASS SPECTROMETRY**

by

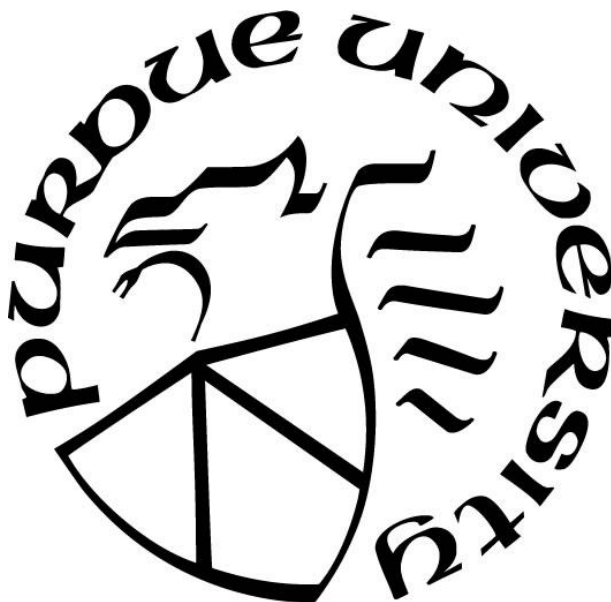
David Land Logsdon II

A Dissertation

Submitted to the Faculty of Purdue University

In Partial Fulfillment of the Requirements for the degree of

Doctor of Philosophy



Department of Chemistry

West Lafayette, Indiana

December 2019

THE PURDUE UNIVERSITY GRADUATE SCHOOL
STATEMENT OF COMMITTEE APPROVAL

Dr. R. Graham Cooks, Chair

Department of Chemistry

Dr. Scott A. McLuckey

Department of Chemistry

Dr. Dor Ben-Amotz

Department of Chemistry

Dr. David H. Thompson

Department of Chemistry

Approved by:

Dr. Christine A. Hrycyna

TABLE OF CONTENTS

LIST OF TABLES	6
LIST OF FIGURES	7
LIST OF REACTION SCHEMES	10
ABSTRACT.....	11
CHAPTER 1. INTRODUCTION	12
CHAPTER 2. HIGH-THROUGHPUT SCREENING OF ORGANIC REACTIONS IN MICRODROPLETS USING DESORPTION ELECTROSPRAY IONIZATION MASS SPECTROMETRY (DESI-MS): HARDWARE AND SOFTWARE IMPLEMENTATION	14
2.1 Introduction.....	14
2.2 System Hardware	17
2.2.1 Fluid Handling Workstation	18
2.2.2 SCARA	19
2.2.3 Piezoelectric Spray Solvent Delivery System (PieSDS)	19
2.2.4 DESI-2D Stage	21
2.3 Software and Communication Protocol	21
2.3.1 Biomek Software	22
2.3.2 SAMI EX.....	23
2.3.3 Integrated Flowrate Controller and Solvent Switching System (IFC3S)	23
Flowrate stability monitoring	24
Cascaded ratio control for accelerated solvent switching	24
Automatic problem identification and troubleshooting in IFC3S	25
Level 1 troubleshooting: purge the tubing for non-critical system failure	25
Level 2 troubleshooting: alert the user of a critical system failure	25
2.3.4 Chemical Reaction Integrated Screening Software (CHRIS).....	26
2.4 Case Study: N-Alkylation, N-Acylation, and N-Sulfonylation Reactions	29
2.4.1 Experimental.....	29
Preparation of the reaction mixtures using the Biomek i7	30
Spotting of the reaction mixtures onto the DESI plates	31
DESI-MS conditions	32

2.4.2	Results and Discussion	32
	Product Peak Intensity Reproducibility.....	33
	MS Spectrum Reproducibility.....	35
2.5	Recent Advancements.....	38
2.6	Conclusions.....	40
CHAPTER 3. HIGH THROUGHPUT EXPERIMENTATION AND CONTINUOUS FLOW EVALUATION OF NUCLEOPHILIC AROMATIC SUBSTITUTION REACTIONS		42
3.1	Introduction.....	42
3.2	Experimental	43
3.2.1	High Throughput Reaction Conditions.....	43
3.2.2	Liquid Handling Robot	45
3.2.3	Customized Heating Block	45
3.2.4	DESI-MS Analysis	45
3.2.5	DESI-MS Analysis Software (CHRIS)	46
3.2.6	Microfluidic System	46
3.2.7	Microfluidic Reaction Conditions	47
3.2.8	Analysis of Microfluidic Reactions	47
3.3	Results and Discussion	48
3.3.1	High throughput experimentation (HTE)	48
3.3.2	Correlation Between DESI and Bulk Reactions	68
3.3.3	Microfluidic Evaluation.....	71
3.4	Conclusions.....	78
CHAPTER 4. HIGH THROUGHPUT SCREENING OF REDUCTIVE AMINATION REACTIONS USING DESORPTION ELECTROSPRAY IONIZATION (DESI-MS)		79
4.1	Introduction.....	79
4.2	Experimental	80
4.2.1	Reaction Mixture Preparation.....	80
4.2.2	DESI Slide Preparation.....	84
4.2.3	DESI-MS Conditions.....	85
4.2.4	Dilution of the 384 well plates for LC-MS and Direct Injection.....	85
4.2.5	LC-MS Conditions.....	86

4.2.6	Direct Injection Conditions.....	86
4.2.7	DESI-MS/MS Data Acquisition	86
4.2.8	CHRIS Data Analysis	87
4.2.9	Custom Python Scripts for Data Processing.....	88
	m/z Value Calculation.....	88
	DESI Data Processing Script.....	88
	LC-MS and Direct Injection Data Processing Script	88
	MS/MS Data Processing Script.....	89
4.3	Results and Discussion	89
4.3.1	Amine and Electrophile Reactivity Trends.....	89
4.3.2	Effect of Reducing Agent, Reaction Time, Acid and Stoichiometry	93
4.3.3	Validation of DESI-MS Results with LC-MS and Direct Injection	96
4.3.4	Advantages of DESI-MS as a Reaction Screening Tool	99
4.3.5	Example Mass Spectra.....	100
4.3.6	Example MS/MS Spectra	103
4.4	Conclusions.....	104
APPENDIX A. CUSTOM PYTHON SCRIPTS		105
	m/z Value Calculation Script	105
	DESI Data Processing Script.....	108
	DESI Data Processing Script Functions.....	109
	LC-MS and Direct Injection Data Processing Script	114
	MS/MS Data Processing Script.....	122
REFERENCES		127
PUBLICATIONS.....		133

LIST OF TABLES

Table 3.1 S _N Ar product formation as a function of reaction solvent, base, and DESI spray solvent.	57
Table 3.2 Summary of Round 2. The bulk reaction results are reported for three different time points (1, 4, 15 hr). DESI experiments were averages of replicates that were done in two different days.	68
Table 3.3 Possible reasons for discrepancy between droplet/thin film and bulk reaction observations.	71
Table 4.1 Comparison of the analysis time, solvent consumption, and sample consumption for each of the analysis techniques used in this study.	99

LIST OF FIGURES

Figure 2.1 Schematic of the desorption electrospray ionization (DESI) source.....	15
Figure 2.2 Line drawn lay-out of the hardware components of the Purdue Make-It system. 1) Biomek i7, 2) servo shuttle, 3) SCARA. 4) LTQ XL, 5) DESI stage, 6) solvent reservoirs, 7) Elveflow pressure controller, 8) Elveflow valve matrix, 9) DESI plate storage, 10 and 11) tables to support the equipment.....	16
Figure 2.3 Photographs showing the key components of the system.	18
Figure 2.4 Simplified engineering diagram of the spray-solvent delivery system.	20
Figure 2.5 Software communication protocol for the system.	22
Figure 2.6 The hierarchical control strategy applied within the IFC3S and the data flow between CHRIS and IFC3S.....	24
Figure 2.7 Scanning pattern used for the DESI-MS analysis. After each line, the current data file is closed, and a new data file is opened. The DESI stage then returns to the home position before moving to the beginning of the next line. When the contact closure signal is received, the acquisition of the next line begins. The red dots represent the rhodamine B fiducial markers. ...	26
Figure 2.8 Screenshot of the web-based, graphical output of CHRIS. Reactions conditions such as reagents, solvent, stoichiometry, etc. can be selected on the left to focus the view on the desired data points. Blue spots represent successful reactions, and red spots represent failed reactions (product detected above/below a user-defined threshold). Each individual spot can be clicked on, which will display its experimental conditions and mass spectrum.	28
Figure 2.9 Deck layout of Biomek i7 during the case study.....	31
Figure 2.10 Duration of action for each component of the make-it system during the 3-by-8h experiment.....	33
Figure 2.11 (Top) Normalized MS intensity of 120 reaction products performed in the 3-by-8h case study. (Bottom) Zoomed-in plot of the first 20 reactions with different yes/no thresholds applied.....	34
Figure 2.12 Trade-off between reproducibility and the rate of false negatives at different normalized intensity thresholds for determining yes/no reactions.	35
Figure 2.13 (Top) The coefficients of the first 3 principle components (PC) of the rhodamine spectra over 3 days. (Bottom) Plot of the % variance captured vs. number of PCs. 8 PCs capture 90% of the variance and 20 PCs 99% of the variance.	37
Figure 2.14 Spot-to-spot method of data acquisition. The spots that are skipped represent locations that were not selected for analysis by the user.....	38
Figure 2.15 Example of MS/MS spot-to-spot data acquisition. Data is acquired only from specific locations provided by the user. Since not all reactions produce product, MS/MS data is typically acquired from fewer spots.....	40

Figure 3.1 Direct comparison of S_NAr reactions using droplet/thin film and microtiter approach A) The droplet/thin film and B) bulk microtiter results for the same set of reaction conditions. Experimental conditions: spray solvent: methanol; reaction solvent: NMP; base: DIPEA. C) Same as B, but the spray solvent was MeOH + 1% FA D) Same as C, but the reaction solvent was 1,4 dioxane. Each cell is an average of two data points. Green cells represent "yes" reactions (product ion intensity > 150 counts). Red cells represent "no" reactions (product ion intensity < 150 counts). B12 can form both single and double addition products; the double addition product can form multiple ions. B12 (S) is the singly charged ion of the single addition product; B12 (D) is the sum of the average intensities of all the double addition products..... 51

Figure 3.2 Heat map of 1,536 reactions from Round 1 of the S_NAr HTE using MeOH with 1% FA as the spray solvent under droplet/thin film or bulk microtiter plate conditions at 150 °C. Green cells represent successful reactions (average product intensity ≥ 150 counts. Red cells represent unsuccessful reactions (average product intensity < 150 counts)..... 53

Figure 3.3 Heat map of 1,536 reactions (768 in droplet/thin film and 768 in bulk microtiter at three time points) from Round 2 of the S_NAr HTE using MeOH with 1% FA as the DESI spray solvent and NMP as the reaction solvent at 150 and 200 °C. Green cells represent successful reactions (average product intensity ≥ 150 counts. Red cells represent unsuccessful reactions (average product intensity < 150 counts). 60

Figure 3.4 Correlation plot for the comparison of droplet/thin film and bulk data from 831 unique S_NAr products in Round 1. Q1: 186 points; Q2: 124 points; Q3: 491 points; Q4: 30 points. 69

Figure 3.5 Two representative examples of heated bulk reaction outcomes showing the impact of thermal degradation (Reaction A: R2-A6 with R1-B12) and the positive effects of heating (Reaction B: R2-A6 with R1-B3). The dashed lines are only to guide the eye..... 70

Figure 3.6 Continuous flow synthesis of S_NAr reactions in a Chemtrix glass chip reactor, SOR 3225. A = amine; B=aryl halide; C = DIPEA..... 72

Figure 3.7 Full scan mass spectra from the continuous flow reactions between **R2-A6** and **R1-B4**. The blue arrow highlights the product peak at m/z 252. The peaks at m/z 100, 122, and 221 are the protonated, sodiated, and sodium bound dimer ions of the solvent NMP. The residence time and temperature of each reaction is listed on the corresponding spectrum. 75

Figure 3.8 Full scan mass spectra from the continuous flow reactions between **R1-A3** and **R1-B2**. No peak is observed at m/z 204 indicating that no product was formed. The peaks at m/z 100, 122, and 221 are the protonated, sodiated, and sodium bound dimer ions of the solvent NMP. The residence time and temperature of each reaction is listed on the corresponding spectrum. 77

Figure 4.1 Layout of the 384 well plate containing the reaction mixtures. The amines (top), electrophiles (middle), and stoichiometries (bottom) were arranged such that each well contains a unique combination of amine, electrophile, and stoichiometry. 83

Figure 4.2 The DESI-MS signal to noise ratio of the final, reduced product as a function of amine and electrophile. Each subplot represents a different amine, and the electrophiles (B1-B24) are represented on the x-axis. The dashed line represents a signal to noise of 3:1..... 91

Figure 4.3 Effect of reducing agent, reaction time, addition of acetic acid, and stoichiometry on the number of successful reactions. A successful reaction is defined as having a signal to noise ratio greater than 3:1 for the final, reduced product.	94
Figure 4.4 Effect of reaction time on the number of successful intermediate reactions. A successful intermediate reaction is defined as having a signal to noise ratio greater than 3:1 for the imine intermediate.....	95
Figure 4.5 Heat maps comparing the peak height of the final, reduced product analyzed by DESI-MS (Top), direct injection (Middle), and LC-MS (Bottom). Dark red indicates the areas of highest intensity, and dark blue indicates the areas of lowest intensity. This data was obtained from the NaBH ₄ , 0h, without acid 384 well plate.	97
Figure 4.6 Example mass spectra from DESI-MS showing the various types of products, by-products, and intermediates monitored in this study. A) Reaction between A1 and B21 showing the final, reduced product. B) Reaction between A4 and B6 showing two additions of the amine to the dielectrophile as well as the reduced, single addition product. C) Reaction between A3 and B3 showing the imine intermediate. D) Reaction between A6 and B11 showing two additions of the electrophile to the amine.	101
Figure 4.7 MS/MS spectra for the product of the reaction between A4 and B1 . The spectra were acquired at three different normalized collision energies (NCEs).....	103
Figure 4.8 Interpreted MS/MS spectrum of the product of the reaction between A4 and B1 . This MS/MS spectrum is used to confirm the identity of the product.	104

LIST OF REACTION SCHEMES

Scheme 2.1 Reagents used for the case study.....	30
Scheme 3.1 Reagents used in Round 1 of the HTE campaign.....	49
Scheme 3.2 Reagents used in Round 2 of the HTE campaign.....	58
Scheme 3.3 Microfluidic evaluation of select 'yes' reactions from the HTE study.....	74
Scheme 3.4 Microfluidic evaluation of some 'no' reactions from the HTE.....	76
Scheme 4.1 Amines used in the high throughput screening experiment.....	81
Scheme 4.2 Electrophiles used in the high throughput screening experiment.....	82

ABSTRACT

This dissertation describes the development of a system for the automated, high-throughput screening of organic reactions. This system utilizes a liquid handling robot for reaction mixture preparation combined with desorption electrospray ionization mass spectrometry (DESI-MS) for reaction mixture analysis. With an analysis speed of ~1 second per reaction mixture, this system is capable of screening thousands of reactions per hour. Reaction mixtures are prepared in 384-well microtiter plates using a liquid handling robot. A sample of each reaction mixture (50 nL) is then transferred to a PTFE coated, glass slide using a pin tool. By offsetting the placement of the pin tool during each transfer, up to 6,144 unique reaction mixtures can be placed on each slide. The slide is then transferred to the DESI stage by a robotic arm, and the DESI-MS analysis begins, taking as little as 7 minutes for 384 reaction mixtures. We utilize a scheduling software to control each component of the system, which automates the entire process from reaction mixture preparation to DESI-MS analysis. In order to efficiently analyze and visualize the extremely large data sets generated by the system, we developed a custom software suite to automatically process each data set. We have used this system to screen several classes of industrially relevant reactions including Suzuki coupling, nucleophilic aromatic substitution, reductive amination, and Sonogashira coupling. We have validated both positive and negative results from the system using flow chemistry, and we have observed excellent agreement between the two methodologies. By being capable of screening thousands of reactions per hour, requiring only microliter quantities of reaction mixtures, and consuming less than a milliliter of solvent during the DESI-MS analysis, this system significantly reduces the time and costs associated with organic reaction screening.

CHAPTER 1. INTRODUCTION

The applications of high-throughput screening (HTS) were first popularized in the late 1990s. They have since proliferated throughout the field of combinatorial (bio)chemistry¹⁻² and have recently captured increased attention from the chemical and (bio)pharmaceutical industry, especially with the second coming of artificial intelligence (AI) and machine learning (ML).³ Within the realm of organic synthesis, generating high-quality and contextual chemical data for the purpose of exploring uncharted chemical space has become a technical bottleneck as sophisticated chemical feature engineering and AI/ML techniques have pushed the boundaries of how much insight may be gained from hundreds of thousands to millions of datapoints.

Conceptually, HTS refers to a method for acquiring and processing a large amount of data per unit time and cost, normally in the order of ~1K-10K data points/day. While the nature of HTS experimentations vary from the biological to the chemical, the objectives of HTS are universal, which is to (1) generate libraries of useful information (e.g. gene sequences⁴, organic reactions⁵, and microbial strains⁶), (2) explore or discover new parameter value ranges within a desired (bio)chemical reaction space (e.g. protein-ligand interactions⁷ and polymorph-specific crystallization⁸⁻⁹), and to (3) optimize a set of known (bio)chemical reaction conditions (e.g. temperature ranges and solvent choices in organic reactions⁵ and catalyst compositions in heterogeneous reactions¹⁰).

The latest progress in the implementation of AI/ML significantly elevates the impact an HTS system can have on the scientific community by enabling deeper comprehension of the accumulated, high-dimensional and complex dataset, and in turn, the screening problem at hand. To attain such feats, HTS has historically involved shrewd design of hardware and software for streamlining the process of rapidly preparing samples, performing assays, and acquiring and processing data in chemically and biologically insightful ways.

Specifically, the ideal HTS system is one which allows for low sample volume, rapid assay, system integration and automation, and in the case of dense datasets, effective data compression. These four fundamental factors of HTS combine to lower the costs of material and labor as well as increase the rate of data generation. As a result, current state-of-the-art HTS technologies often involve the use of nanoliter-to-picoliter fluid handling robots to mix and deposit samples in parallel,

such as in microarrays or microfluidics, coupled with rapid spectroscopic- and spectrometric-based analytical techniques, including UV/Vis, IR, Raman, NMR and MS.¹¹⁻¹²

This thesis describes the development of a DESI-MS based, automated, high throughput reaction screening system. The original proof of concept work for this system was carried out by Wleklinski *et al*¹³, and in the years since, we have been continuously developing and improving the system. The system consists of three main components: a liquid handling robot for reaction mixture preparation, a robotic arm for transfer of the reaction mixtures from the liquid handling robot to the DESI stage, and a DESI stage attached to a mass spectrometer for reaction mixture analysis. Custom built software combined with commercial software is used to integrate each hardware component and allow for automated operation.

This thesis contains three main content chapters. Chapter 2 of this thesis describes the high throughput screening system in significant detail. Each hardware component is described, and an in-depth description of the software that is used to integrate each hardware component is included. This chapter also details an experiment that was conducted to evaluate the reproducibility of the system.

Chapter 3 describes the application of the high throughput system to the screening of nucleophilic aromatic substitution reactions. This study includes a comparison of droplet reactions with heated batch reactions and also provides several examples where the high throughput screening results were validated using flow chemistry.

Chapter 4 describes the application of the high throughput system to the screening of reductive amination reactions. This study highlights the extremely high throughputs that are capable with the system. During this study, almost 2,000 unique reactions were screened in a single day starting from commodity chemicals. This work also compares the DESI-MS screening results with those from LC-MS and direct injection MS.

CHAPTER 2. HIGH-THROUGHPUT SCREENING OF ORGANIC REACTIONS IN MICRODROPLETS USING DESORPTION ELECTROSPRAY IONIZATION MASS SPECTROMETRY (DESI-MS): HARDWARE AND SOFTWARE IMPLEMENTATION

2.1 Introduction

Recently, Wleklinski *et al* developed a novel HTS method capable of screening up to ~3600 reactions/hour based on a novel phenomenon of accelerated reactions in microdroplets coupled with desorption electrospray ionization mass spectrometry (DESI-MS).¹⁴ DESI-MS is an ambient ionization technique whereby analytes from an inert surface are desorbed in the form of charged droplets and are directed to the inlet of a mass spectrometer such as an ion-trap¹⁵. The reagents of interest are first prepared in microwell plates and then “spotted” onto an inert substrate, such as polytetrafluoroethylene (PTFE). This DESI substrate is subsequently sprayed with charged solvent droplets causing the spotted reagents to desorb, producing charged microdroplet reaction mixtures. The charged microdroplets evaporate and the remaining ions are guided towards the MS via a metal ion-transfer line as the reaction occurs prior to MS analysis. Consequently, through a mechanical movement of the DESI substrate underneath the sprayer an ion map of the entire reaction set can be generated (Figure 2.1).

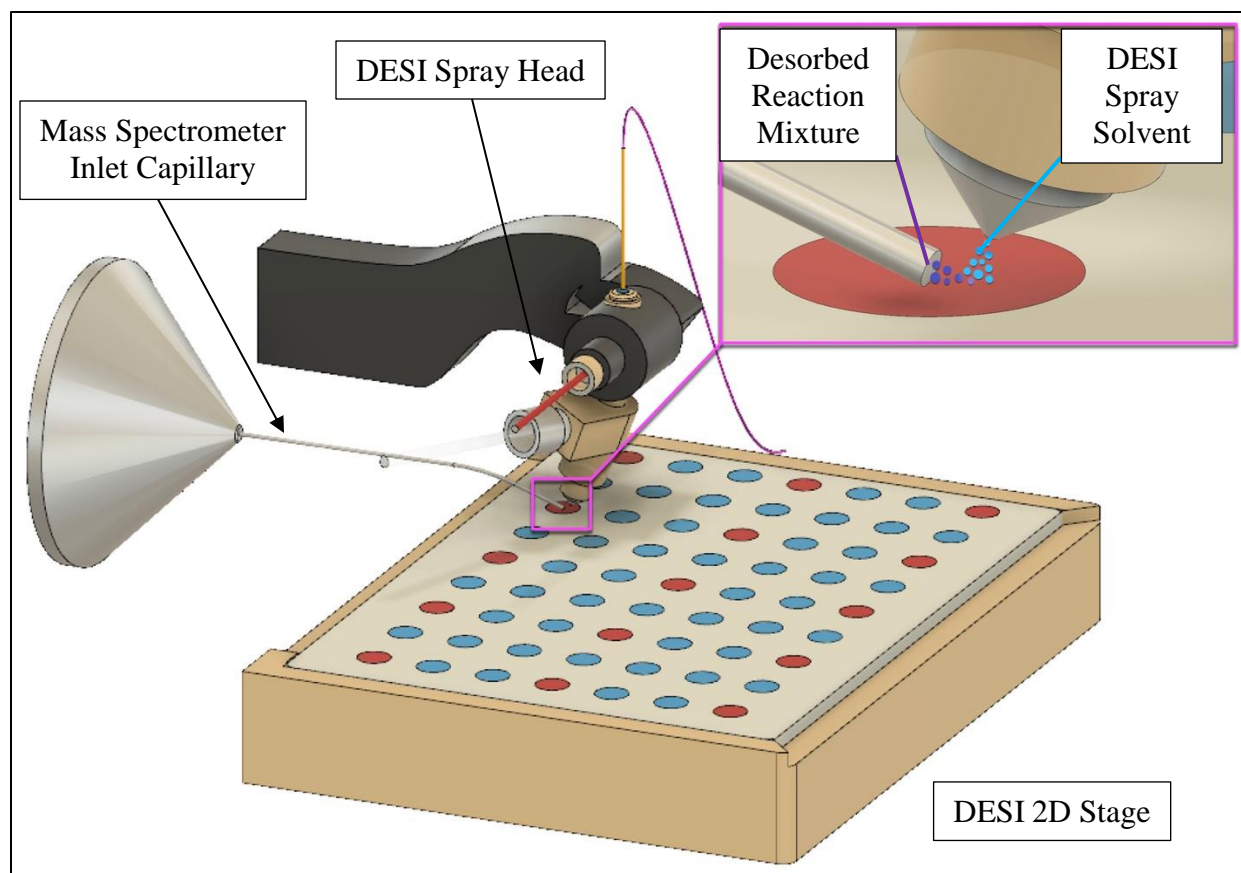


Figure 2.1 Schematic of the desorption electrospray ionization (DESI) source.

To advance the implementation of the novel DESI-MS HTS method by the chemical and (bio)pharmaceutical community at large, an integrated approach to hardware and software design for creating a replicable HTS platform is essential. In this article, we describe our DESI-MS system implementation to accomplish this goal. The platform is comprised mainly of commercially available hardware augmented with a few custom-designed but readily 3D-printable parts (Figure 2.2). The different devices are actuated in an integrated manner using a combination of commercial software and the corresponding software development kits (SDKs) and in-house programs developed using open-source packages. To describe the system's build process, the paper is divided into four additional sections. Section 2, which is divided further into four in-depth subsections, describes the role of each hardware and custom designed component, including the fluid handling robot, the selective compliance articulated robot arm (SCARA), the piezoelectric DESI spray solvent delivery system (PieSDS), and the DESI-2D stage coupled to a mass spectrometer. Section 3 follows with details of (1) the integration of commercial software, the

SDKs, and our in-house software, (2) the description of our in-house software, and (3) the workflow of all programs to control the integrated system during an HTS experiment. A case study of the HTS system is described in Section 4 where we demonstrate the system simultaneously performing and analyzing three classes of reactions, namely N-Alkylation, N-Acylation, and N-Sulfonylation over 8 hours per day for 3 consecutive days. The acquired MS spectra are then used to evaluate the data reproducibility and validate the system's robustness. Finally, we discuss important recent improvements that have been made to the system in Section 5.

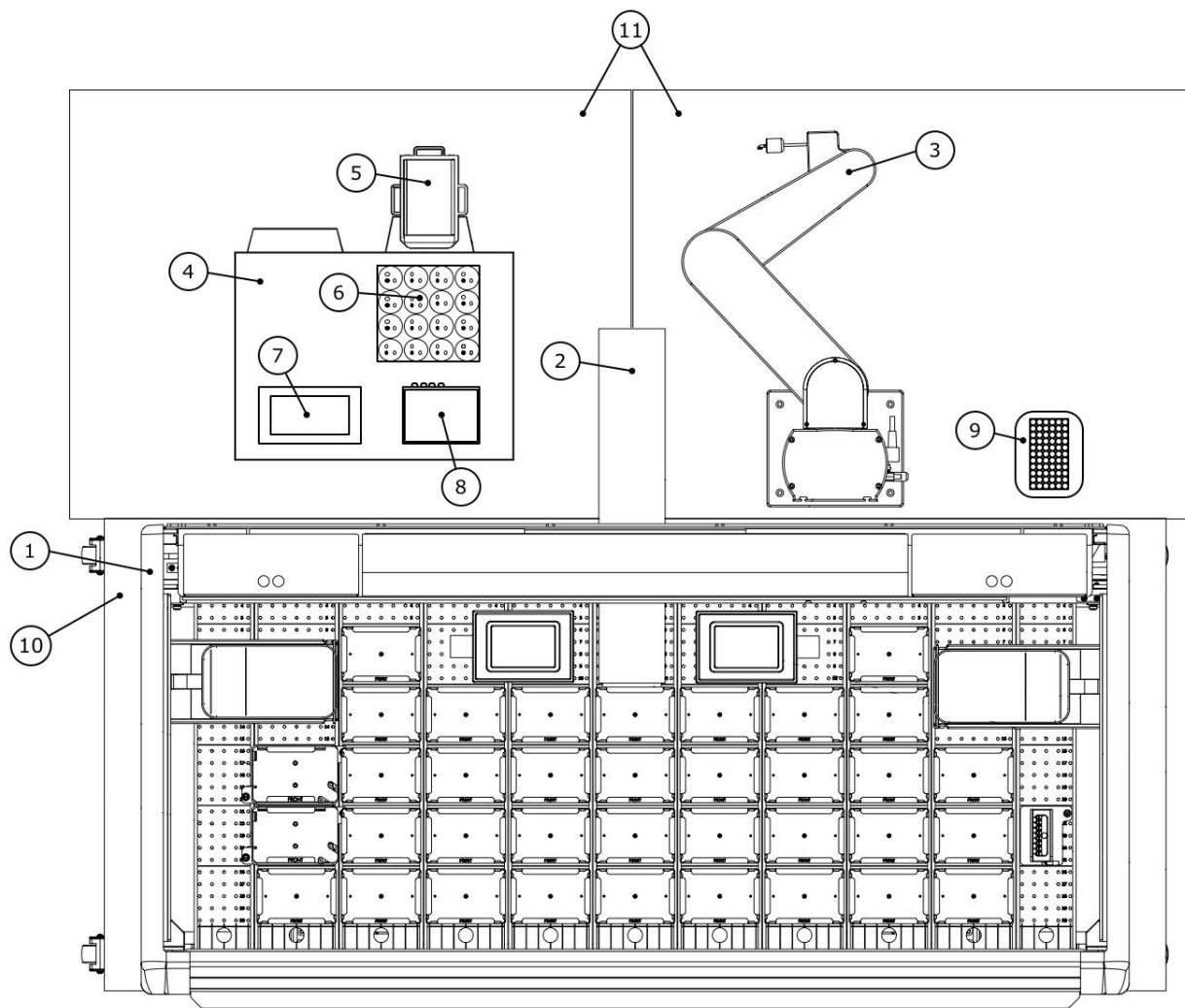


Figure 2.2 Line drawn lay-out of the hardware components of the Purdue Make-It system. 1) Biomek i7, 2) servo shuttle, 3) SCARA. 4) LTQ XL, 5) DESI stage, 6) solvent reservoirs, 7) Elveflow pressure controller, 8) Elveflow valve matrix, 9) DESI plate storage, 10 and 11) tables to support the equipment.

2.2 System Hardware

The DESI-MS HTS platform consists of five centerpiece hardware components (Figure 2.3), namely (A) a fluid handling workstation (Biomek i7, Beckman Coulter Inc.), (D) a SCARA robot (PF3400, Precise Automation Inc.), (D and E) a DESI-2D imaging stage (DESI 2D, Prosolia Inc.), (D) an LTQ XL mass spectrometer (Thermo Scientific), and (F) a DESI spray solvent delivery system (Elveflow). During an HTS experiment, the Biomek i7 mixes reagents in microwell plates and using a pin tool shown in (B), deposits the resulting mixtures in arrays of spots onto an inert PTFE substrate. The PTFE substrate is hosted on top of a 3D-printed plate holder shown in (C), which is custom-designed to manage the different landing configuration of the different devices as it travels through the platform from preparation to analysis and finally to storage. Post-pinning, a magnetic-based servo shuttle, shown in (D), transfers the substrate to a location behind the Biomek i7. The SCARA then transports the substrate onto the DESI 2D stage which is attached to the LTQ XL. The DESI stage is connected to a piezoelectric solvent delivery system (or PieSDS for short) which delivers the DESI spray solvent during the analysis. More details of each hardware and its subcomponents are described in the following subsections.

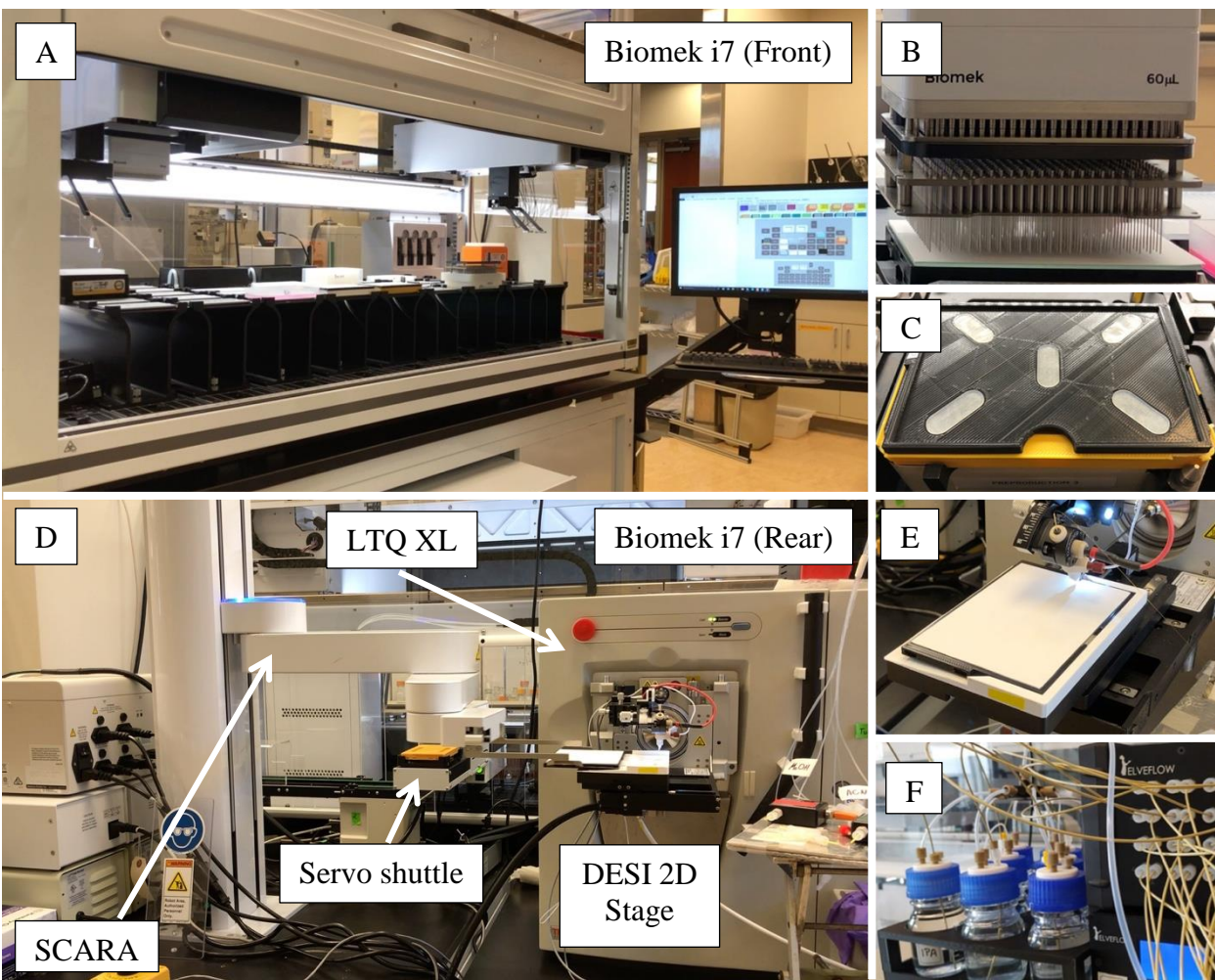


Figure 2.3 Photographs showing the key components of the system.

2.2.1 Fluid Handling Workstation

The Biomek i7 is a dual-arm liquid handling system with multichannel (384 format) and Span-8 (8 channels) heads for the disposable tips. The multichannel head is used for the pipetting of 384 samples simultaneously at the same conditions (volume, height, speed, mixing, layout, etc), while Span-8 channels operate independently and can transfer the samples in unique patterns. In addition to pipetting, the reagents can be transferred using a pin tool (Double Float Plate Replicator, V&P Scientific). The pin tool consists of an array of 384 stainless steel slotted pins (Figure 2.3 B), which are designed to transfer 50 nL of liquid by a combination of surface tension and capillary action. The pin tool can be magnetically loaded to and unloaded from the multichannel head. The pins are re-usable and can be cleaned by sonication. First, pins are dipped

into the source plate, then the hanging drop of solvent-solute mixture is transferred to destination plate by touching the pins to the surface.

The high capacity robotic deck contains forty passive plate holders for standard or deep-well plates. Each holder can be used for a single plate or stacks of plates if needed for long-term experiments. An orbital shaker is included for vigorous mixing of reagents in plates. Two ultrasonic bathes for pin cleaning and two waste stations for used tips are also included. Two grippers can move independently to transfer plates within the deck or to the server shuttle, where they can be reached by the SCARA.

To facilitate manipulation of the glass plates on the deck of the fluid handling robot, we fabricated custom plastic plate carriers (Figure 2.3 C). The carriers have the footprint of a standard well plate, and the top surfaces of the plate and carrier are flush with each other to facilitate pinning. Since each plate requires a dedicated carrier for the duration of the experiment and experiments potentially include large numbers of plates, 3D printing served as a convenient and cost-effective method for fabricating the carriers. We also fabricated a riser plate which supports each carrier when it is on the deck of the Biomek i7 (yellow portion in Figure 2.3 C). The purpose of the riser plate is to prevent the SCARA grip points on the plate carrier from being obstructed by the framework of the servo shuttle carriage.

2.2.2 SCARA

The SCARA is a model PF400 from Precise Automation (Fremont, CA) controlled by Beckman SAMI EX software using PreciseSCARAModule 5.0. The SCARA is used to transfer plate carriers between the fluid handling robot and the DESI stage. The servo shuttle transports plate carriers out of the fluid handling robot, at which point the SCARA grabs and transports them to the DESI stage for analysis. When analysis is completed, the SCARA transports the plate carriers to the storage station.

2.2.3 Piezoelectric Spray Solvent Delivery System (PieSDS)

The PieSDS system was first developed by Szilagyi *et al* to enable fast switching between different spray solvents and precise control of the flowrate during the DESI-MS analysis¹⁶. For implementation with DESI-MS HTS platform, the hardware and software features of the system

were extended to allow reliable autonomous operation. The system is composed of a combination of commercially available hardware. A piezoelectric pressure controller (Elveflow OB1 MK3), which has two independent pressure channels, with a range of 0-2 bar, is used to deliver solvents from a reservoir. Given its piezoelectric nature, the OB1 MK3 has low response (9 ms) and settling times (40 ms), and the pressure fluctuations are as low as 0.005 %. The switching between solvents is enabled by the use of piezoelectric valve array (Elveflow MUX flow switch matrix). The MUX has 16, two position, on-off valves having valve opening/closing time of 25 ms and a hold-up volume of <10 nL. The flowrates are measured with a thermoelectric flowrate sensor (Elveflow MFS2). The MFS2 has a dead volume in the range of μLs , which is not negligible when purging is needed in-between solvent switching. To the best knowledge of the authors, the applied devices were the most performant available in the market in their category. The engineering diagram of the SDS, enabling accurate, independent control of two solvent streams and quick solvent switching, is illustrated in Figure 2.4.

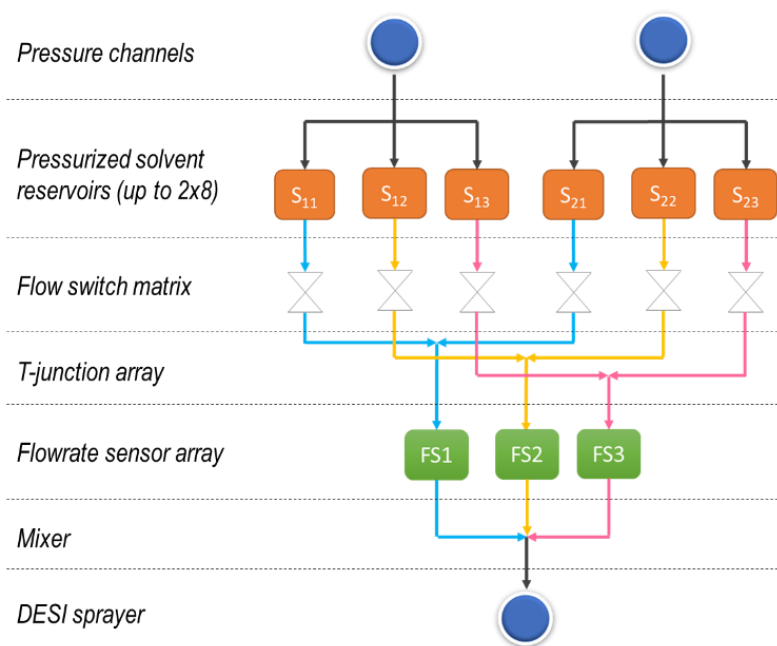


Figure 2.4 Simplified engineering diagram of the spray-solvent delivery system.

During screening, one OB1 channel symmetrically pressurizes up to 8 solvent reservoirs (Figure 2.3 F). To enable solvent composition control, only one MUX valve is open per pressure channel. The solvents connected to the same pressure channel thus cannot be combined with one

another. Each flowrate sensor is calibrated for a particular solvent, and different solvents coming from the two pressure channels are merged by a T-junction. Solvent switching is then facilitated by changing the opening configuration of different MUX valves. The previous solvent needs to be cleaned out from the mixer and the silica capillary between the mixer and the DESI sprayer. In the developed configuration the considerable dead volume of the MFS2s is removed from the common rail, which improves the solvent switching time.

2.2.4 DESI-2D Stage

We modified the surface of the DESI stage to include a custom receiver for the plate carriers (Figure 2.3 E). The receiver includes grooves that interface with rails on the sides of the plate carriers. The grooves are tapered in three dimensions in order to guide the plate carrier into exactly the right position as the SCARA pushes the plate carrier into place. The guide grooves also ensure that the plate carrier does not come into contact with either the DESI sprayer or the mass spectrometer sampling capillary during loading and unloading. Once loaded in the receiver, the plate carrier is held in place by friction between the bottom of the plate carrier and floor of the receiver.

2.3 Software and Communication Protocol

The DESI-MS HTS system is operated using several software packages which communicate with each other. The process begins with a prompt for user input (Figure 2.5 1A and 1B). A user is prompted with a simple-to-use, data entry GUI where essential parameters, such as the plate layout, reaction conditions, and DESI-MS settings, are entered. The GUI is built on top of four main applications, each orchestrating and integrating the five main devices within the system. These applications are the Biomek Software (Beckman Coulter), SAMI EX (Beckman Coulter), Integrated Flowrate Controller and Solvent Switching Software (IFC3S, developed in-house), and the Chemical Reaction Integrated Screening Software (CHRIS, developed in-house). The Biomek software controls the Biomek i7 with a set of pre-programmed methods for preparing the reaction mixtures. It interacts with the automation workflow scheduling software, SAMI EX, which enables networking between the SCARA arm and the Biomek i7 for the entirety of the experiment. The IFC3S controls the flow of multiple spray solvents during DESI analysis while CHRIS obtains and

analyzes the MS data corresponding to each reaction spot on the DESI substrate. The details of each of these applications are discussed in the subsections below.

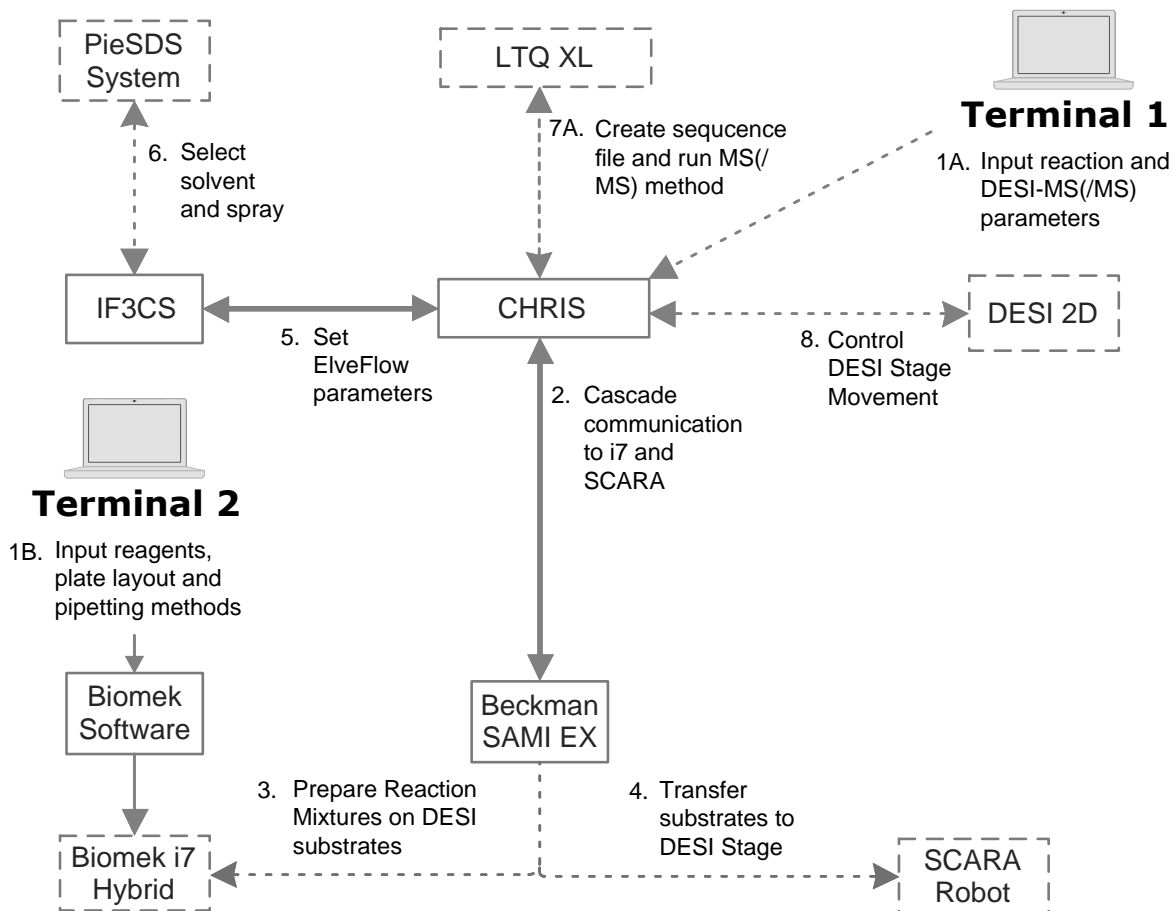


Figure 2.5 Software communication protocol for the system.

2.3.1 Biomek Software

The Biomek software controls the Biomek i7 fluid handling robot to create methods for preparing the reaction mixtures. Specifically, it has the ability to define new liquid types and labware that develops precise and customized pipetting techniques. It also has the capacity to integrate with LIMS systems to import work orders and export data. New methods can be easily created through a user-friendly interface. The user can control various aspects of the pipetting process including the aspiration/dispensing height and speed, mixing within the plate, tip touching, tip pre-wetting, air gaps, blowout volumes, movement speed within the well and between plates,

etc. The software analyses and verifies the validity of the created steps and prevents the method from running until any errors are fixed. Also, it gives the estimated time to finish the method, so the user may optimize this time by re-arranging the steps or pipetting conditions. The Biomek software is capable of programming simultaneous actions if it involves different parts of the robotic deck. For example, the pin-tool held by multichannel head may be cleaned in the sonication bath while the Span-8 head is pipetting reagents on the other side of the deck.

2.3.2 SAMI EX

SAMI EX is an automation workflow scheduling software from Beckman Coulter. It is designed to have a graphical workflow interface that enables simple method creation at a high level without needing to describe the details of how every plate must move across the system. It handles inputs within the hardware constraints and enables feedback to select appropriate actions during the course of a run based on sample data generated in real time. SAMI EX is also equipped with “SILAS” software modules, which are the communication protocols for interacting and integrating with other devices connected to the whole platform. A script-based SILAS module is used whenever appropriate for integrating our in-house software (i.e. CHRIS and IF3CS) with the rest of the system’s software via SAMI EX. The full hardware layout including fluid handling robot, SCARA, and mass spectrometer including DESI stage is therefore represented within SAMI EX.

2.3.3 Integrated Flowrate Controller and Solvent Switching System (IFC3S)

The IFC3S enables programmatic switching of DESI spray solvents and flowrate control of two independent solvent streams during an HTS experiment while communicating with CHRIS (Figure 2.6). It is written in LabView using the ElveSys LabView SDK, which consists of LabView drivers for all ElveFlow devices. The first version of the IFC3S has been discussed previously (Szilagyi et al. 2019), however, using the SDK, a significantly more capable control software and GUI was recently developed for this platform. Specifically, beyond the precise flowrate controller tuning that was implemented in the initial incarnation of the device, there are several other features required for reliable, automated operation, which are described below.

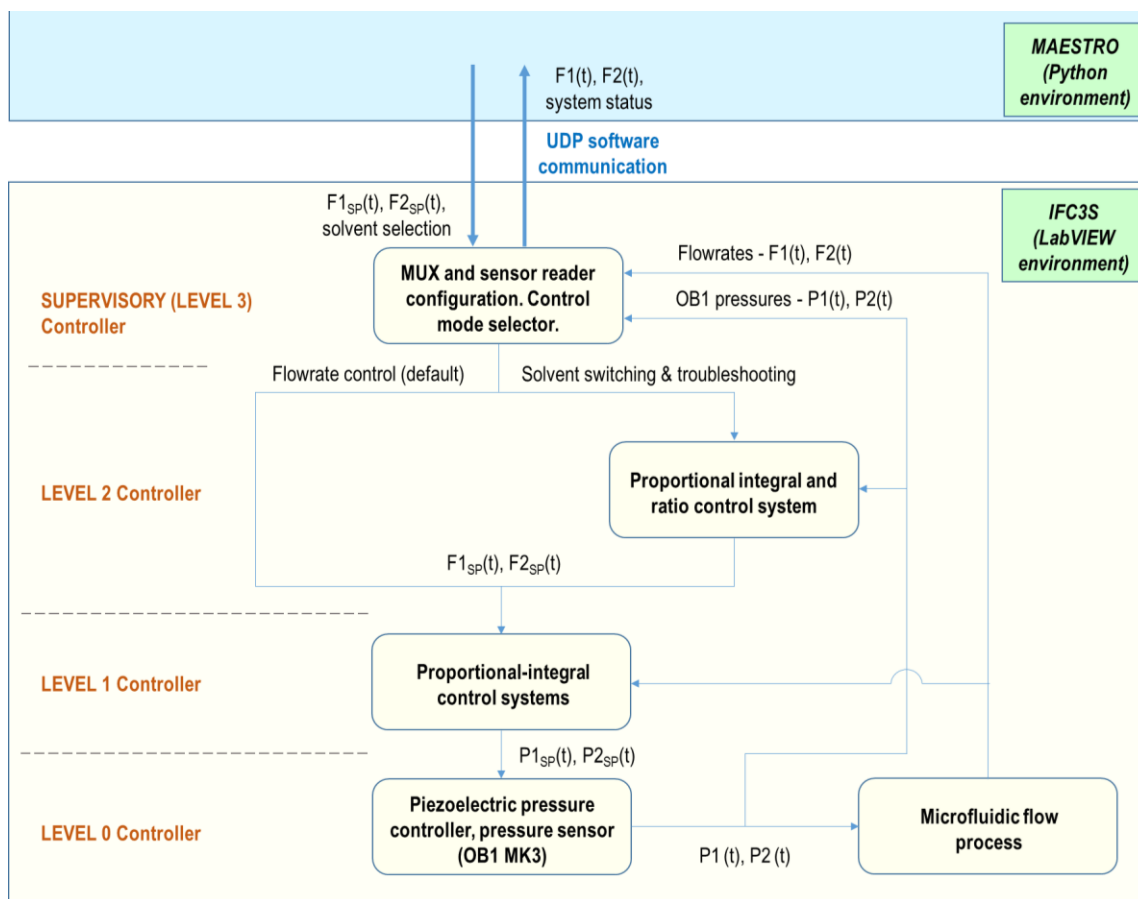


Figure 2.6 The hierarchical control strategy applied within the IFC3S and the data flow between CHRIS and IFC3S.

Flowrate stability monitoring

The flowrate stability is critical to the outcome of DESI. Hence, the control and monitoring of its stability prior to and during the experiment is essential. As a prerequisite for feedback control, the difference between the setpoint and actual flowrate is calculated, and the variance of the data series generated over a certain time interval is calculated. The flowrate is considered stable if the variance is under $0.03 \mu\text{L}/\text{min}$. Some variance under the $0.03 \mu\text{L}/\text{min}$ threshold is always generated by the measurement noise and the flowrate feedback control loops.

Cascaded ratio control for accelerated solvent switching

In the context of HTS it is necessary to minimize the downtimes, therefore, to accelerate the auxiliary operations. Such an operation is the cleaning of the previous solvent mixture from the tubing after changing the MUX configuration. Given the dead volume of the mixer and

common rail, the cleaning time with the generally applied 2-4 $\mu\text{L}/\text{min}$ flowrate takes ~2-4 minutes, which is clearly unacceptable for HTS. A control strategy that minimizes the solvent switching time was developed, which consists the following sequence of events: (1) Switch the independent flowrate control to ratio control, where the target is the ratio of the flowrate setpoints. This ensures that the mixer and tubing will be filled with the desired solvent composition; (2) A master PI controller is added for pressure control, where the manipulated variable is the flowrate of the ratio controller, and the controlled variable is the maximum of the two pressure channels; (3) During the solvent switching (at constant pressure) the flowrate varies due to the change of viscosity in the tubing. Stabilization of the flowrate indicates that no more viscosity change happens, hence, the solvent switching is completed. This control strategy inherently minimizes the solvent switching time while ensuring the desired solvent composition.

Automatic problem identification and troubleshooting in IFC3S

Destabilization and failure of the DESI spray solvent flow clearly leads to the failure of DESI analysis, which must be detected in early stages so that appropriate actions can be taken. A two-level problem identification and troubleshooting protocol is enabled in the IFC3S.

Level 1 troubleshooting: purge the tubing for non-critical system failure

Numerous events may lead to the destabilization of the flowrate, with the most common being bubble formation or clogging. The flowrate destabilization is detected by IFC3S and communicated to CHRIS to pause the DESI acquisition. The system is then flushed using the maximal safe operating pressure. Flushing the tubing can remove bubbles or contaminants from the lines. If this simple method fails, the Level 2 troubleshooting is activated.

Level 2 troubleshooting: alert the user of a critical system failure

Every failure that leads to zero flowrate (gas or liquid leakage, depletion of pressure source, etc.) or a failed Level 1 troubleshooting is considered a critical system failure. These events are communicated to CHRIS to pause the DESI acquisition, and IFC3S sends automatic text and e-mail messages to the user indicating that the system needs human intervention.

2.3.4 Chemical Reaction Integrated Screening Software (CHRIS)

CHemical Reaction Integrated Screening (CHRIS) is an in-house software suite developed to integrate all parts of the DESI-MS system and to acquire mass spectrometry data. CHRIS subsequently searches the acquired data for m/z values that correspond to the starting materials, intermediates, by-products, and products of the reactions. The main part of CHRIS is written in Python 3 but utilizes Visual Basic to generate the Xcalibur sequence file and Visual C++ 5.0 to interact with the mass spectrometer. Both scripts integrate with the Xcalibur SDK. The program is currently installed on a Purdue server and is accessible locally and via the internet.

During an experiment, CHRIS receives a signal from SAMI which indicates that the plate is ready. It then creates an output folder to hold the data and an Xcalibur sequence file. CHRIS then waits for another SAMI signal which indicates that the plate has been successfully transferred from the Biomek i7 to the DESI stage. CHRIS then sends a contact closure signal to the mass spectrometer start the acquisition. Data is acquired by scanning over the plate line by line with each new line being a separate data file (Figure 2.7). At the end of the experiment, CHRIS sends a signal to SAMI to notify that the experiment is completed, and SAMI moves the plate from the DESI stage to the storage space.

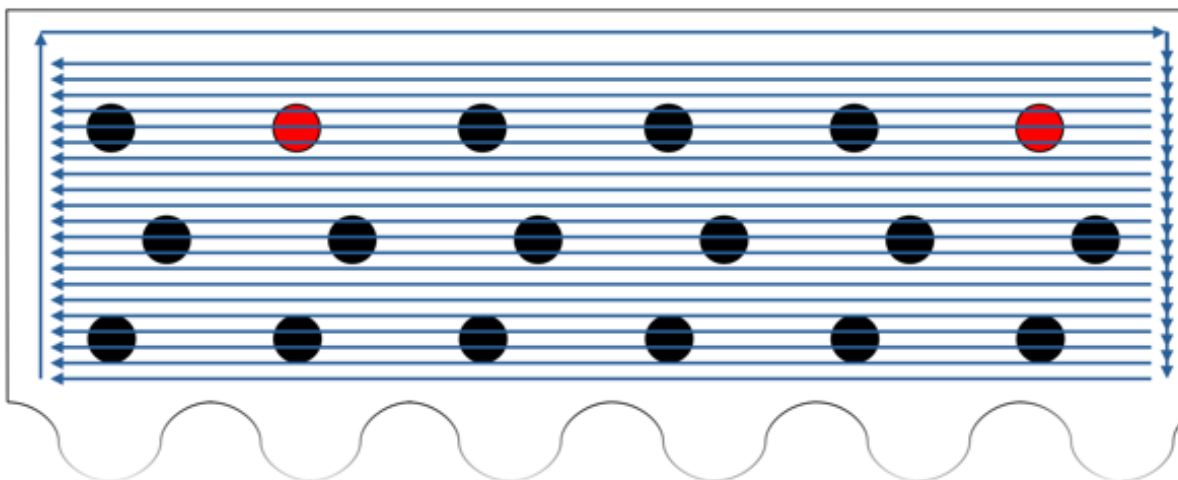


Figure 2.7 Scanning pattern used for the DESI-MS analysis. After each line, the current data file is closed, and a new data file is opened. The DESI stage then returns to the home position before moving to the beginning of the next line. When the contact closure signal is received, the acquisition of the next line begins. The red dots represent the rhodamine B fiducial markers.

After the DESI-MS data is collected, CHRIS analyses and processes the data using the following procedure. First, the Thermo RAW files are converted to a text format using msconvert from ProteoWizard¹⁷. These text files are then searched for the intensities corresponding to m/z 443, which identifies the locations of the 384 rhodamine B fiducial markers. A digital 2D matrix with the location of the rhodamine spots is subsequently generated. This matrix is then used to interpolate the coordinates and find the corresponding mass spectra for all spots on the DESI plate. A second digital 2D matrix is generated which contains the reaction details for each spot. This includes reaction conditions and all m/z values from starting materials, products, and any known by-products/intermediates. This second matrix is generated from a file which details the layout of each 384 well plate. The information in these two matrices is then combined, the first identifying where to look and the second what to look for, to calculate the intensities of all relevant m/z values for each spot. Output files are then generated which include lists of starting material intensities, product/by-product/intermediate intensities, and other ion intensities (unknown m/z values with ion counts above a defined threshold) as well as a graphical representation of the output via a web server (Figure 2.8).

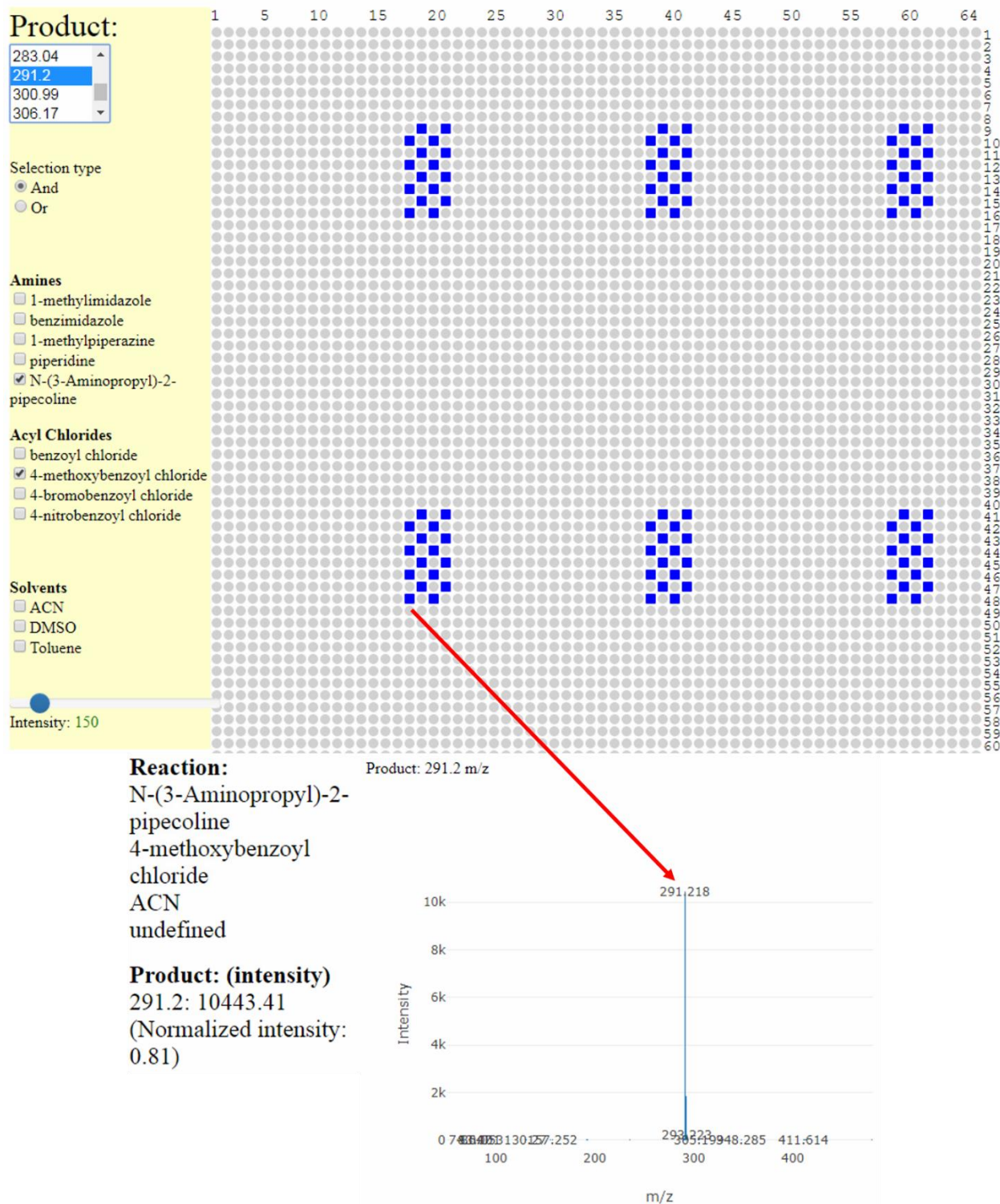


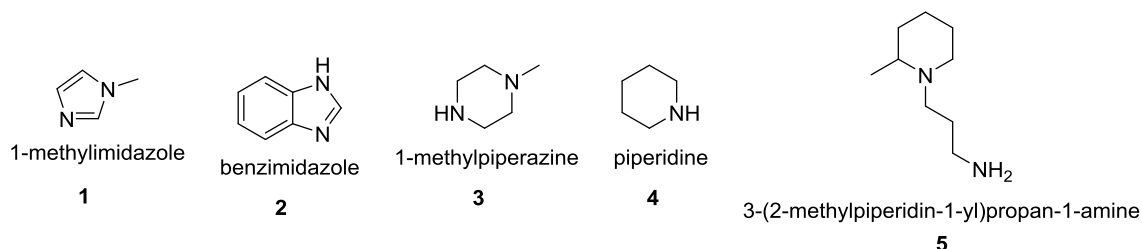
Figure 2.8 Screenshot of the web-based, graphical output of CHRIS. Reactions conditions such as reagents, solvent, stoichiometry, etc. can be selected on the left to focus the view on the desired data points. Blue spots represent successful reactions, and red spots represent failed reactions (product detected above/below a user-defined threshold). Each individual spot can be clicked on, which will display its experimental conditions and mass spectrum.

2.4 Case Study: N-Alkylation, N-Acylation, and N-Sulfonylation Reactions

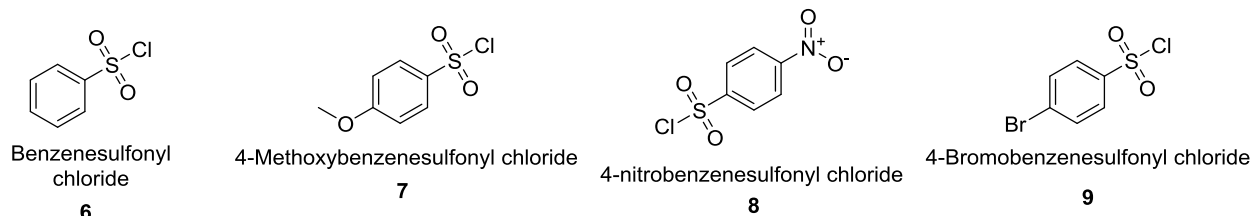
2.4.1 Experimental

The robustness and reproducibility of the system was evaluated by screening three classes of reactions: amine alkylation, amine acylation and amine sulfonylation. A variety of amines and electrophiles were used, and three different reaction solvents as well as three different DESI spray solvents were evaluated. The final concentration of all the reagents was 50 mM, and the ratio of amine to electrophile was 1:1. Acetonitrile (ACN), dimethyl sulfoxide (DMSO) and toluene were used as reaction solvents. The reagents used for these experiments were selected to provide structural diversity which would in turn impart various reactivity trends (Scheme 2.1).

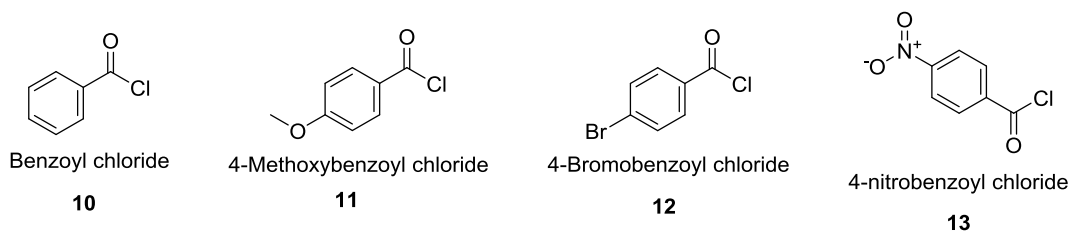
Amines



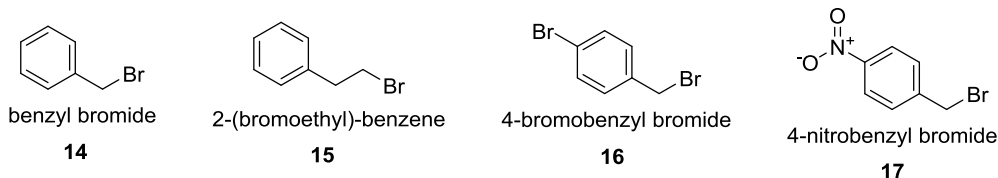
Sulfonyl Chlorides



Acyl Chlorides



Alkyl Bromides



Scheme 2.1 Reagents used for the case study.

Preparation of the reaction mixtures using the Biomek i7

Stock solutions (100 mM) were prepared for each reagent in each of the three reaction solvents in 3 mL glass vials. These vials were then placed into 24-position racks that fit onto the deck of the Biomek i7 (Figure 2.9). The Span-8 head was then used to transfer the reagent stock solutions into a 96 deep-well plate (for the amines) and three separate 96-well standard plates (one for each electrophile). Transfer from these intermediate plates to the 384-well final plates was also performed by the Span-8 head resulting in a total volume of 50 μ L for each reaction mixture (25 μ L of the amine and 25 μ L of the electrophile). The intermediate transfer of the stock solutions to

the 96-well plates allow for rapid 384-well plate preparation by the Span-8 head. The reaction mixtures were then carefully mixed in the 384-well final plates by pipetting up and down simultaneously using the multichannel head.

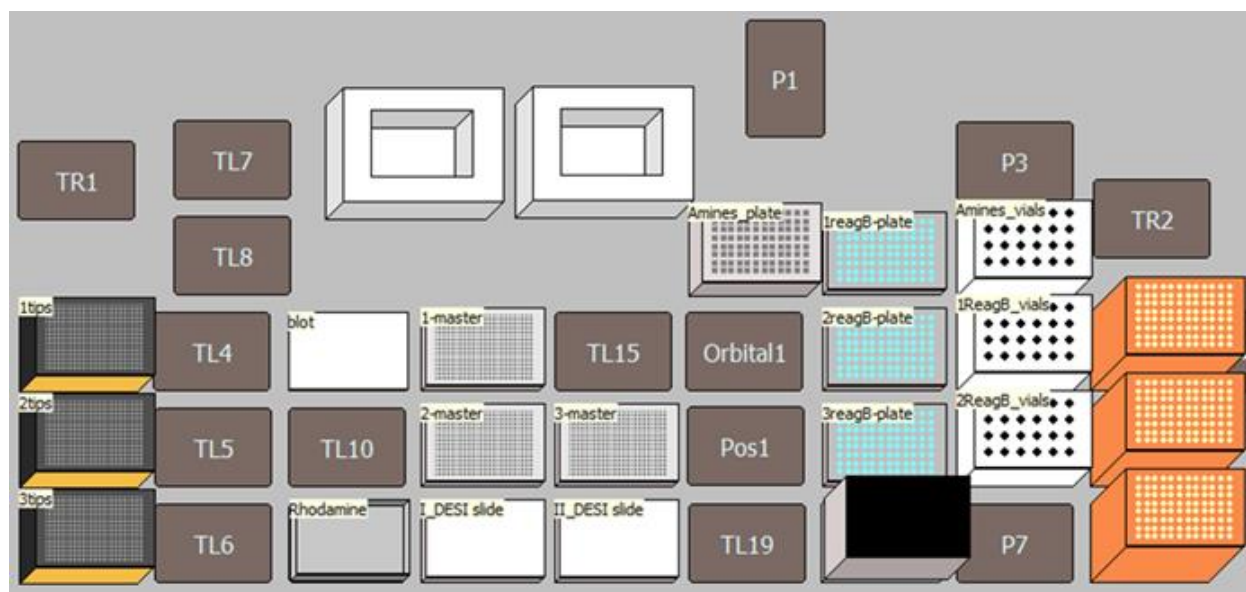


Figure 2.9 Deck layout of Biomek i7 during the case study.

Each reaction class (alkylation, acylation, and sulfonylation) was placed in a separate 384-well final plate. The layout of each final plate was the same and contained three segments containing five rows each (120 wells per segment) with one empty row (row P). Each 120 well segment contained the 20 unique combinations of amine and electrophile in sextuplicate, and each segment represented a different reaction solvent (ACN, DMSO, or toluene). Each 120 well segment was then further divided into three 40 well segments, containing the 20 unique combinations of amine and electrophile in duplicate, which were used during the DESI analysis to evaluate the effect of different DESI spray solvents.

Spotting of the reaction mixtures onto the DESI plates

Reaction mixtures from the 384-well final plates were transferred to the DESI plates using the 384-pin tool (50 nL/spot). Three different DESI plates were created each day (i.e. within 8h). The first DESI plate contained only acylation reactions. Eight replicates of the acylation 384-well final plate were spotted onto the DESI plate to create a density of 3,072 spots/plate. The second plate

contained both alkylation and sulfonylation reactions. Four replicates of each of the two 384-well final plates were transferred resulting in a final density of 3,072 spots/plate. The third plate contained all three reaction types. Seven replicates of acylation final plate, four replicates of alkylation final plate, and four replicates of the sulfonylation final plate were spotted onto the same DESI plate resulting in a density of 5,760 spots/plate. Thus, over three days there were 90 replicates of each unique N-Acylation reaction, 48 replicates of each unique N-sulfonylation reaction, and 48 replicates of each unique N-Alkylation reaction. A unique reaction consists of a unique combination of amine, electrophile, reaction solvent, and DESI spray solvent.

DESI-MS conditions

The mass spectrometer (Thermo LTQ XL) was operated in positive ion mode with an m/z range of 50-500. The DESI spray angle was 55° , and the spray tip was placed around 1 mm from the surface of the DESI plate and 2 mm from the mass spectrometer inlet capillary. A voltage of 5kV was applied to the DESI solvent flow. The DESI-MS imaging lateral resolution was 350 μm , and with an instrument scan time of 80 ms, the resulting DESI stage speed was 4,376 $\mu\text{m}/\text{sec}$.

2.4.2 Results and Discussion

During the HTS experiment, different components of the system operate in unison at different periods and for different durations (Figure 2.10). The results of the 3-by-8h experiments were used to study the robustness of the system as measured by the reproducibility of the data generated. We analyzed a total of 540 unique reactions, where each reaction has either 48 or 90 replicates, for a total of 35,712 data points collected across 3 days. The reproducibility of the system is discussed in the context of whether the mean and variance of the MS peak intensity distribution associated with the reaction products lead to variations in a “yes/no” decision of whether the reaction is successful. Specifically, we analyzed the acquired HTS data using two approaches, namely (1) statistical analysis of reaction product peak intensity across all the replicates and (2) principal component analysis (PCA) of the whole MS spectrum associated with a reaction spot on the DESI substrate.

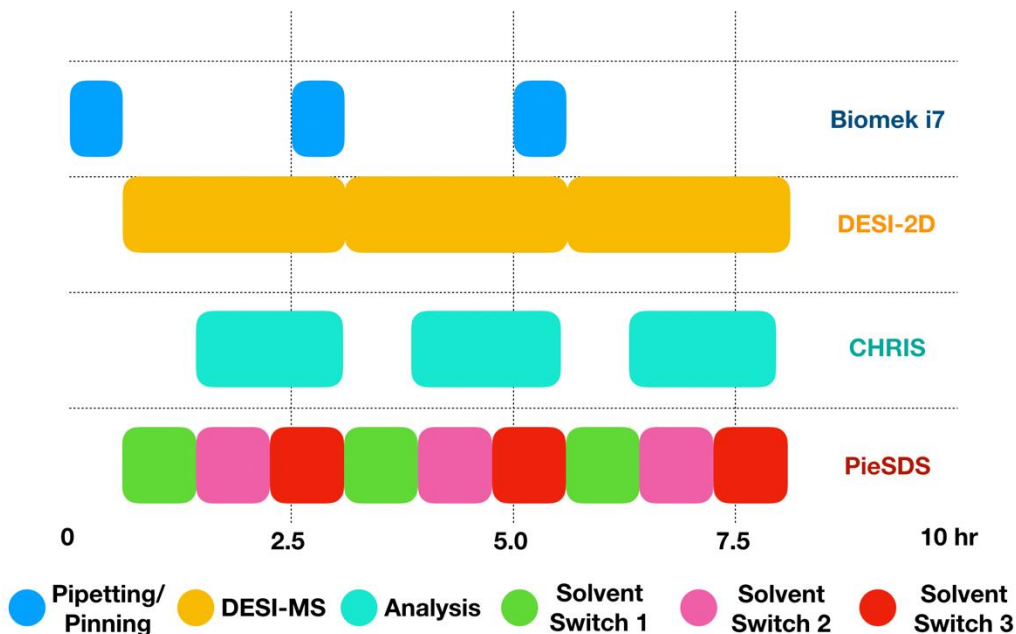


Figure 2.10 Duration of action for each component of the make-it system during the 3-by-8h experiment.

Product Peak Intensity Reproducibility

We chose to analyze the normalized peak intensity for each expected product, which is the height of the peak at the expected product's m/z divided by the total ion current for that scan. This information reveals whether a reaction is a success (produces the expected product) depending on whether the peak is above a certain, pre-determined threshold. One can pre-determine an intensity threshold corresponding to a yes/no decision based on heuristic knowledge of the sensitivity of the DESI-MS experiment. We identified that a normalized peak intensity above 0.003 represents a yes reaction because this corresponds to a signal to noise ratio of approximately 3:1. Naturally, the consistency of our decision-making regarding reactions whose normalized product intensity is around the 0.003 threshold is less reliable (Figure 2.11). That is, reaction products whose intensities lie close to the threshold will have higher rates of false positive and/or false negatives.

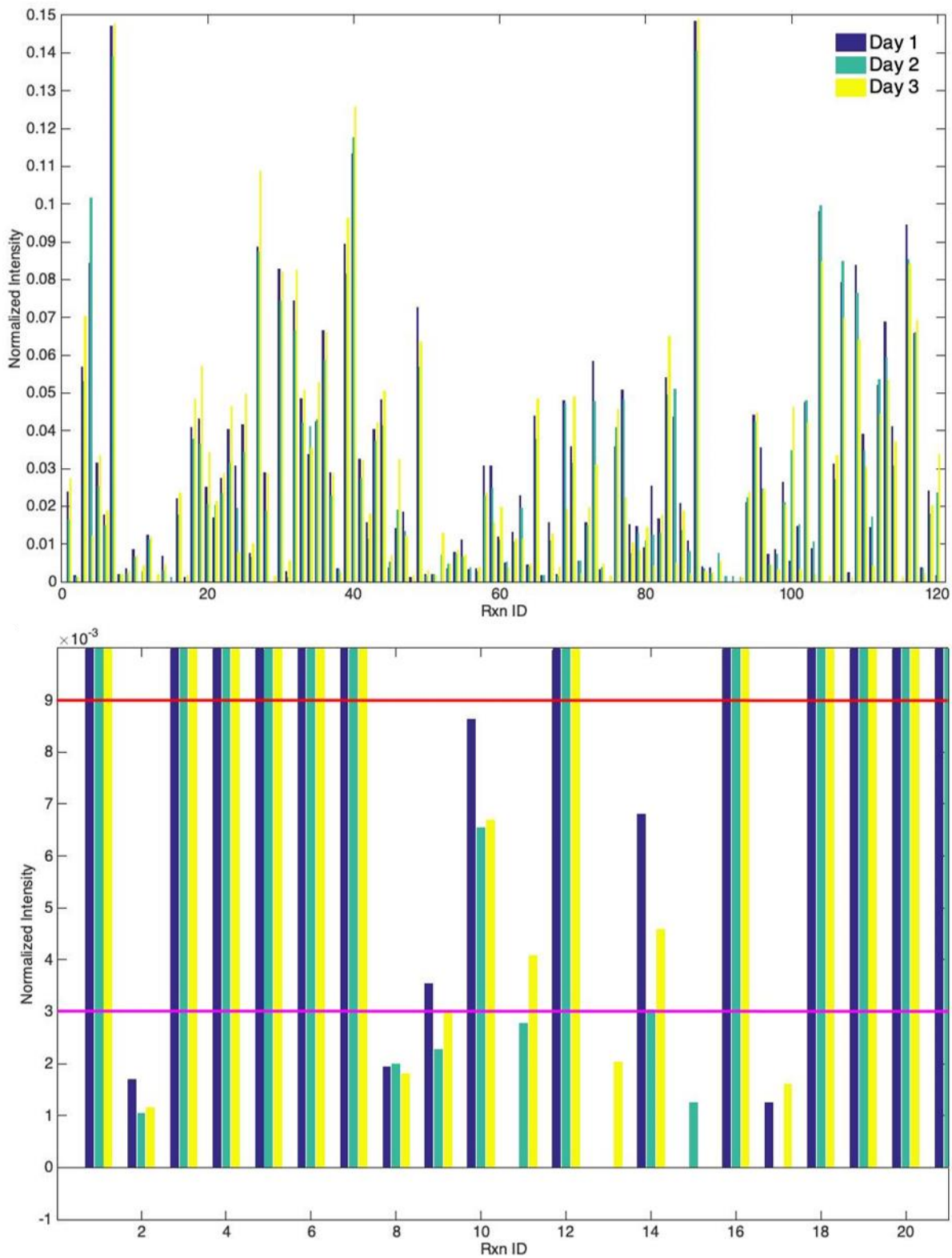


Figure 2.11 (Top) Normalized MS intensity of 120 reaction products performed in the 3-by-8h case study. (Bottom) Zoomed-in plot of the first 20 reactions with different yes/no thresholds applied.

In choosing an intensity threshold, one can improve the reproducibility of the yes/no decisions by generally increasing the intensity threshold, but this comes at the expense of increasing the rate of false negatives (Figure 2.12). At the threshold where the rate of false negatives is lowest, we found that 94% of all reactions are reproducible at the 3,072 and 5,760 reaction spot density over the 3 days of experimentation. The 15% inconsistency means that we may have a yes decision on one of the plates but not all of the plates across different days. Evidence suggests that 60% of the inconsistencies (4% of the reactions), is due to ion suppression while the rest (2% of reactions) is due to the current DESI detection limit. Collectively, the source of irreproducibility may be due to several factors, including inconsistency in reaction mixture pinning and fluctuations in solvent delivery that may not have been captured by the flow sensor and therefore not corrected by the IF3CS control system.

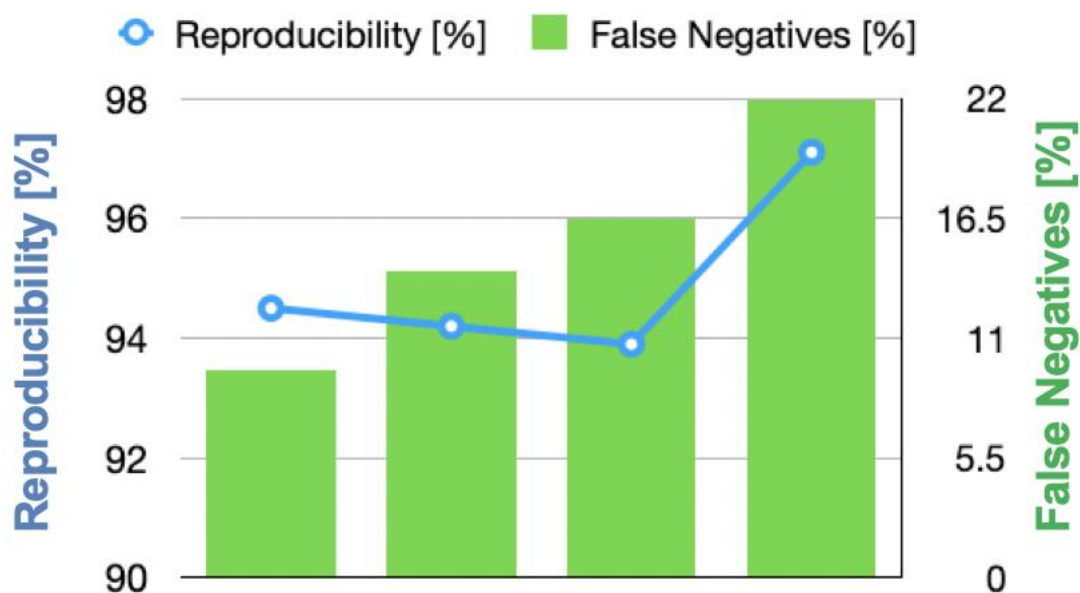


Figure 2.12 Trade-off between reproducibility and the rate of false negatives at different normalized intensity thresholds for determining yes/no reactions.

MS Spectrum Reproducibility

The second approach for robustness analysis of the system concerns the use of the entire MS spectrum of a reaction spot and is intended to study the variability of the product and background peaks from one reaction spot to the next and from plate to plate across the three days of

experimentation. Given the tremendous sensitivity of the DESI-MS method and that the method is performed in an open, ambient environment, a DESI-MS analysis of the same reaction but from different spots or plates can yield different spectra. In order to capture this variability, we use principal component analysis (PCA) to compare the spectra of a standard reagent, namely rhodamine, replicated over multiple plates. There are 384 rhodamine spots per plate and 3 plates per day for a total of 3,456 replicates. The PCA analysis of these spectra showed that 8-20 spectral components capture ~90-99% of the variability between spots from different plates (Figure 2.13 Bottom). In other words, 20 different sets of peaks associated with each rhodamine spectra vary significantly from spot-to-spot. Figure 2.13 (Top) shows a plot of the coefficients of the 3 most significant principle components (PCs). They occupy the same space between substrates and suggest that the variability of the MS spectrum, while large, is fully characterized and reveals the reproducibility of each HTS experiment and across plates.

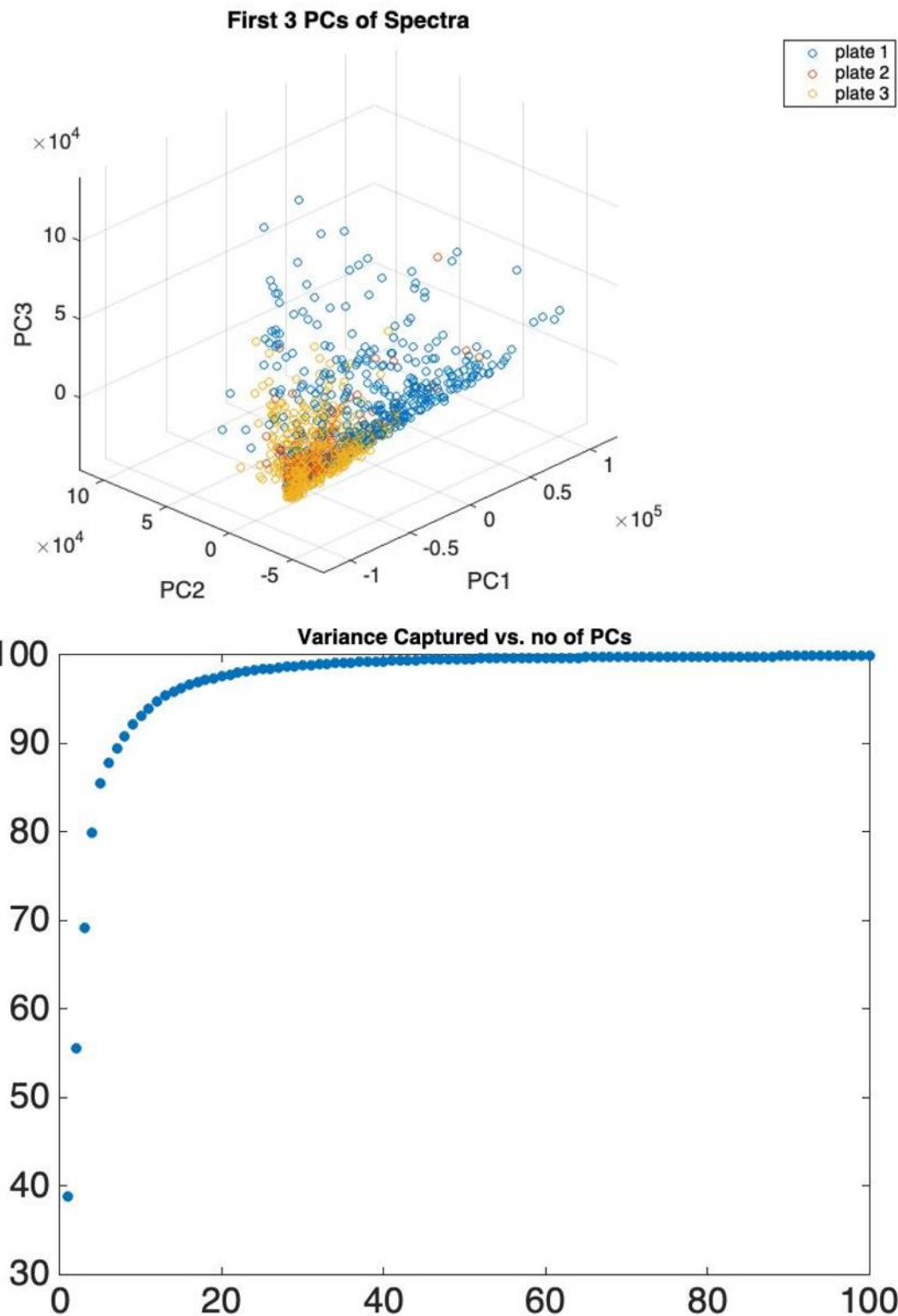


Figure 2.13 (Top) The coefficients of the first 3 principle components (PC) of the rhodamine spectra over 3 days. (Bottom) Plot of the % variance captured vs. number of PCs. 8 PCs capture 90% of the variance and 20 PCs 99% of the variance.

2.5 Recent Advancements

Since we completed the case study described previously, we have made significant improvements to our data collection procedures. The first of these improvements is that we now collect data only from the center of each spot. Our previous method of data collection (Figure 2.7) scanned over the entire surface of the DESI plate. Whether a plate contained only 384 or the full 6,144 spots, the analysis time was always the same (approximately three hours). The new, spot-to-spot method of data collection acquires data only from locations that the user specifies, which significantly shortens the analysis time of plates containing fewer than 6,144 spots. (Figure 2.14).

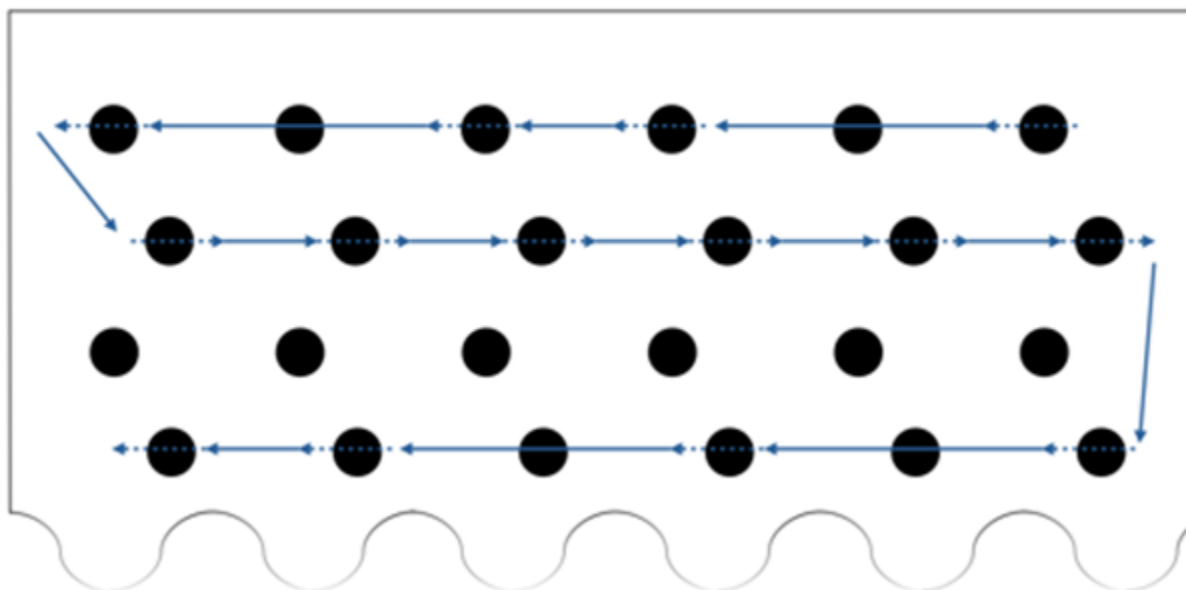


Figure 2.14 Spot-to-spot method of data acquisition. The spots that are skipped represent locations that were not selected for analysis by the user.

For the spot-to-spot method to work, the locations of all 6,144 spots must be known before the analysis begins. This is accomplished by using the pin tool to place a dark dye solution in three corners of each DESI plate (top left, top right, and bottom left). The user then locates the center of the DESI spray using the camera on the DESI stage. The DESI stage is then moved sequentially to each of the three pinned dye spots, the center of the DESI spray is aligned with the center of the dye spot using the camera, and the location of the DESI stage is recorded. Using the coordinates of these three spots, the locations of all 6,144 spots are then calculated. When the analysis begins, the DESI stage moves sequentially to each spot selected by the user and acquires data for

approximately one second. A plate containing only 384 spots can be acquired in under seven minutes, while this same plate would take three hours using the previous method.

A second improvement is that we can now analyze data in real time using CHRIS. Previously, data could only be analyzed after the entire data set had been collected. For large data sets, this meant that there were delays of an hour or more before any data could be reviewed. With the latest version of CHRIS, outputs like the one seen in Figure 2.8 are generated in real time. Spots appear in the output as they are analyzed, and the user can determine the success or failure of the reaction and view the associated mass spectrum in real time.

A final improvement is that MS/MS acquisition has been incorporated into CHRIS. Users first acquire full scan data using the procedures described previously. Once the data is analyzed by CHRIS, the user is provided a file which contains the data for each spot including reaction conditions, m/z values and corresponding intensities for starting materials, products, and other ions of interest, and importantly the XY coordinates of each spot. The user then creates a list of m/z values along with their corresponding XY coordinates for MS/MS analysis. The MS/MS analysis can then be performed on the same DESI plate that was used for the full scan analysis or an exact copy of the DESI plate that was made during the pinning process. The user first calculates the locations of all 6,144 spots using the coordinates of the three dye spots as described above, and the MS/MS analysis then proceeds in a spot-to-spot fashion only acquiring data from the locations specified by the user (Figure 2.15). The DESI spray rasters back and forth over each spot for approximately 30 seconds, during which product ion spectra are collected using three different relative collision energies (10%, 20%, and 30%). The MS/MS data is saved in the form of one RAW file per spot with an automatically generated name containing the XY coordinates and m/z value.

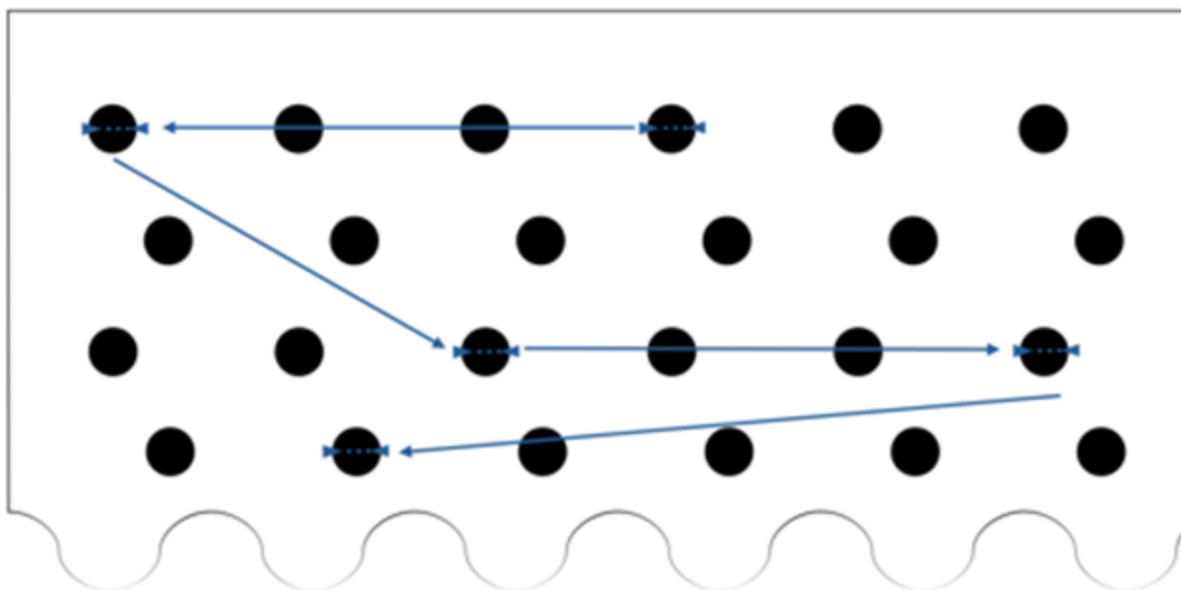


Figure 2.15 Example of MS/MS spot-to-spot data acquisition. Data is acquired only from specific locations provided by the user. Since not all reactions produce product, MS/MS data is typically acquired from fewer spots.

2.6 Conclusions

In this work, we designed and built a novel DESI-MS HTS platform comprised of commercial and custom-made hardware and software. We evaluated the robustness and reproducibility of the system by performing a 24h HTS experiment spanned across 3 days. The experiment involves determining the success of three classes of organic reactions, namely amine alkylation, amine acylation and amine sulfonylation, where a variety of amines and electrophiles were used, and three different reaction solvents as well as three different DESI spray solvents were evaluated. We noted that there is a trade-off between the reproducibility of the yes/no decisions and the rate of false negatives for the data generated, which can be modulated by choosing the threshold intensity. We found that results from 94% of all the reactions tested are reproducible over 3 days at both 3,072 and 5,760 reaction spot density. We attributed the sources of inconsistencies to factors such as inconsistency in reaction mixture pinning and fluctuations in spray solvent delivery. These issues are not fundamental and may be resolved in the future. At the time of writing, the platform was also updated with several features including (1) a new, spot-to-spot method of data collection, which allows users to acquire data only from user-specified locations, (2) a capability for data analysis in real time, and (3) on-demand MS/MS analysis of a reaction products. It is noteworthy

that the system's throughput may be significantly improved upon when coupled with a reagent preparation system and that its impact can be readily extended towards biological applications whereby analytes from cells and tissue samples instead of reaction mixtures are of interest and can be deposited on the DESI substrate. As such, these are opportunities for future work.

CHAPTER 3. HIGH THROUGHPUT EXPERIMENTATION AND CONTINUOUS FLOW EVALUATION OF NUCLEOPHILIC AROMATIC SUBSTITUTION REACTIONS

3.1 Introduction

High throughput experimentation (HTE) allows the implementation of large numbers of experiments in parallel, expending minimum amounts of compounds and time, and consuming less labor per experiment.¹⁸⁻¹⁹ This technique can boost lab productivity by rapid generation of comprehensive data for the selected transformations.^{18, 20} HTE based experiments focused across a range of settings have spread in biology, drug discovery²¹, medicinal chemistry²²⁻²³ and catalysis.^{19, 24-25} Analysis of the resulting large data sets to extract a deeper understanding of the chemical transformation can be a bottleneck. The discovery and optimization of reaction conditions prior to chemical process development can be accelerated when HTE is coupled with MS analysis.^{13, 24, 26} These impacts are particularly evident in the pharmaceutical and biopharmaceutical industries where reduction in the time of each experimental cycle is a necessity due to the great value of these product classes.²⁷⁻²⁸

The HTE technologies reported herein are based on two techniques: (i) desorption electrospray ionization (DESI) and (ii) bulk microtiter (small scale batch) reactions. DESI is an ambient ionization technique in which electrospray droplets are directed onto a surface generating a thin film of solvent (~500 μm in diameter)²⁹. Analytes present on the surface desorb into this thin film, and are then transferred into the mass spectrometer by secondary droplets (typically 1 micron in diameter³⁰), which are generated from small splashes caused by the continuously arriving electrospray droplets. The electrospray is rastered over the surface using a moving x-y stage to generate a 2D array of chemical reactivity. The thin films and droplets generated in the DESI process can promote reaction acceleration³¹; thereby allowing the simultaneous synthesis and analysis of reaction mixtures in a high throughput manner. This has been demonstrated previously with both amine alkylation and Suzuki coupling reactions in studies of modest scope.¹⁴ In this study, DESI is also used to analyze the results of the bulk microtiter reactions, and with an analysis time of a few seconds per reaction mixture, DESI enables a far more rapid evaluation of these results than other techniques such as LC-MS, which typically takes several minutes for each sample. It is important to note that we will typically refer to the droplet/thin film accelerated

reactions as DESI reactions in this paper. This is not to be confused with the DESI analysis of the bulk microtiter reactions.

Nucleophilic aromatic substitution (S_NAr) reactions are versatile transformations in the modern organic chemistry arsenal³² and one of the important reactions used for making pharmacologically³³⁻³⁴ and biologically active molecules.³⁵⁻⁴⁰ The reaction mechanism⁴¹⁻⁴² involves a stepwise addition–elimination sequence⁴³⁻⁴⁵ wherein the first step involves a nucleophilic attack of the substrate to provide a Meisenheimer complex followed by the loss of the leaving group through either catalyzed or non-catalyzed pathways.⁴⁵⁻⁴⁷ The reaction typically involves an amine as the nucleophile,⁴¹ although a wide variety of non-nitrogenous nucleophiles may be used. This study reports HTE evaluation of S_NAr reactions performed in both droplets/thin film and bulk microtiter formats with analysis by DESI-MS.

After HTE optimization, validation of the reaction hotspots was performed in flow to increase confidence in the HTE findings. Microfluidic reactions are attractive alternatives for these transformations in organic synthesis, since continuous flow methods have shown great potential to achieve faster syntheses in a greener way⁴⁸ for more than a decade. Rapid multistep microfluidic synthesis of small drug molecules using ESI-MS analysis has been reported by our group⁴⁹⁻⁵². Although the S_NAr reaction is already known in flow⁵³, we selected a broader range of substrates for this study in an effort to develop efficient flow-enabled routes to biologically as well as pharmaceutically important synthons.¹⁰ The preparation of automated S_NAr reaction mixtures for both HTE methods was performed in glass-lined 96-well metal plates using sixteen different amines and thirteen different aryl halides. Additional variables, including base, reaction solvent, DESI spray solvent, temperature, and reaction time, were evaluated.

3.2 Experimental

All chemicals and reagents were purchased from Sigma-Aldrich (St Louis, Missouri) and used without any purification.

3.2.1 High Throughput Reaction Conditions

High throughput S_NAr experimentation in bulk was performed in 96-well metal block assemblies (Analytical Sales and Services, Inc., NJ, USA). The reaction mixtures were prepared

in 1 mL glass inserts of the 96-well metal block. All the reagent transfers and mixing were performed using a Beckman Coulter i7 liquid handling robot. The stock solutions were 111 mM for amines and aryl halides, and the base stock solution concentration was 1.25 M in NMP or 1,4-dioxane. The final reaction concentrations were 50 mM (1 equiv.) both for the amines and aryl halides, and 125 mM (2.5 equiv.) for the bases. All solutions were prepared in the appropriate solvent, and they were added to the 96-well plate in a ratio of 9:9:2 (amine:aryl halide:base). Additional solvent was used instead of base for the ‘no base’ condition. Four identical 96 well plates were prepared, each utilizing one of four different base conditions: N,N-Diisopropylethylamine (DIPEA), Sodium tert-butoxide (NaO^tBu), Triethylamine (TEA) and no base (control). Each reaction mixture (40 μ L) was then transferred to a 384 well plate. For DESI-MS HTE, aliquots from all four 96 well metal plates were deposited into one 384 well plate, followed by transfer of 50 nL of each reaction mixture in the 384 well plate to a PTFE surface (a porous polytetrafluoroethylene sheet glued onto a glass support) using a 384-format stainless steel pin tool. This final transfer is necessary because the reaction mixtures must be on a surface to enable DESI-MS analysis. Up to sixteen 384 well plates can be pinned onto one PTFE surface (also referred to as the DESI slide) by slightly offsetting the location of the pins relative to the surface during each transfer and resulting in a total of up to 6,144 spots per DESI slide as described by Wleklinski et. ¹⁴ It is important to note that these reaction mixtures were placed onto the surface prior to any incubation steps for evaluation of the droplet/thin film reactions.

For bulk HTE, the remaining reaction solutions in the metal blocks were heated in the customized heating block at 150 °C or 200 °C for varying times to affect the bulk reaction. The cover on top of the glass inserts (top of the metal block) is made by chemically resistant perfluoroalkoxy (PFA) film. Double silicone rubber mats were used on top of the PFA film, providing a tight seal that is enough to heat the solution above the boiling point with less than 5% solvent loss and no cross talk between wells. After heating, the well plates were cooled, and samples of the reaction mixtures were transferred to the PTFE surface using the same procedure described above. These thermally activated bulk microtiter reaction mixtures were spotted onto the same PTFE surface using the same transfer method as the non-incubated mixtures to enable direct comparison, using rhodamine B as a fiducial marker. The PTFE surface was then analyzed using DESI-MS, and the MS data was analyzed using in-house software called Chemical Reaction Integrated Screening (CHRIS) to produce heat maps of the reaction outcomes.

3.2.2 Liquid Handling Robot

Samples in 96 well aluminum blocks fitted with glass vial liners (Analytical Sales and Services, Inc., NJ, USA) or 384 well polypropylene plates (Analytical Sales and Services, Inc., NJ, USA) were prepared both for DESI and bulk HTE using a Biomek i7 (Beckman Coulter, Inc., Indianapolis, IN) liquid handling robot. A 384-tip head was used to transfer a single volume of 384 samples under the same speed of aspiration and dispensing conditions. Also, the heights of pipetting at the source and destination positions, pattern of pipetting, etc. remained constant for each transfer. An 8-channel head provided more flexibility in the amount of liquid transferred. Moreover, the 8-channel tip head provided better flexibility in terms of the layout of source and destination platforms, speed, pipetting height, and reaction stoichiometry. The Biomek i7 deck is also capable of accommodating all necessary labware including robotic tips, plates, reservoirs, etc. for assembling one reaction step. Chemically resistant polypropylene and disposables tips (Beckman Coulter, Inc., Indianapolis, IN) were used to make the reaction mixtures. The reservoirs of reagents solutions were polypropylene multi-well plates and reservoirs, as well as custom made Teflon reservoirs. The plate preparation methods were made using the Biomek point-and-click programming tool.

3.2.3 Customized Heating Block

Home built heating devices made of aluminum heater blocks containing four, 100 W cartridge heaters were fabricated to accommodate standard size 96 well plates. A CNi series temperature controller (Omega Engineering) enabled precise temperature control and a solid-state relay was used to modulate the 120 Vac power to the heaters.² The heating blocks tolerate temperatures ranging from -20 °C to 200 °C.

3.2.4 DESI-MS Analysis

DESI-MS analysis was performed following the previously published method of Wleklinski et al¹⁴. However, in this work, the density of reaction spots was 3,072 spots/plate instead of 6,144/plate. The Biomek i7 robot was used to prepare the DESI slide using reagents that were pipetted into standard polypropylene 384-well plates. Porous polytetrafluoroethylene (PTFE) sheets (EMD, Millipore Fluoropore, Saint-Gobain) were glued (Scotch Spray mount) onto glass

slides (Foxx Life Sciences) to make the DESI slides. No signs of interference from the glue were observed. The reagents were mixed, and rhodamine B dye in a separate reservoir was added to the robotic deck as a fiducial marker. The liquids (50 nL) were deposited onto a porous PTFE surface using the magnetic pin tool at 3,072 spot densities. A linear ion trap mass spectrometer (LTQ XL; Thermo Scientific, San Jose, CA) equipped with a commercial DESI-imaging source (DESI 2D source, Prosolia Inc., Indianapolis, IN) was used to collect the DESI-MS data. Xcalibur v. 4.0 software was used to control the instrument and run the worklists for DESI-MS data acquisition. The DESI spray angle was 56° using MeOH or MeOH with 1% formic acid (FA) as spray solvent with an applied voltage of 5 kV. Mass spectra were collected in positive ion mode over the m/z range of 50-500. The DESI-MS imaging lateral resolution was 350 μm . This was achieved using a stage speed of 4,376 $\mu\text{m}/\text{sec}$ and an instrument scan time of 80 ms. The time to acquire data from one DESI slide was approximately 3 h, resulting in an analysis time of \sim 3.5 seconds per reaction mixture. For data processing, data were visualized using in-house software designed¹⁴ to automatically search for the m/z values of reactants, intermediates, and byproducts. The analysis using the in-house software generates a heat map indicating ‘yes/no’ output for each spot on the PTFE surface of the DESI slide.

3.2.5 DESI-MS Analysis Software (CHRIS)

The Chemical Reaction Integrated Screening (CHRIS) tool is an in-house software suite developed to search the captured data for m/z values that correspond to the starting materials, intermediates, by-products, and products. CHRIS is used here to generate a yes/no report, through a web interface and displays the mass spectrum of any spot as well as spreadsheets with the intensity for the selected molecules, the possible contaminants, or unknown by-products as guided by the user.

3.2.6 Microfluidic System

All microfluidic validation reactions were performed using a Labtrix S1 system (Chemtrix, Ltd, Netherlands). The system was described previously in Jaman et al.² The micro reactor 3225 is made of glass and used for all conducted reactions. The staggered orientated micro reactor (SOR) chip 3225 (four inlets and one outlet, volume 10 μl) have channel width 300 μm and channel depth

120 μm . The Labtrix unit is enabled to pump five syringes into the micro reactor positioned on a heating and cooling unit. All the gastight glass syringes were bought separately from Hamilton Company (Hamilton, Reno, Nevada). All operations are controlled via a ChemTrix GUI software, connected to the Labtrix S1 casing using a USB cable.

3.2.7 Microfluidic Reaction Conditions

Solutions of amines (100 mM, 1 equiv) and aryl halides (100 mM, 1 equiv) in NMP were loaded individually into two separate 1 mL Hamilton gastight glass syringes (Hamilton Company, Reno, NV). DIPEA (150 mM, 1.5 equiv) solution in NMP was loaded into another 1 mL Hamilton gastight glass syringe. Each solution was continuously dispensed into the SOR 3225 reactor to engage the reactants. All the $\text{S}_{\text{N}}\text{Ar}$ reactions were run at 100 $^{\circ}\text{C}$ and/or 150 $^{\circ}\text{C}$ using residence times of 30 sec, 1 min, 3 min, and 5 min. The products were collected without quenching and stored at -80 $^{\circ}\text{C}$. TLC analyses were performed at the end of the reactions and the findings confirmed by subsequent ESI-MS analysis after extraction in ether and dilution into methanol.

3.2.8 Analysis of Microfluidic Reactions

A Thermo Fisher TSQ Quantum Access MAX mass spectrometer connected to a Dionex Ultimate 3000 Series Pump and WPS-3000 Autosampler (Thermo Fisher Scientific, Waltham, MA), was used to acquire electrospray ionization mass spectra (ESI-MS) of the samples. The analysis was performed in full scan mode, monitoring each analysis in both positive and negative ion modes. The optimized parameters for the ESI source and MS are as follows: spray solvent, MeOH; spray voltage +5 kV (positive mode) and -5.0 kV (negative mode); capillary temperature, 250 $^{\circ}\text{C}$; Sheath gas pressure, 20; scan time, 0.5 s; Q1 peak width (FWHM), 0.70 Th; micro scans, 1. The autosampler settings were as follows: MS acquire time, 2 min; sample injection volume, 1 μL . The data from MS spectrometer was processed using Thermo Fisher Xcalibur software.

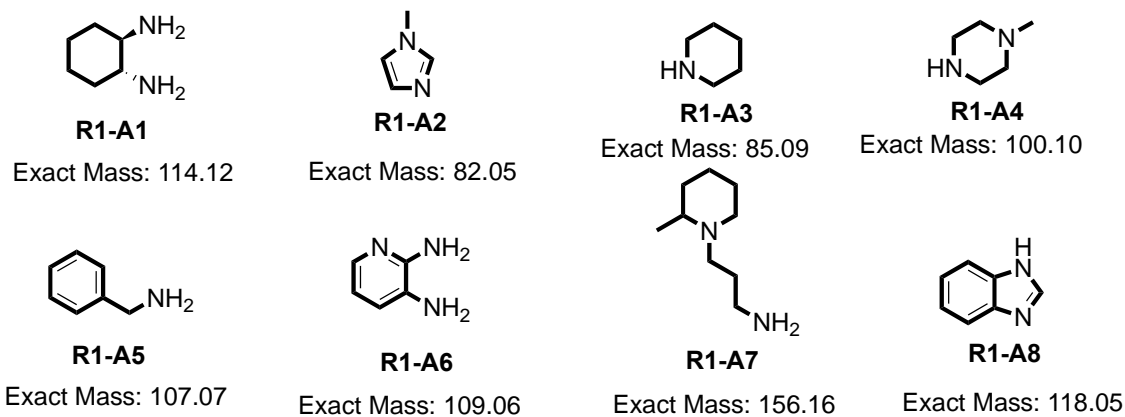
3.3 Results and Discussion

3.3.1 High throughput experimentation (HTE)

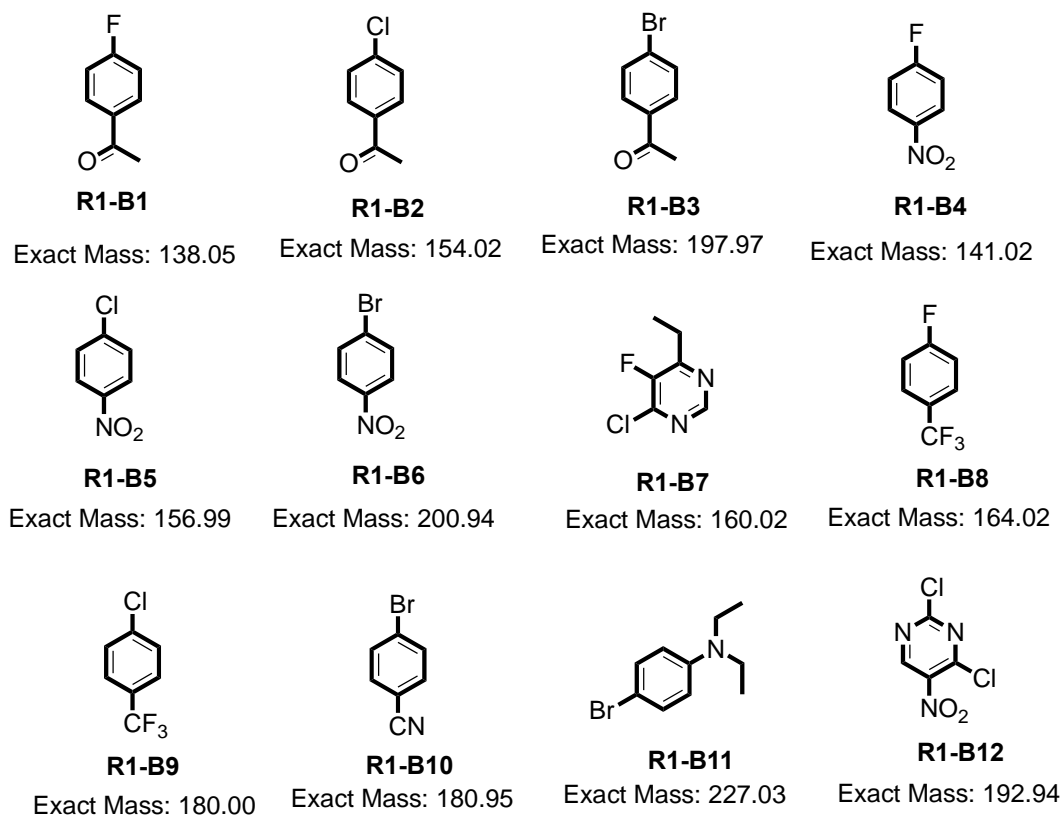
Two high throughput experimentation methods were tested: reactions in droplets/thin films (DESI used for both synthesis and analysis) and reactions in bulk microtiter plates (DESI used for analysis only). N-Methyl-2-pyrrolidone (NMP) and 1,4 dioxane were chosen as the polar aprotic solvents for the reaction because all the reagents dissolved in these polar aprotic reaction media.⁵⁴ DESI-MS analysis allowed rapid investigation of reactions that were capable of producing a diverse product profile. The spray solvents were MeOH or MeOH with 1% formic acid (FA). Full scan mass spectra in positive mode were recorded for each reaction mixture.

Eight amines and twelve aryl halides (Scheme 3.1) were tested in our first round of experiments using different bases in two solvents, NMP and 1,4-dioxane. The bulk HTE reactions were heated for S_NAr reaction product formation at 150 °C for 15h. The DESI droplet/thin film reactions were performed under ambient conditions in the time it took to spray each pixel in the array.

Amines



Aryl halides



Scheme 3.1 Reagents used in Round 1 of the HTE campaign.

The amine and aryl halide ratios used were 1:1 while 2.5 equivalent of different bases were used. All the amines and aryl halides for this reaction were explored without additional protection/deprotection steps. A Beckman-Coulter Biomek i7 liquid handling robot was used to prepare the reaction mixtures in either 96 well glass lined metal blocks or 384 well plates. A total

of 400 μL of the reaction solution was prepared in each well of the 96 well plates for the bulk microtiter reactions while just 50 nL was used for the DESI experiments.

We performed the high-throughput experiments in two rounds, differing primarily in the amine nucleophiles used. Results for a subset of the data from Round 1 is shown in Figure 3.1. Each square in Figure 3.1 represents a unique reaction condition and is an average of two separate reaction replicates. The peak intensities of the products in the corresponding full scan mass spectra were used to evaluate the success or failure of each reaction. A successful reaction was defined as having an average product peak intensity of at least 150 counts (S/N \sim 3) in the centroided mass spectrum.

A)

	R1-B1	R1-B2	R1-B3	R1-B4	R1-B5	R1-B6	R1-B7	R1-B8	R1-B9	R1-B10	R1-B11	R1-B12 (S)	B12 (D)
R1-A1													
R1-A2													
R1-A3													
R1-A4													
R1-A5													
R1-A6													
R1-A7													
R1-A8													

B)

	R1-B1	R1-B2	R1-B3	R1-B4	R1-B5	R1-B6	R1-B7	R1-B8	R1-B9	R1-B10	R1-B11	R1-B12 (S)	B12 (D)
R1-A1													
R1-A2													
R1-A3													
R1-A4													
R1-A5													
R1-A6													
R1-A7													
R1-A8													

C)

	R1-B1	R1-B2	R1-B3	R1-B4	R1-B5	R1-B6	R1-B7	R1-B8	R1-B9	R1-B10	R1-B11	R1-B12 (S)	B12 (D)
R1-A1													
R1-A2													
R1-A3													
R1-A4													
R1-A5													
R1-A6													
R1-A7													
R1-A8													

D)

	R1-B1	R1-B2	R1-B3	R1-B4	R1-B5	R1-B6	R1-B7	R1-B8	R1-B9	R1-B10	R1-B11	R1-B12 (S)	B12 (D)
R1-A1													
R1-A2													
R1-A3													
R1-A4													
R1-A5													
R1-A6													
R1-A7													
R1-A8													

Figure 3.1 Direct comparison of S_NAr reactions using droplet/thin film and microtiter approach
 A) The droplet/thin film and B) bulk microtiter results for the same set of reaction conditions. Experimental conditions: spray solvent: methanol; reaction solvent: NMP; base: DIPEA. C) Same as B, but the spray solvent was MeOH + 1% FA D) Same as C, but the reaction solvent was 1,4 dioxane. Each cell is an average of two data points. Green cells represent "yes" reactions (product ion intensity > 150 counts). Red cells represent "no" reactions (product ion intensity < 150 counts). B12 can form both single and double addition products; the double addition product can form multiple ions. B12 (S) is the singly charged ion of the single addition product; B12 (D) is the sum of the average intensities of all the double addition products.

Twelve successful reactions were found for the droplet reactions, whereas 41 successful reactions were found for the same conditions in bulk (Figure 3.1, A & B). Some of the reactions were favorable under droplet conditions; however, S_NAr reactions typically require heating,⁵⁵ so

it was not surprising that more ‘yes’ reactions were observed in the bulk reaction conditions. Moreover, MeOH with 1% FA was found to be a better spray solvent than MeOH due to the better product ionization in presence of acid⁵⁶⁻⁵⁷ (Figure 3.1, C). This change increased the number of successful reactions detected in bulk by 30%. It is also worth noting that the reaction worked better in NMP than 1,4 dioxane (54 ‘yes’ reactions vs 40 ‘yes’ reactions) (Figure 3.1, C &D). Since NMP is much more polar,⁵⁴ we attribute these finding to the stabilization of the sigma complex transition state found after the addition step.

Figure 3.2 shows the heat map of the Round 1 reactions in both DESI and bulk using MeOH with 1% FA as spray solvent. In general, electron donating groups (EDG) in the amine nucleophile and electron withdrawing groups (EWG) in the aryl halide substrate favored product formation.⁴¹⁻⁴² For these experiments, the most reactive amines were 1-methylpiperazine (**R1-A4**) and 3-(2-methylpiperidin-1-yl) propan-1-amine (**R1-A7**), both of which possess electron donating groups. Similarly, a strong electron withdrawing nitro group in 1-fluoro-4-nitrobenzene (**R1-B4**), 1-chloro-4-nitrobenzene (**R1-B5**), 1-bromo-4-nitrobenzene (**R1-B6**), and 2,4-dichloro-5-nitropyrimidine (**R1-B12**) increases the reaction of these aryl halides. 4-Bromo-N,N-diethylaniline (**R1-B11**) did not work well due to the presence of the electron donating diethyl amine group. All other aryl halides reacted to the same extent. Also, ortho substituents in amine nucleophile or aryl halide substrate retarded the reaction due to steric hindrance.⁵⁸ Thus, pyridine-2,3-diamine, **R1-A6** or 2,4-dichloro-5-nitropyrimidine (**R1-B12**) did not react well, although (1R,2R)-cyclohexane-1,2-diamine (**R1-A1**) reactions were facile since the two adjacent amino groups are on different faces of the cyclohexane ring. 1-Methyl-1H-imidazole (**R1-A2**), a tertiary amine, did not react.

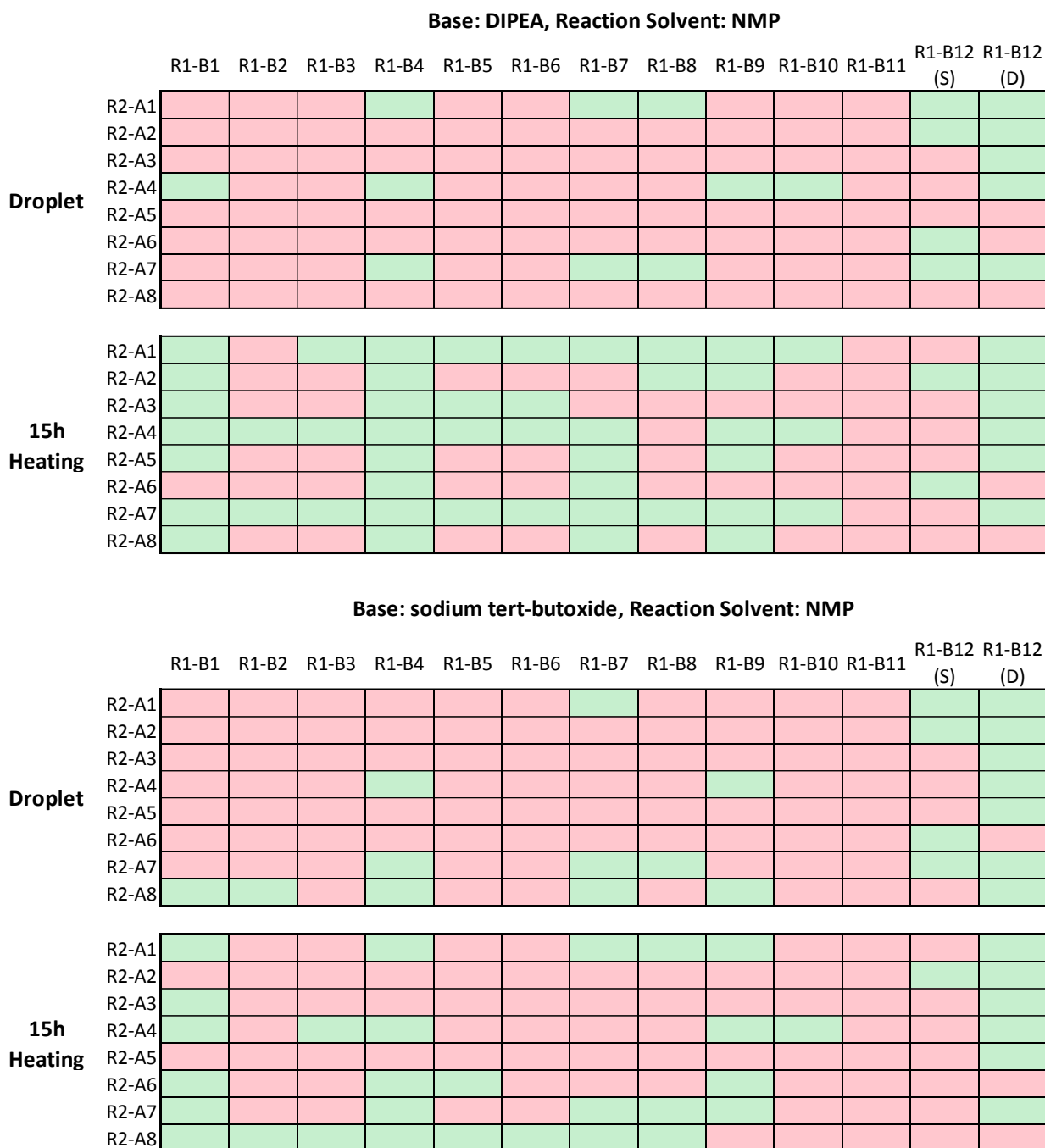
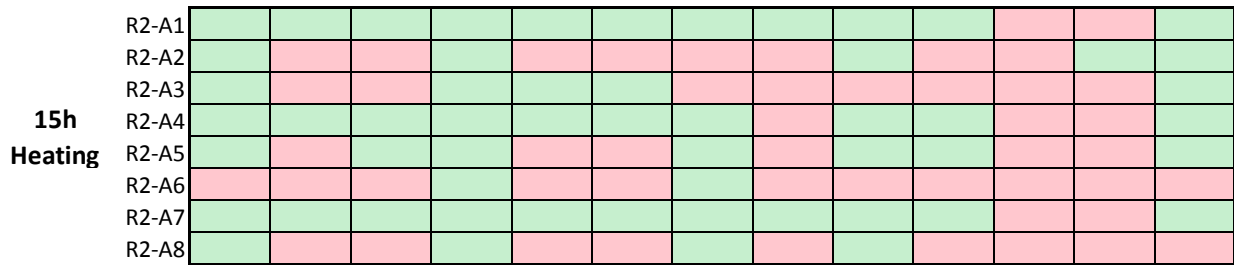
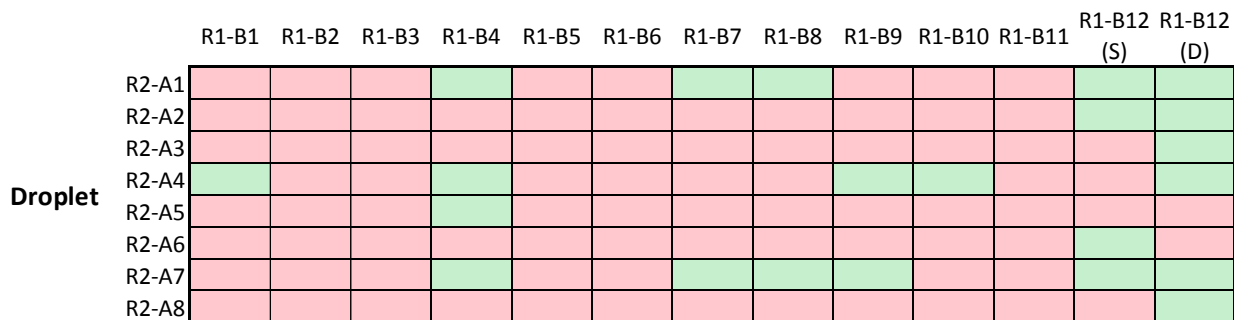


Figure 3.2 Heat map of 1,536 reactions from Round 1 of the S_NAr HTE using MeOH with 1% FA as the spray solvent under droplet/thin film or bulk microtiter plate conditions at 150 °C. Green cells represent successful reactions (average product intensity >= 150 counts). Red cells represent unsuccessful reactions (average product intensity < 150 counts).

Figure 3.2 continued

Base: TEA, Reaction Solvent: NMP



No Base, Reaction Solvent: NMP

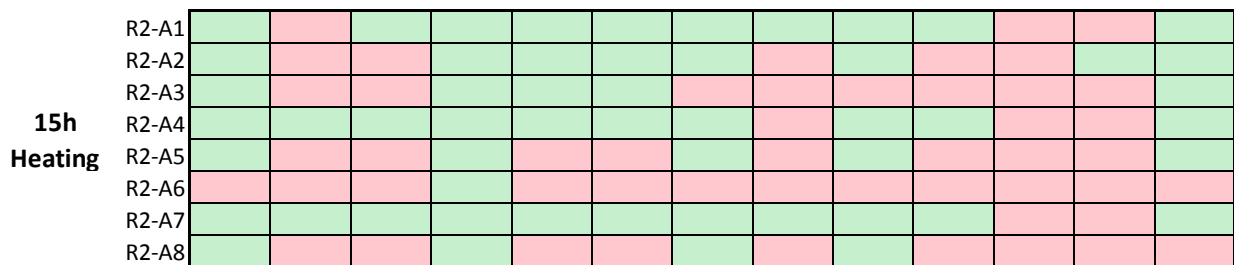
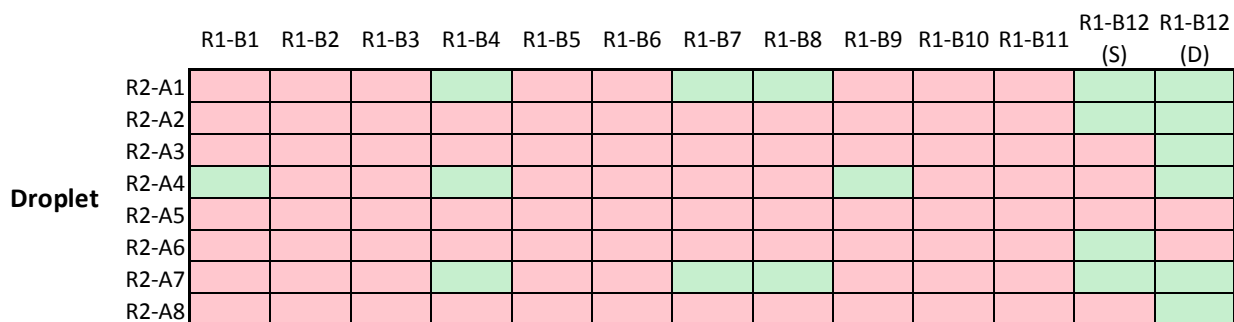


Figure 3.2 continued

Base: DIPEA, Reaction Solvent: 1,4-dioxane

	R1-B1	R1-B2	R1-B3	R1-B4	R1-B5	R1-B6	R1-B7	R1-B8	R1-B9	R1-B10	R1-B11	R1-B12 (S)	R1-B12 (D)
Droplet	R2-A1												
	R2-A2												
	R2-A3												
	R2-A4												
	R2-A5												
	R2-A6												
	R2-A7												
	R2-A8												
15h Heating	R2-A1												
	R2-A2												
	R2-A3												
	R2-A4												
	R2-A5												
	R2-A6												
	R2-A7												
	R2-A8												

Base: sodium tert-butoxide, Reaction Solvent: 1,4-dioxane

	R1-B1	R1-B2	R1-B3	R1-B4	R1-B5	R1-B6	R1-B7	R1-B8	R1-B9	R1-B10	R1-B11	R1-B12 (S)	R1-B12 (D)
Droplet	R2-A1												
	R2-A2												
	R2-A3												
	R2-A4												
	R2-A5												
	R2-A6												
	R2-A7												
	R2-A8												
15h Heating	R2-A1												
	R2-A2												
	R2-A3												
	R2-A4												
	R2-A5												
	R2-A6												
	R2-A7												
	R2-A8												

Figure 3.2 continued

Base: TEA, Reaction Solvent: 1,4-dioxane

		R1-B1	R1-B2	R1-B3	R1-B4	R1-B5	R1-B6	R1-B7	R1-B8	R1-B9	R1-B10	R1-B11	R1-B12 (S)	R1-B12 (D)
Droplet	R2-A1													
	R2-A2													
	R2-A3													
	R2-A4													
	R2-A5													
	R2-A6													
	R2-A7													
	R2-A8													
15h Heating	R2-A1													
	R2-A2													
	R2-A3													
	R2-A4													
	R2-A5													
	R2-A6													
	R2-A7													
	R2-A8													

No Base, Reaction Solvent: 1,4-dioxane

		R1-B1	R1-B2	R1-B3	R1-B4	R1-B5	R1-B6	R1-B7	R1-B8	R1-B9	R1-B10	R1-B11	R1-B12 (S)	R1-B12 (D)
Droplet	R2-A1													
	R2-A2													
	R2-A3													
	R2-A4													
	R2-A5													
	R2-A6													
	R2-A7													
	R2-A8													
15h Heating	R2-A1													
	R2-A2													
	R2-A3													
	R2-A4													
	R2-A5													
	R2-A6													
	R2-A7													
	R2-A8													

The structures of piperidine (**R1-A3**), and 1-methylpiperazine (**R1-A4**) are similar, but **R1-A4** always worked better than **R1-A3** due to the presence of an electron donating group (EDG) that enhances its reactivity. Moreover, benzylamine (**R1-A5**), pyridine-2,3-diamine (**R1-A6**), and benzimidazole (**R1-A8**) showed lower reactivity due to the presence of an electron withdrawing

aromatic moiety in these molecules, making them less nucleophilic toward the addition step in the reaction mechanism.

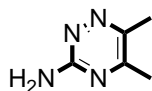
The summary of successful S_NAr reactions detected upon analysis of 1,536 unique droplet/thin film and bulk reactions is shown in Table 3.1. Among all the reactions, 311 'yes' reactions were observed in bulk while less than half that number were observed (153) when run in the short time/low temperature droplet/thin film format.

Table 3.1 S_NAr product formation as a function of reaction solvent, base, and DESI spray solvent.

Number of successful reactions in droplet/thin film format								
Base	DIPEA		NaO ^t Bu		TEA		No Base	
Reaction solvent→ Spray solvent ↓	NMP	Dioxane	NMP	Dioxane	NMP	Dioxane	NMP	Dioxane
MeOH	12	--	10	--	21	--	13	--
MeOH with 1% FA	18	22	22	09	22	21	19	20
Number of successful reactions in bulk microtiter format								
MeOH	41	--	18	--	40	--	41	--
MeOH with 1% FA	54	40	35	08	55	32	54	33

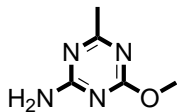
Our initial HTE campaign was followed by a second round of S_NAr reactions using a family of biologically active amines. Reaction in this round employed the same aryl halides (except that **R1-B10** was exchanged for 1-bromo-4-(trifluoromethyl) benzene, **R2-B10**) with a different set of eight amines (Scheme 3.2). The reaction conditions for Round 2 were similar to Round 1, except that (i) all reactions were performed in NMP, (ii) time points of 1 h, 4 h, and 15 h at 150 °C were used for the bulk microtiter reactions, and (iii) methanol with 1 % FA was the only DESI spray solvent used.

Amines



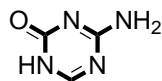
R2-A1

Exact Mass: 124.07



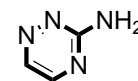
R2-A2

Exact Mass: 140.07



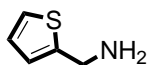
R2-A3

Exact Mass: 112.04



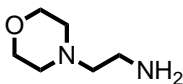
R2-A4

Exact Mass: 96.04



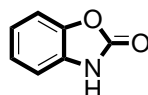
R2-A5

Exact Mass: 113.03



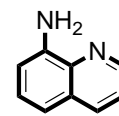
R2-A6

Exact Mass: 130.11



R2-A7

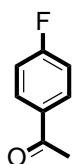
Exact Mass: 135.03



R2-A8

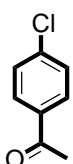
Exact Mass: 144.07

Aryl halides



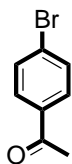
R1-B1

Exact Mass: 138.05



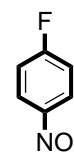
R1-B2

Exact Mass: 154.02



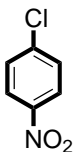
R1-B3

Exact Mass: 197.97



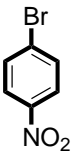
R1-B4

Exact Mass: 141.02



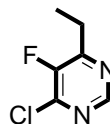
R1-B5

Exact Mass: 156.99



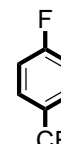
R1-B6

Exact Mass: 200.94



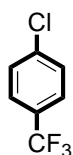
R1-B7

Exact Mass: 160.02



R1-B8

Exact Mass: 164.02



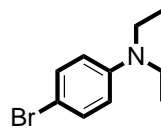
R1-B9

Exact Mass: 180.00



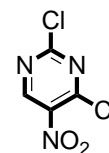
R2-B10

Exact Mass: 223.94



R1-B11

Exact Mass: 227.03



R1-B12

Exact Mass: 192.94

Scheme 3.2 Reagents used in Round 2 of the HTE campaign.

Figure 3.3 shows the heat maps from Round 2. Unfortunately, this set of reactions did not work very well because most of the amines have electron withdrawing groups in the aromatic moiety, thus making them less nucleophilic toward the addition step. Thiophen-2-ylmethanamine (**R2-A5**), and 2-morpholinoethan-1-amine (**R2-A6**), worked comparatively better than the other

amines due to their electron donating moiety. Again, **R1-B4**, **R1-B5**, **R1-B6**, **R1-B7**, and **R1-B12** worked better due to the presence of their strong electron withdrawing nitro and chloro groups.

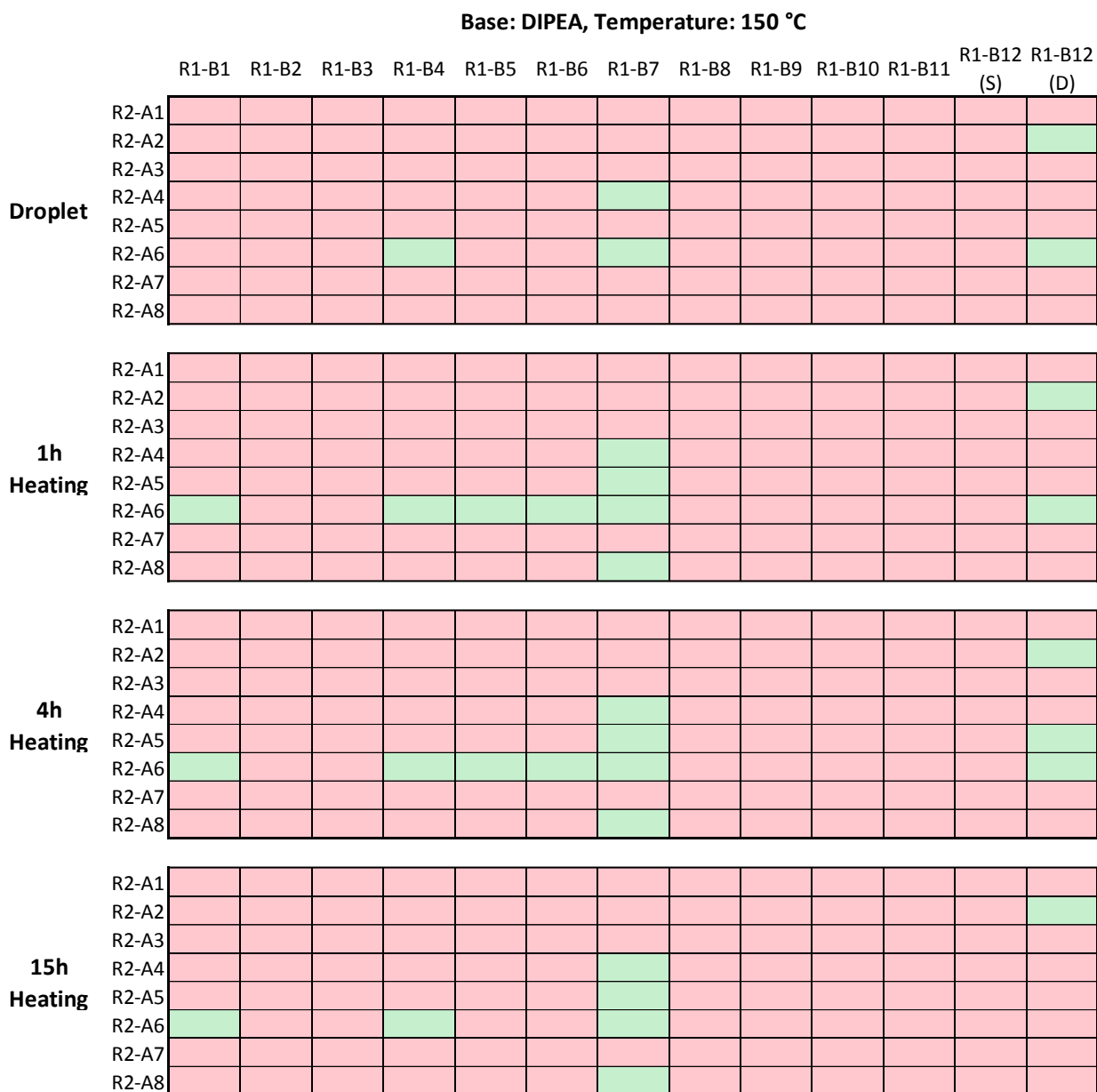


Figure 3.3 Heat map of 1,536 reactions (768 in droplet/thin film and 768 in bulk microtiter at three time points) from Round 2 of the S_NAr HTE using MeOH with 1% FA as the DESI spray solvent and NMP as the reaction solvent at 150 and 200 °C. Green cells represent successful reactions (average product intensity ≥ 150 counts). Red cells represent unsuccessful reactions (average product intensity < 150 counts).

Figure 3.3 continued

Base: sodium tert-butoxide, Temperature: 150 °C

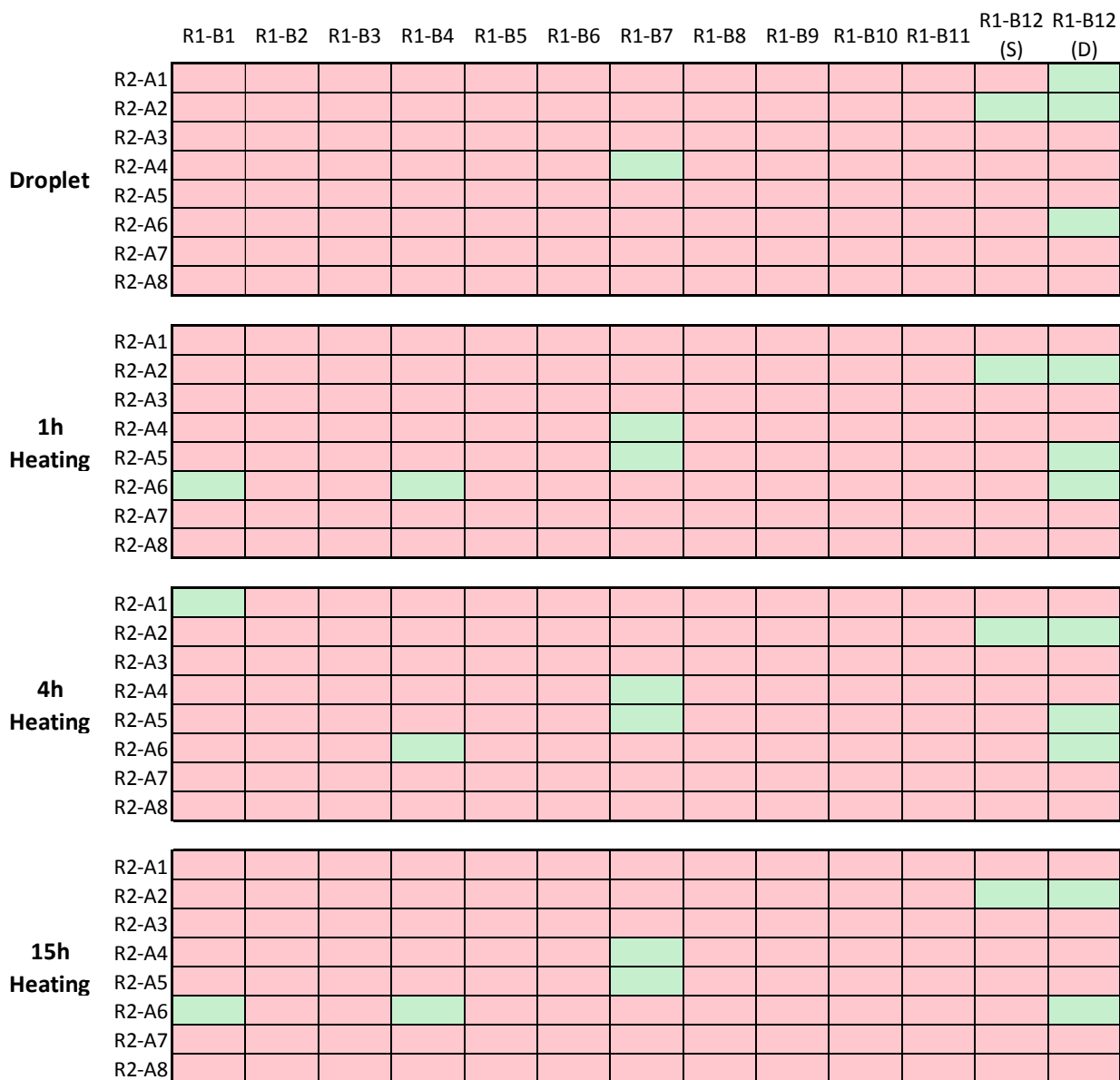


Figure 3.3 continued

Base: TEA, Temperature: 150 °C

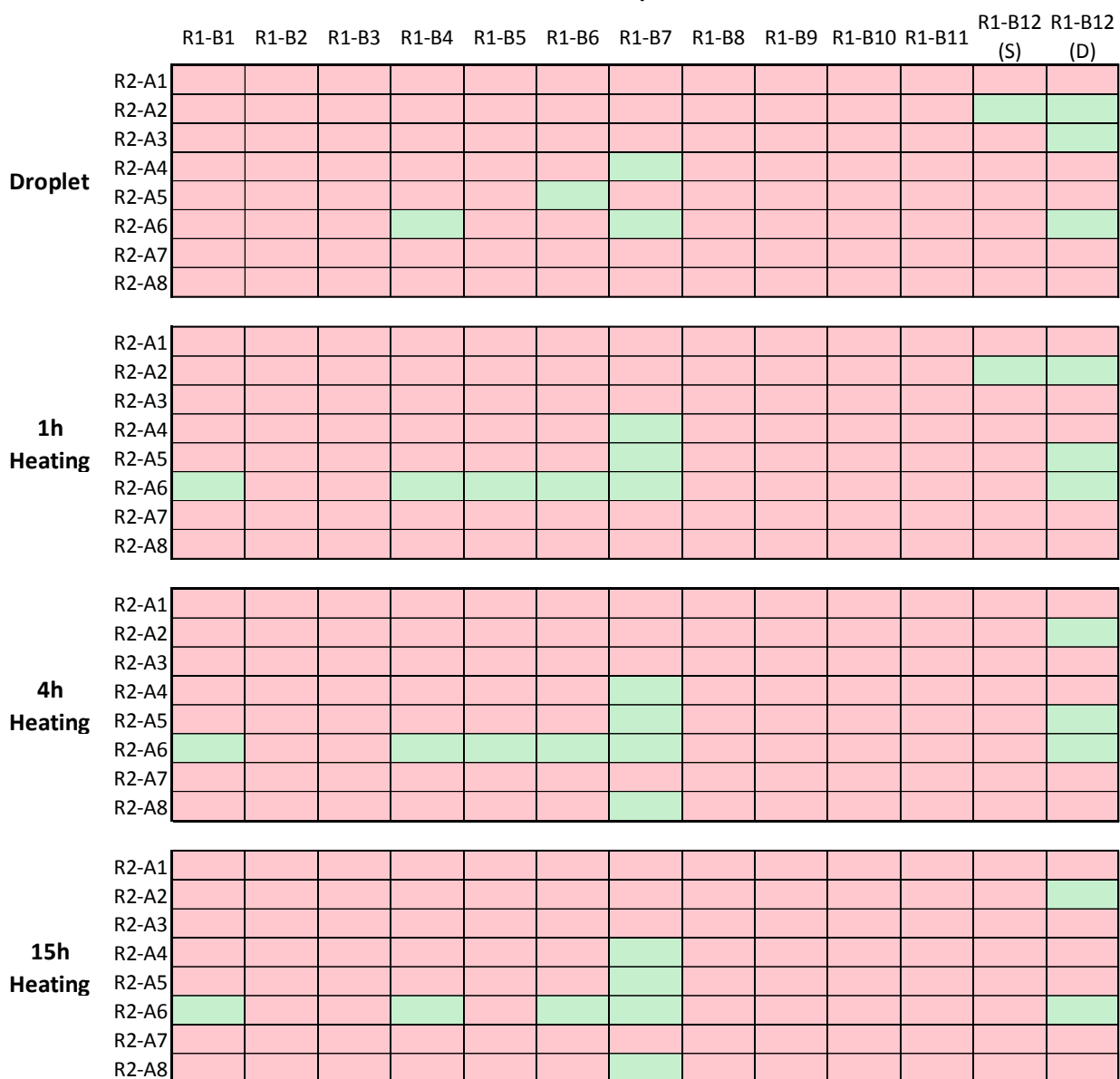


Figure 3.3 continued

No Base, Temperature: 150 °C

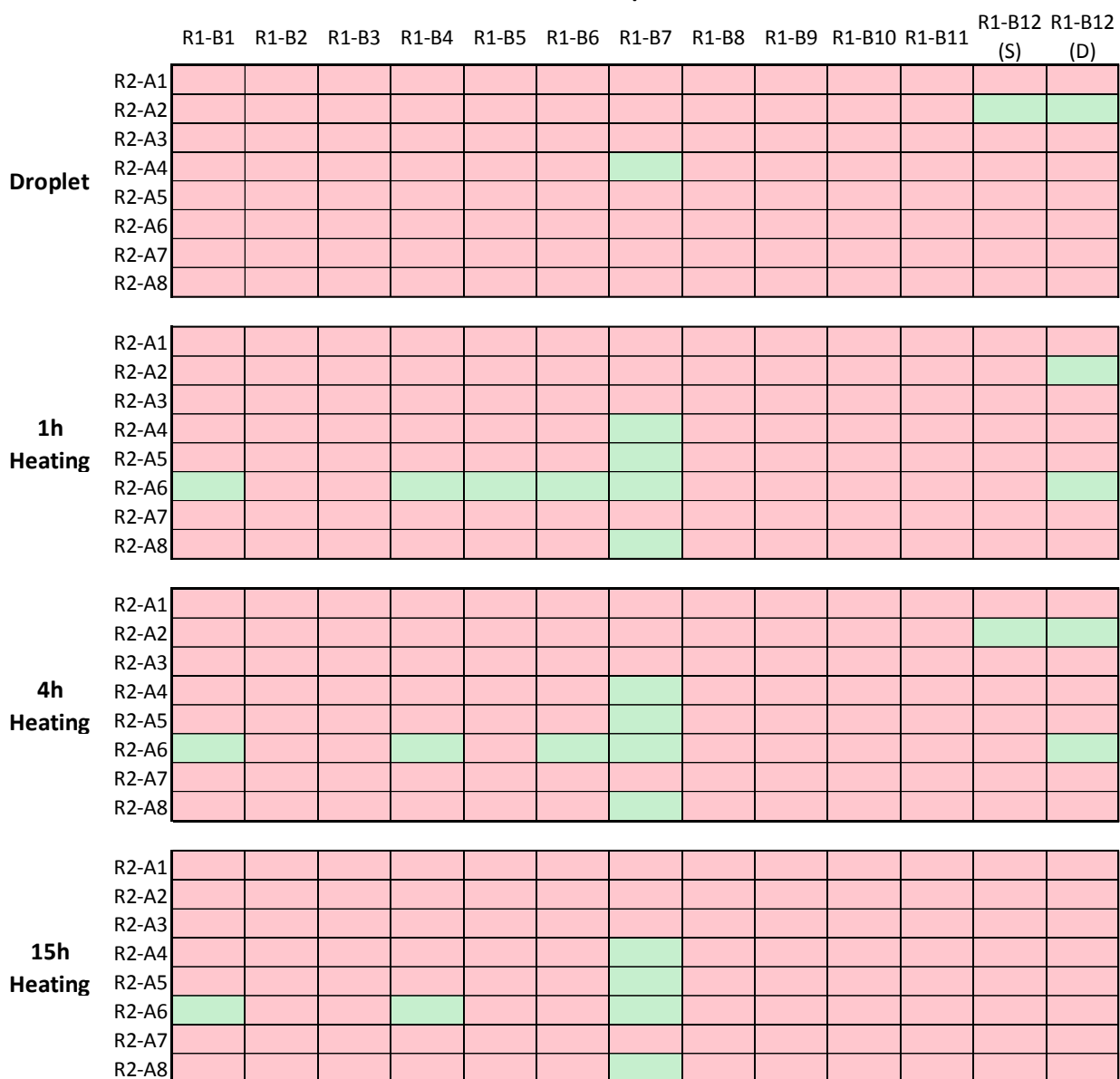


Figure 3.3 continued

Base: DIPEA, Temperature: 200 °C

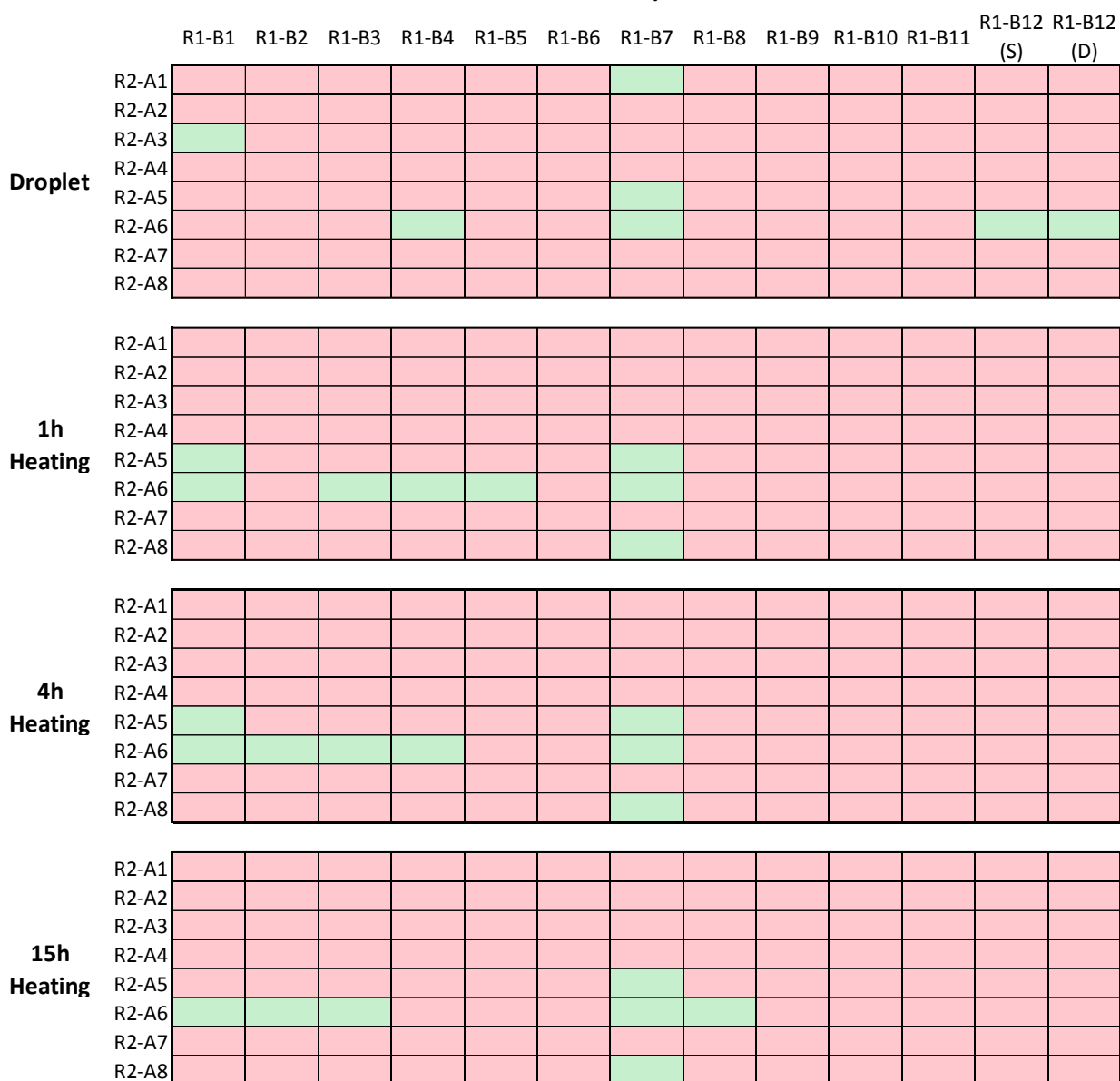


Figure 3.3 continued

Base: soduim tert-butoxide, Temperature: 200 °C

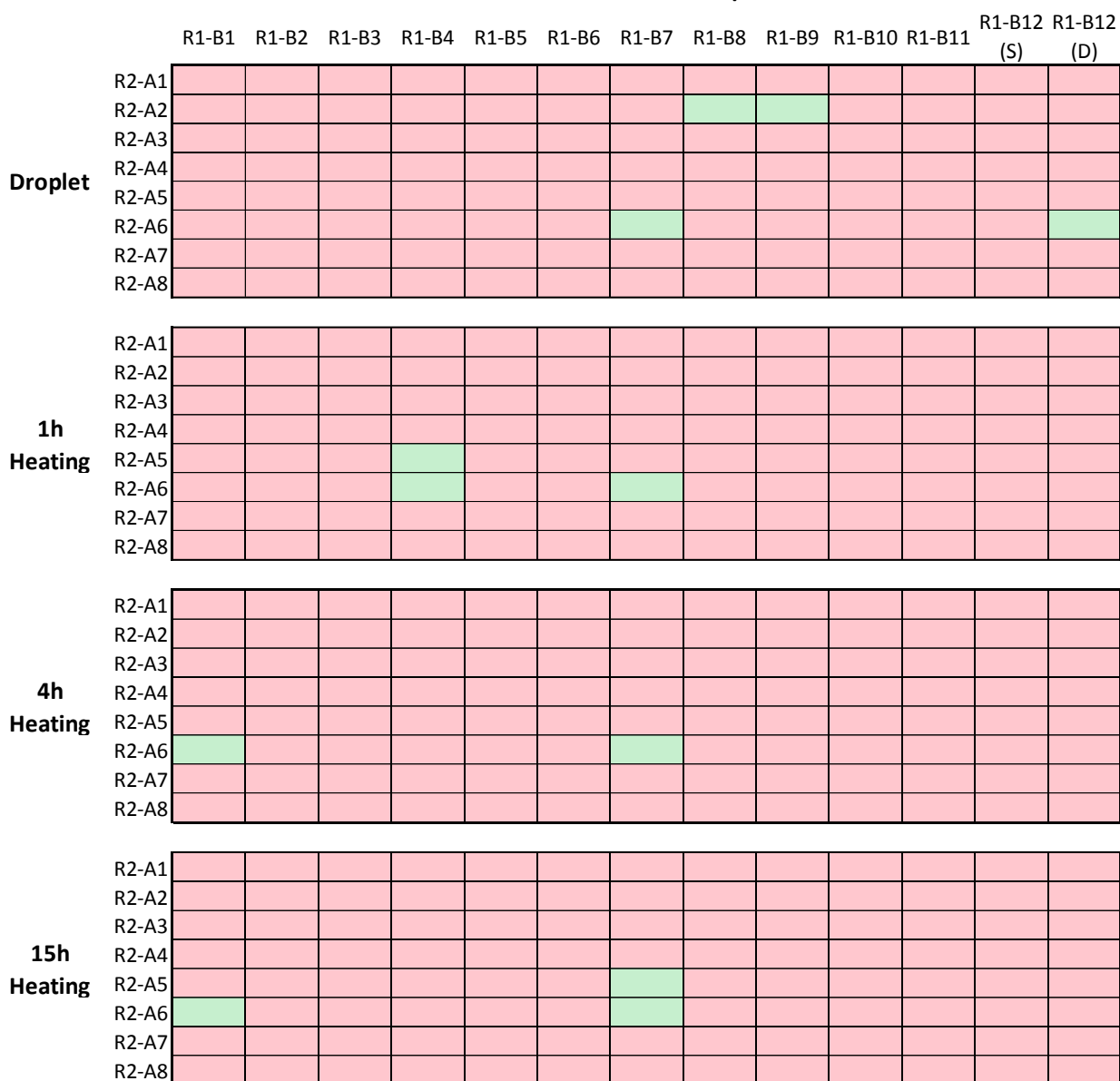


Figure 3.3 continued

Base: TEA, Temperature: 200 °C

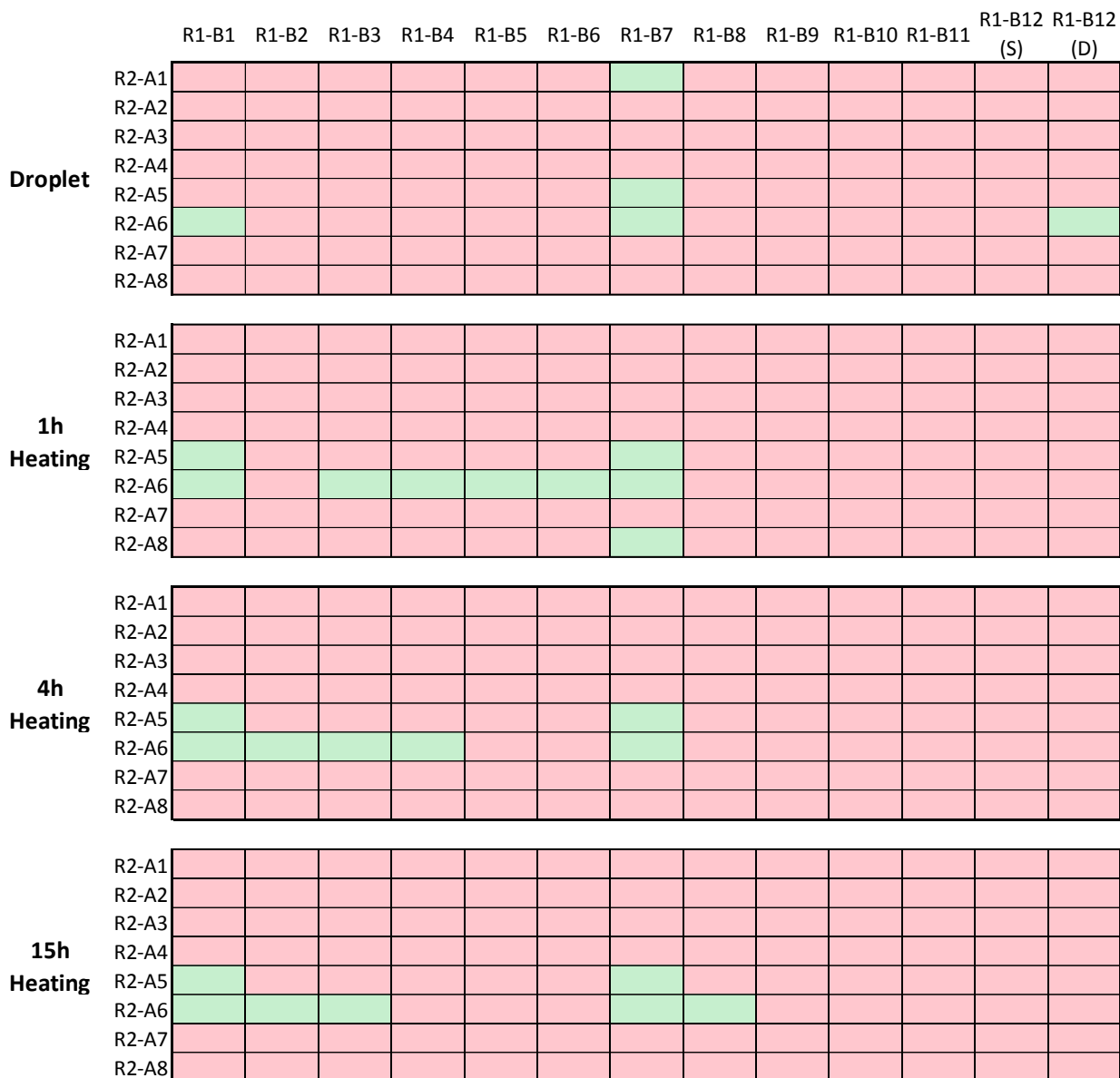


Figure 3.3 continued

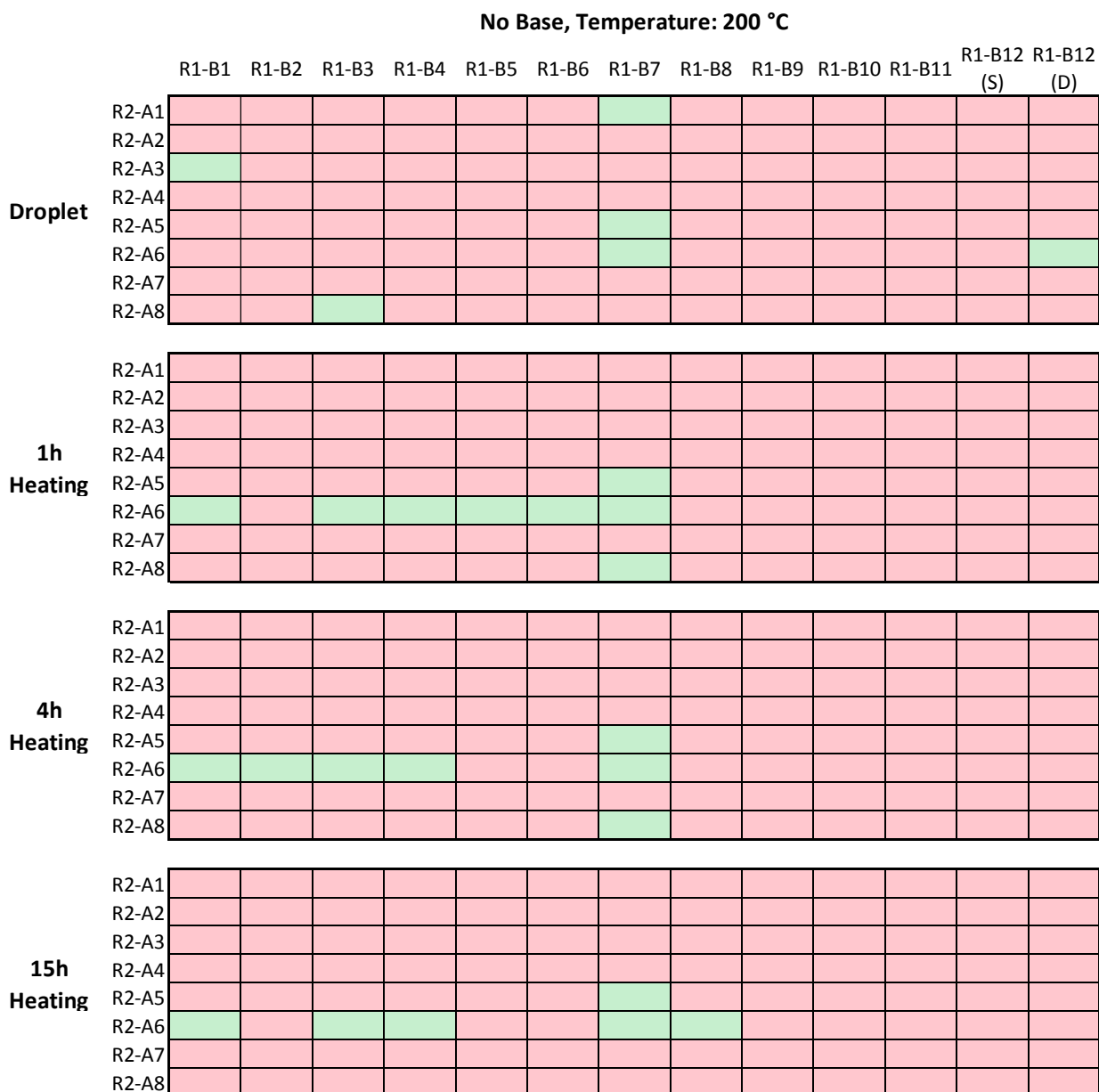


Table 3.2 summarizes of the Round 2 S_NAr HTE reactions both in DESI and bulk at different time points. Only 18 reactions gave substantial amounts of product in DESI, whereas 38 reactions worked in bulk after 1 h heating. Efforts to push the reaction at higher temperatures and longer times (200 °C for 15 h), did not improve the outcome (Figure 3.3 B). Heating helped to promote reactions with the most reactive aryl halides (**R1-B1** through **R1B7**) with the most reactive amine being 2-morpholinoethan-1-amine, **R2-A6**; however, very high heating appeared

to promote product degradation. In most cases, higher reaction temperatures and longer reaction times did not promote product formation.

Table 3.2 Summary of Round 2. The bulk reaction results are reported for three different time points (1, 4, 15 hr). DESI experiments were averages of replicates that were done in two different days.

	DIPEA			NaO ^t Bu			TEA			No Base						
	DESI	Bulk			DESI	Bulk			DESI	Bulk			DESI	Bulk		
Time (h)		1	4	15		1	4	15		1	4	15		1	4	15
150 °C	4	8	9	6	4	8	7	7	7	11	11	9	3	11	9	6
200 °C	7	8	9	6	4	3	2	3	5	9	7	7	6	8	7	6

3.3.2 Correlation Between DESI and Bulk Reactions

Figure 3.4 depicts the product intensities in the heated bulk microtiter reactions of Round 1 as a function of product intensities obtained in DESI. This correlation plot gives a simple, yet effective visual interpretation of agreement between the droplet/thin film and bulk reactions. Although a comprehensive statistical correlation analysis is beyond the scope of this study, the threshold intensity moves the comparison back to the binary “yes”-“no” information space and splits the correlation plot into four quadrants. Q2 and Q3 are the regions of good agreement between droplet/thin film and bulk. The reactions in Q1 are positives in bulk and negative in droplet/thin film. In the context of droplet reaction-guided bulk reaction design, these reactions would have been missed although a false negative in the less sensitive DESI experiment is not a serious problem. Q4 points are positives in the droplet/thin film but negatives in the bulk experiment. This latter case is also misleading, since these positive droplet reactions outcomes do not translate as positives under bulk reaction conditions. This is a more serious problem although it only occurs in a small fraction of the reactions examined.

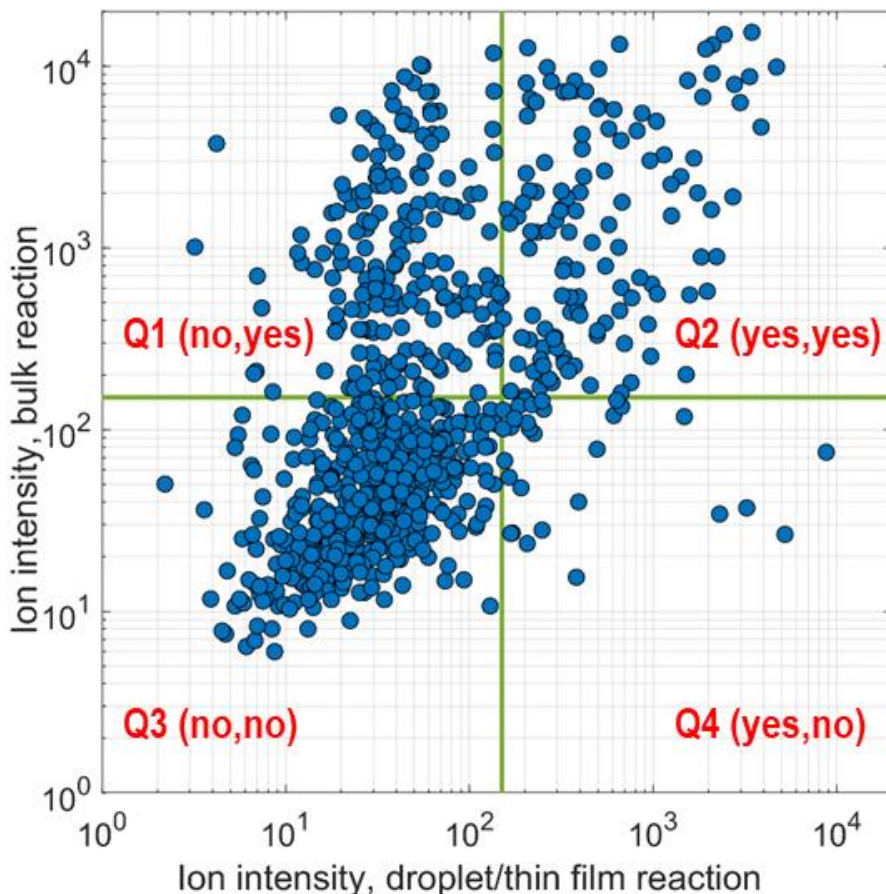


Figure 3.4 Correlation plot for the comparison of droplet/thin film and bulk data from 831 unique SNAr products in Round 1. Q1: 186 points; Q2: 124 points; Q3: 491 points; Q4: 30 points.

Round 2 containing bulk microtiter reaction data at two temperatures and three reaction times, permits a more detailed comparison of droplet/thin film and bulk reactions and sheds light on why there are reaction outcomes that appear in Q1 and Q4. For a bulk reaction, the reaction time and temperature are among the most important conditions; however, the droplet/thin film reaction format cannot reliably recapitulate these conditions. For example, reaction A (Figure 3.5) showed only positive hits at 150 °C, but only negatives at 200 °C, whereas the opposite behavior is observed in the case of Reaction B. Hence, in 50 % of these bulk reactions there is a discrepancy between the observed outcomes for droplet/thin film DESI and bulk microtiter reactions. Ideally, the optimum droplet/thin film and optimum bulk conditions should be comparable.

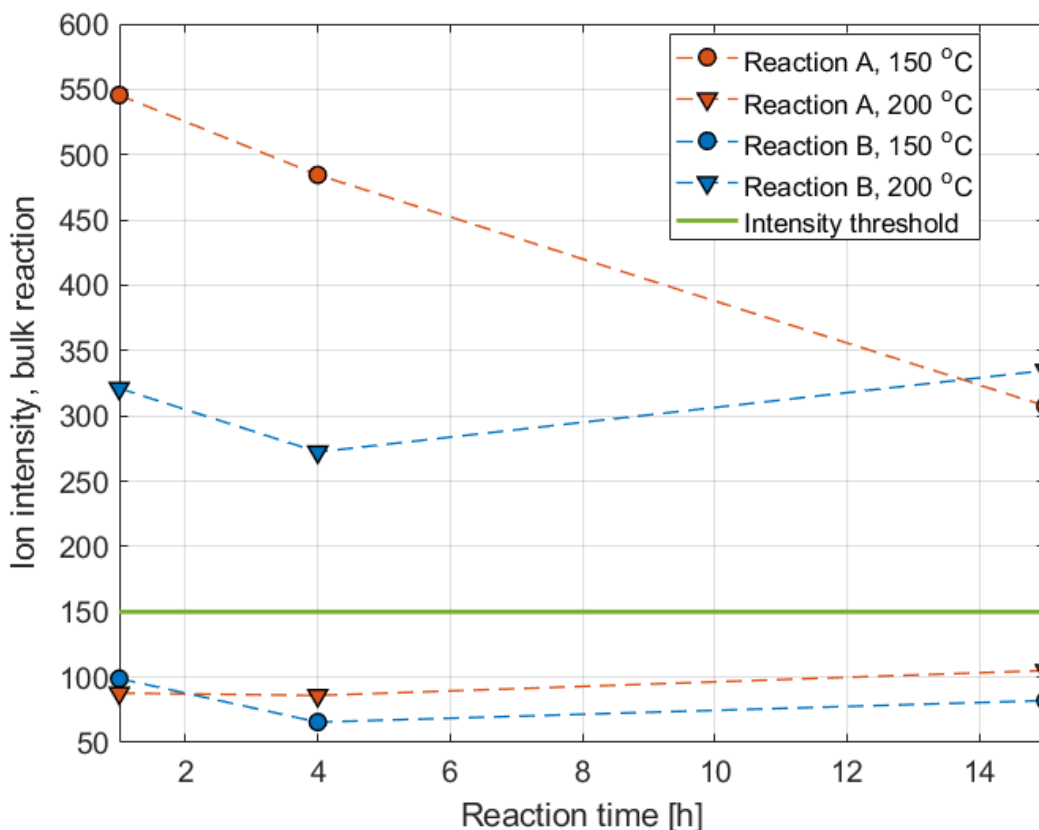


Figure 3.5 Two representative examples of heated bulk reaction outcomes showing the impact of thermal degradation (Reaction A: R2-A6 with R1-B12) and the positive effects of heating (Reaction B: R2-A6 with R1-B3). The dashed lines are only to guide the eye.

Reaction A is an example of thermal degradation: the reactions at 200 °C were all negatives and, although there are only positives at 150 °C, the product intensity decreases with time. Since this reaction was a “yes” in the droplet/thin film format, the thermal decomposition explains some of the false positives. In sharp contrast, reaction B showed positives at high temperature, and negatives at low temperature. The fact that this reaction was a “no” under droplet/thin film conditions suggests that the positive effect of heating cannot be predicted by accelerated reactions (one of the proposed mechanisms of reaction acceleration is the lowering of the activation energy barrier, which is a kinetic effect).³¹ We hypothesize that the high temperature shifted the chemical equilibrium towards product formation. The second SNAr dataset contains 13 such reactions (reactions with more “yes” outcomes at 200 °C than at 150 °C) that were all negatives under droplet/thin film conditions. Table 3.3 summarized the possible reasons for differences in the results from the droplet/thin film and bulk reactions.

Table 3.3 Possible reasons for discrepancy between droplet/thin film and bulk reaction observations.

Mechanism	From	To	Result
Thermal degradation in bulk	Q2	Q4	False positive
Incomplete bulk reaction (by reaction time or temperature)	Q2	Q4	False positive
Thermodynamic control in bulk	Q3	Q2	False negative

3.3.3 Microfluidic Evaluation

After identifying reaction hotspots from HTE, we sought to validate some of the good reaction conditions to build confidence in the high-throughput results. For all microfluidic reactions, the reactions were explored for 30 sec, 1 min, 3 min, and 5 min residence times at 100 °C and/or 150 °C using a 1:1 ratio of amines and aryl halides in NMP (Figure 3.6). DIPEA (2.5 equiv.) was used as base since it showed the most promising results for both Rounds 1 and 2. Reactions in 1,4-dioxane were not possible in flow due to the low solubility of the base, resulting in reactor clogging when this solvent was used.

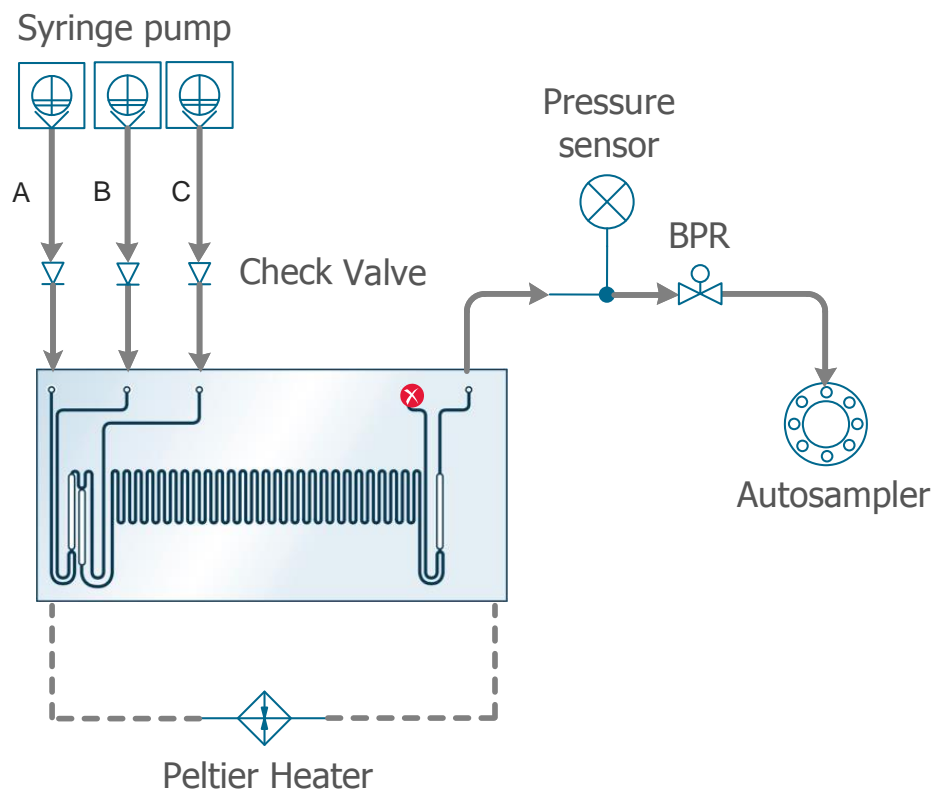
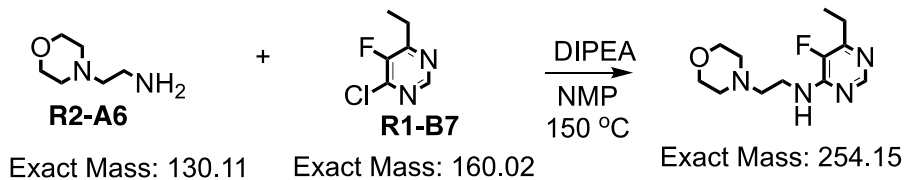
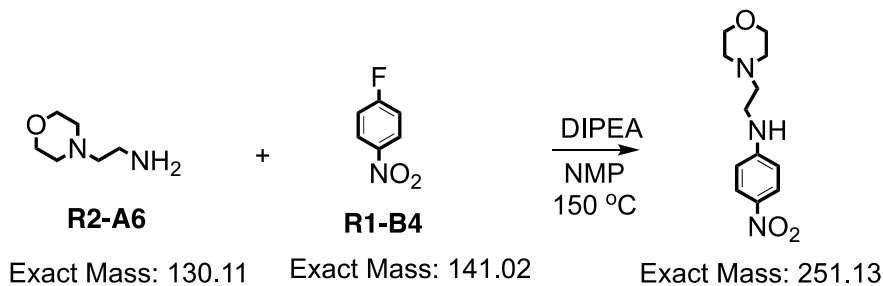
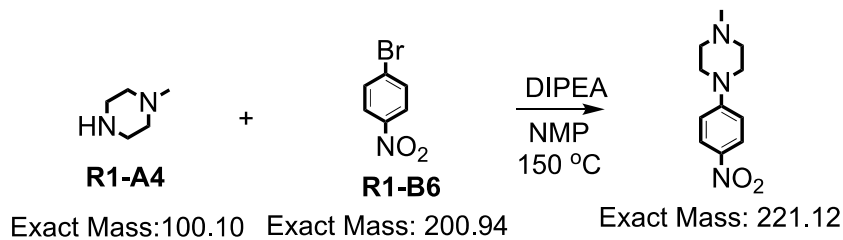
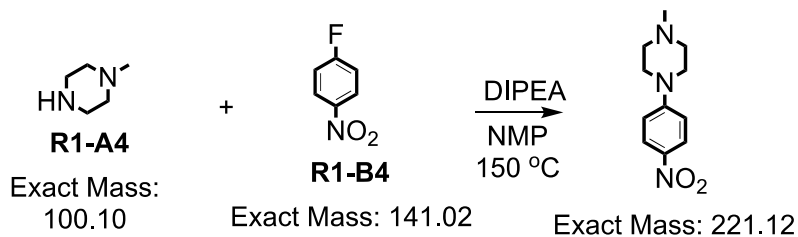
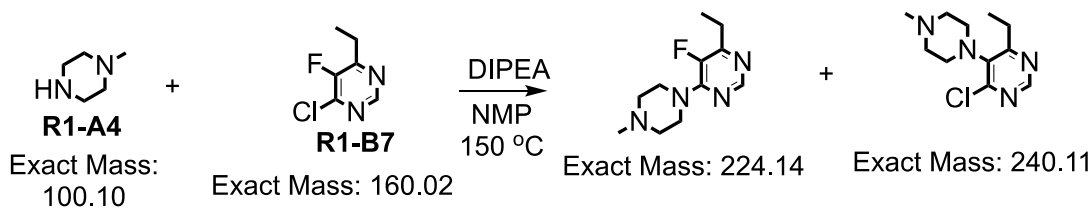
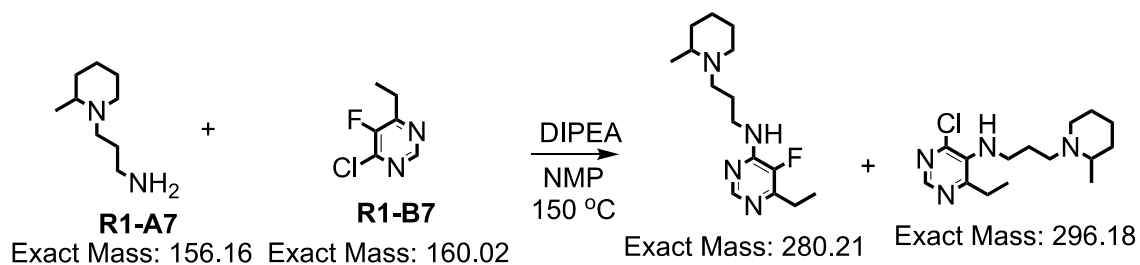


Figure 3.6 Continuous flow synthesis of SNAr reactions in a Chemtrix glass chip reactor, SOR 3225. A = amine; B=aryl halide; C = DIPEA.

Formation of the expected products in flow was confirmed by TLC and electrospray ionization-mass spectrometry (ESI-MS). We also found that the results of the microfluidic reactions were comparable to bulk and droplet screening experiments. Scheme 3.3 shows the ‘yes’ reactions that were conducted in flow, including amines with EWGs that were found to produce successful reactions. The reaction of 4-chloro-6-ethyl-5-fluoropyrimidine (**R1-B7**) with 3-(2-methylpiperidin-1-yl) propan-1-amine (**R1-A7**) and 1-methylpiperazine (**R1-A4**) always produced the chloride eliminated products. Since 1-Methyl-1H-imidazole (**R1-A2**) does not have a reactive amine site, it is not surprising that it did not participate in an SNAr reaction. It should be noted that there is a possibility of obtaining a false positive result in MS for the reaction between 1-methyl-1H-imidazole (**R1-A2**) and 4-bromo-N,N-diethylaniline (**R1-B11**) because the m/z of the aryl halide starting material isotopic ($M+2$) peak and the product ion m/z are same. Despite this, we were able to confirm that no product was formed from this reaction because the ratio of the bromine isotope peaks intensities always remained at 1:1. 2-Morpholinoethan-1-amine, **R2-A6**, was the only reactive amine in the Round 2 reaction set, and continuous flow experiments

confirmed this result (Figure 3.7). We also examined some negative outcomes identified by HTE and almost no product peak was found when those reaction conditions were evaluated under continuous flow (Scheme 3.4 and Figure 3.8).



Scheme 3.3 Microfluidic evaluation of select 'yes' reactions from the HTE study.

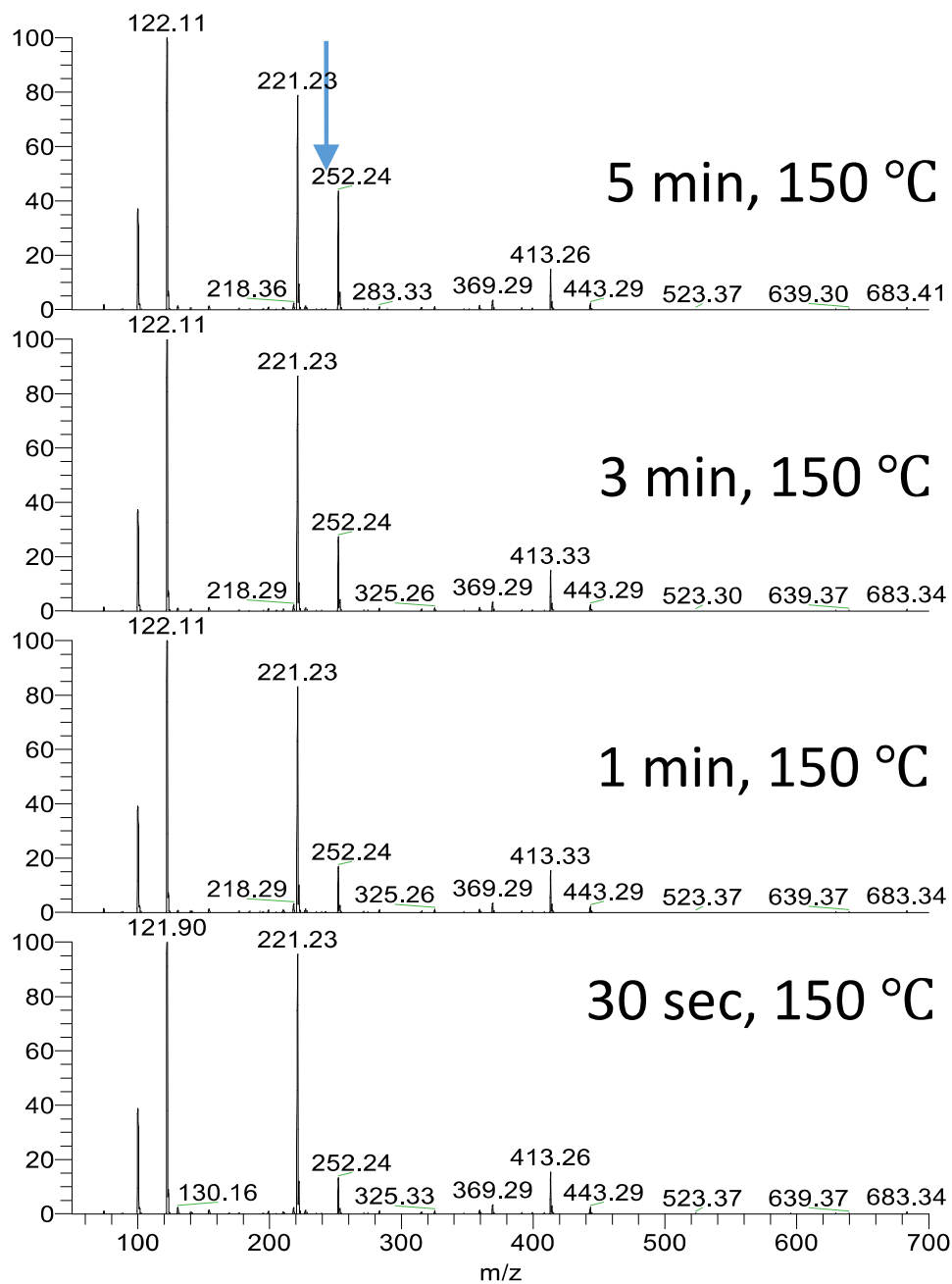
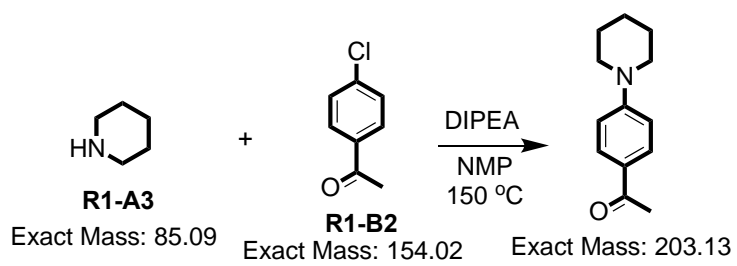
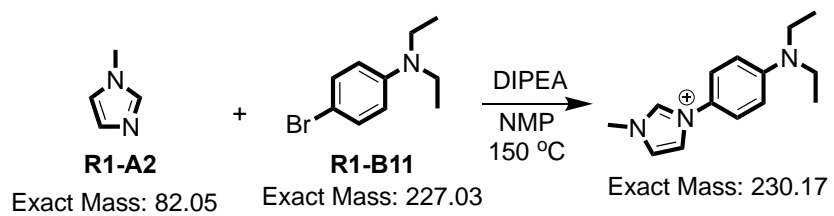


Figure 3.7 Full scan mass spectra from the continuous flow reactions between **R2-A6** and **R1-B4**. The blue arrow highlights the product peak at m/z 252. The peaks at m/z 100, 122, and 221 are the protonated, sodiated, and sodium bound dimer ions of the solvent NMP. The residence time and temperature of each reaction is listed on the corresponding spectrum.



Scheme 3.4 Microfluidic evaluation of some ‘no’ reactions from the HTE.

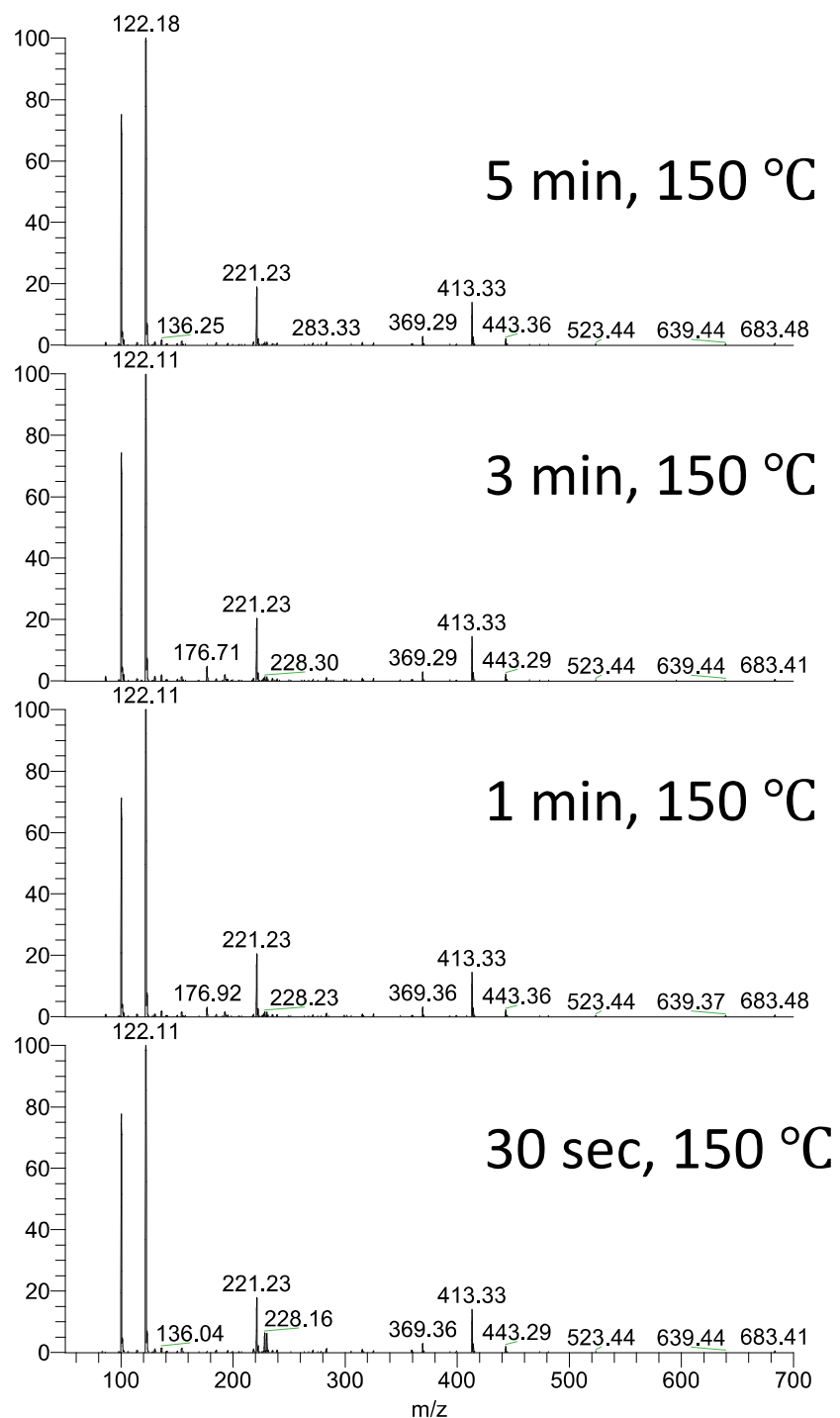


Figure 3.8 Full scan mass spectra from the continuous flow reactions between **R1-A3** and **R1-B2**. No peak is observed at m/z 204 indicating that no product was formed. The peaks at m/z 100, 122, and 221 are the protonated, sodiated, and sodium bound dimer ions of the solvent NMP. The residence time and temperature of each reaction is listed on the corresponding spectrum.

3.4 Conclusions

The power of HTE both in droplet/thin film and bulk microtiter reaction modes enables chemists to rapidly perform large arrays of rationally designed experiments. Moreover, it makes it possible to derive multidimensional hypotheses that can be explained from easily collected large data sets. This investigation led to a robotic HT technique to execute SNAr reactions in 96-well arrays which was coupled with a fast DESI-MS analysis that boosts the speed of the reaction optimization process. Extremely high throughputs can be achieved using DESI because both synthesis and analysis can occur simultaneously; however, we found that many reactions required incubation at elevated temperatures in order to observe product. Even with the added time of incubation, the analysis times reachable with DESI (~3.5 sec/sample) result in sample throughputs that far exceed traditional techniques. A total of sixteen amines and thirteen aryl halides were used for HTE evaluation. A total 1,536 unique reactions in droplet mode and 1,536 reactions in bulk were performed using four different bases in two different solvents, producing a total of 170 successful droplet reactions and 351 successful in bulk microtiter reactions. Expectations for the impact of electron donating and withdrawing substituents on SNAr reactions were also met in the HTE. A few of the successful reactions identified by HTE were evaluated under continuous flow conditions. Our findings showed that the positive conditions identified by HTE were true positives. Furthermore, the same was true for negative reaction conditions. Although many unsuccessful reaction conditions were identified by HTE, these negative results are valuable in that they can support machine learning efforts.⁵⁹⁻⁶⁰ Since negative data is rarely published, the resulting gaps in the data available impedes the progress of groups trying to develop machine learning algorithms that can predict the success or failure of organic reactions.

A rapid method of identifying SNAr reaction conditions that generate biologically important synthons is described. Our findings show that HTE can be used to rapidly identify the most important reaction parameters for faster optimization of microfluidic reactions while also eliminating wasted effort spent exploring failed reaction conditions. Increasing the number of successful reactions can also populate libraries with more compounds for physicochemical and biological evaluation. Further, applying this process to other common important classes of reactions, may accelerate library synthesis and the identification of optimal conditions for challenging substrates. This type of data could also be used to identify new reactions and patterns of the chemical reactivity, which may facilitate new synthetic pathways.

CHAPTER 4. HIGH THROUGHPUT SCREENING OF REDUCTIVE AMINATION REACTIONS USING DESORPTION ELECTROSPRAY IONIZATION (DESI-MS)

4.1 Introduction

Reductive amination is among the most widely used reactions by medicinal chemists in industry.³⁴ It is a method of introducing nitrogen into a molecule that offers superior control over alternative reactions, such as amine alkylation using alkyl halides, in which overalkylation is a common issue.⁶¹ The reaction involves the nucleophilic attack of an amine on an aldehyde or ketone forming an imine after dehydration. The imine (or iminium if protonated) is reduced by the reducing agent forming the product. Weakened reducing agents such as sodium cyanoborohydride (NaCNBH_3) or sodium triacetoxyborohydride ($\text{NaBH}(\text{OAc})_3$) are often used because they are strong enough to reduce the imine or iminium intermediate but not strong enough to reduce the aldehyde or ketone starting material. Reductive amination reactions can be carried out under a variety of conditions depending on what type of substrates are involved. The choice of reducing agent, solvent, stoichiometry, acid catalyst, and reaction time can all have a significant impact on the outcome of the reaction. This makes the reductive amination reaction an excellent candidate to study using high throughput experimentation (HTE).

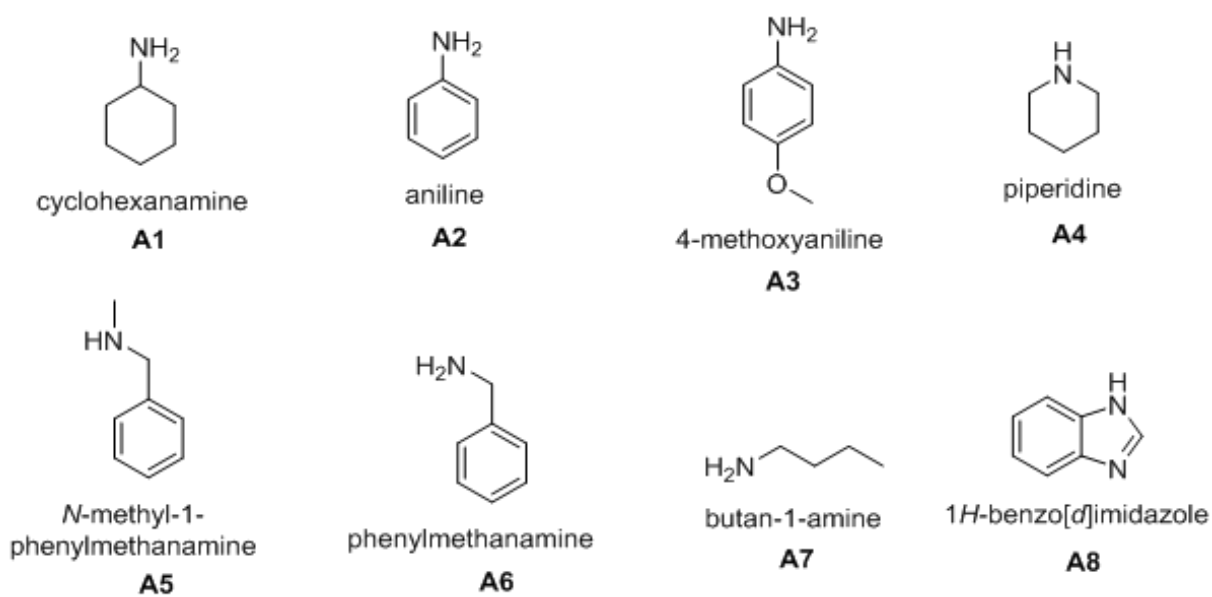
This study reports the screening of nearly 4,000 unique reductive amination reaction using a DESI-MS based, high-throughput reaction screening system. This system combines a liquid handling robot for fast reaction mixture preparation with DESI-MS for rapid analysis. The original concept of using DESI-MS for reaction screening was developed by our group¹³; however, other groups have since been inspired by our work and have implemented DESI-MS reaction screening in their labs.⁶² The purpose of this study is to demonstrate the extremely high throughputs that are capable with the latest generation of our system. Starting from commodity chemicals, we were able to screen 1,920 unique reactions in a single day. We evaluate the performance of 8 amines combined with 24 electrophiles (12 aldehydes and 12 ketones) under a variety of reaction conditions including different reducing agents (NaCNBH_3 , $\text{NaBH}(\text{OAc})_3$, and sodium borohydride (NaBH_4)), stoichiometries, reaction times, and the presence or absence of an acid catalyst.

4.2 Experimental

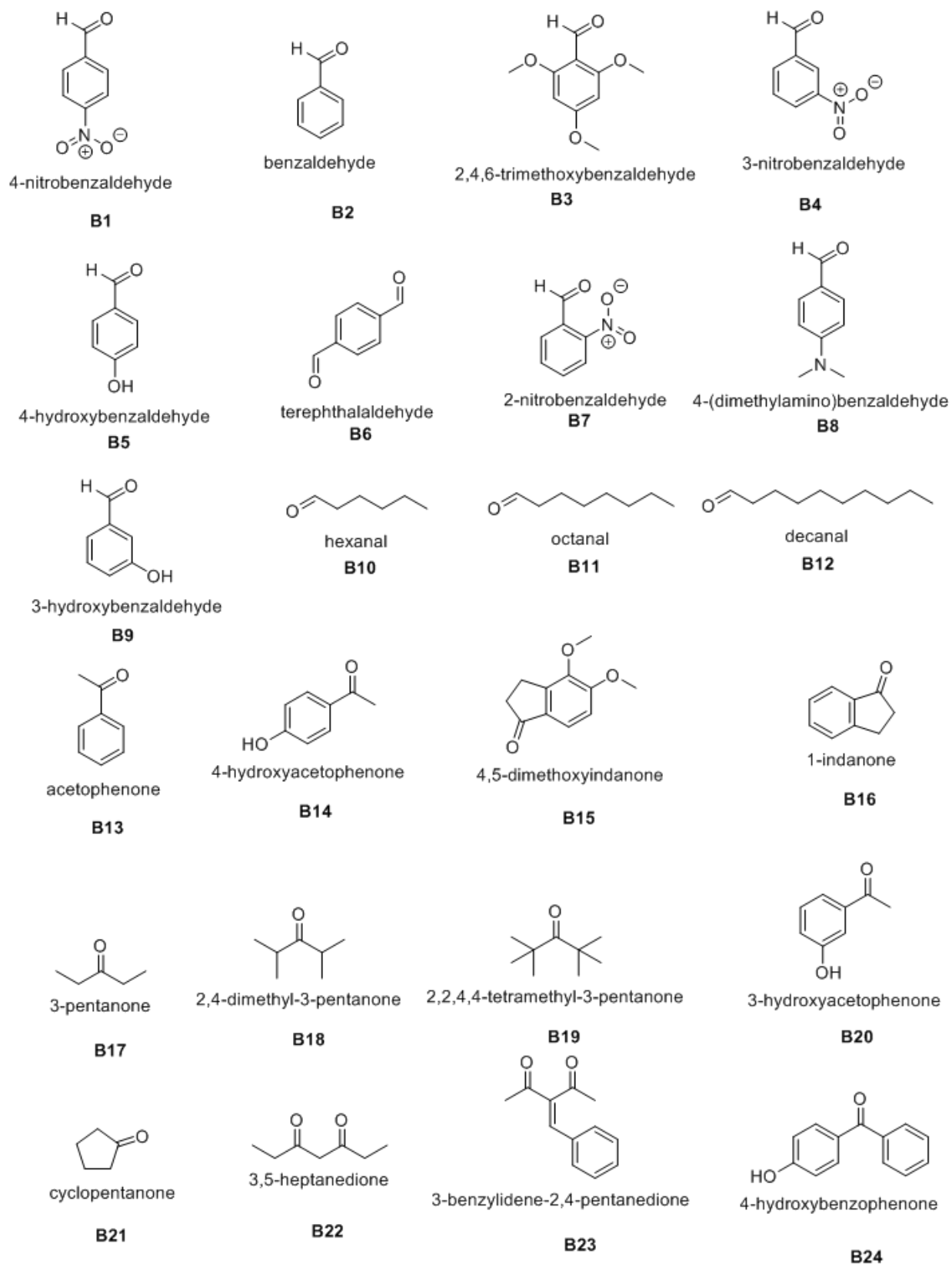
All chemicals and reagents were purchased from Sigma-Aldrich (St Louis, Missouri) and used without any purification.

4.2.1 Reaction Mixture Preparation

All reaction mixtures were prepared in 384 well microtiter plates (Analytical Sales & Services, max volume: 120 uL) using a Biomek i7 liquid handling robot (Beckman Coulter). Stock solutions of each amine (Scheme 4.1, 450 mM), electrophile (Scheme 4.2, 150 mM), NaBH_4 (150 mM), NaCNBH_3 (150 mM), $\text{NaBH}(\text{OAc})_3$ (225 mM), and acetic acid (500 mM) were prepared in methanol. The stock solutions were added to the 384 well plate using the pattern shown Figure 4.1. For the 3:1 (amine:electrophile) stoichiometry reactions, 30 uL of each amine stock solution was added to the appropriate wells. For the 1:1 stoichiometry reactions, 20 uL of methanol followed by 10 uL of each amine stock solution and was added the wells. Next, 30 uL of each electrophile stock solution was added to the plate. Using the 384 multichannel head of the Biomek i7, 30 uL of the reducing agent stock solution was added to all wells of the plate at once. Each reducing agent stock solution was prepared immediately before the addition step to reduce degradation. The plate was then mixed by aspirating and dispensing within the well plate several times, and then 45 uL of each well was transferred to a new 384 well plate. Using the 384 multichannel head of the Biomek i7, 5 uL of the acetic acid stock solution was added to this new plate.



Scheme 4.1 Amines used in the high throughput screening experiment.



Scheme 4.2 Electrophiles used in the high throughput screening experiment.

	1	2	3	4	5	6	7	8	9	10	11	12	13	14	15	16	17	18	19	20	21	22	23	24
A	A1																							
B	A2																							
C	A3																							
D	A4																							
E	A5																							
F	A6																							
G	A7																							
H	A8																							
I	A1																							
J	A2																							
K	A3																							
L	A4																							
M	A5																							
N	A6																							
O	A7																							
P	A8																							
	1	2	3	4	5	6	7	8	9	10	11	12	13	14	15	16	17	18	19	20	21	22	23	24
A	B1	B2	B3	B4	B5	B6	B7	B8	B9	B10	B11	B12	B13	B14	B15	B16	B17	B18	B19	B20	B21	B22	B23	B24
B	B1	B2	B3	B4	B5	B6	B7	B8	B9	B10	B11	B12	B13	B14	B15	B16	B17	B18	B19	B20	B21	B22	B23	B24
C	B1	B2	B3	B4	B5	B6	B7	B8	B9	B10	B11	B12	B13	B14	B15	B16	B17	B18	B19	B20	B21	B22	B23	B24
D	B1	B2	B3	B4	B5	B6	B7	B8	B9	B10	B11	B12	B13	B14	B15	B16	B17	B18	B19	B20	B21	B22	B23	B24
E	B1	B2	B3	B4	B5	B6	B7	B8	B9	B10	B11	B12	B13	B14	B15	B16	B17	B18	B19	B20	B21	B22	B23	B24
F	B1	B2	B3	B4	B5	B6	B7	B8	B9	B10	B11	B12	B13	B14	B15	B16	B17	B18	B19	B20	B21	B22	B23	B24
G	B1	B2	B3	B4	B5	B6	B7	B8	B9	B10	B11	B12	B13	B14	B15	B16	B17	B18	B19	B20	B21	B22	B23	B24
H	B1	B2	B3	B4	B5	B6	B7	B8	B9	B10	B11	B12	B13	B14	B15	B16	B17	B18	B19	B20	B21	B22	B23	B24
I	B1	B2	B3	B4	B5	B6	B7	B8	B9	B10	B11	B12	B13	B14	B15	B16	B17	B18	B19	B20	B21	B22	B23	B24
J	B1	B2	B3	B4	B5	B6	B7	B8	B9	B10	B11	B12	B13	B14	B15	B16	B17	B18	B19	B20	B21	B22	B23	B24
K	B1	B2	B3	B4	B5	B6	B7	B8	B9	B10	B11	B12	B13	B14	B15	B16	B17	B18	B19	B20	B21	B22	B23	B24
L	B1	B2	B3	B4	B5	B6	B7	B8	B9	B10	B11	B12	B13	B14	B15	B16	B17	B18	B19	B20	B21	B22	B23	B24
M	B1	B2	B3	B4	B5	B6	B7	B8	B9	B10	B11	B12	B13	B14	B15	B16	B17	B18	B19	B20	B21	B22	B23	B24
N	B1	B2	B3	B4	B5	B6	B7	B8	B9	B10	B11	B12	B13	B14	B15	B16	B17	B18	B19	B20	B21	B22	B23	B24
O	B1	B2	B3	B4	B5	B6	B7	B8	B9	B10	B11	B12	B13	B14	B15	B16	B17	B18	B19	B20	B21	B22	B23	B24
P	B1	B2	B3	B4	B5	B6	B7	B8	B9	B10	B11	B12	B13	B14	B15	B16	B17	B18	B19	B20	B21	B22	B23	B24
	1	2	3	4	5	6	7	8	9	10	11	12	13	14	15	16	17	18	19	20	21	22	23	24
A	3:1	3:1	3:1	3:1	3:1	3:1	3:1	3:1	3:1	3:1	3:1	3:1	3:1	3:1	3:1	3:1	3:1	3:1	3:1	3:1	3:1	3:1	3:1	
B	3:1	3:1	3:1	3:1	3:1	3:1	3:1	3:1	3:1	3:1	3:1	3:1	3:1	3:1	3:1	3:1	3:1	3:1	3:1	3:1	3:1	3:1	3:1	
C	3:1	3:1	3:1	3:1	3:1	3:1	3:1	3:1	3:1	3:1	3:1	3:1	3:1	3:1	3:1	3:1	3:1	3:1	3:1	3:1	3:1	3:1	3:1	
D	3:1	3:1	3:1	3:1	3:1	3:1	3:1	3:1	3:1	3:1	3:1	3:1	3:1	3:1	3:1	3:1	3:1	3:1	3:1	3:1	3:1	3:1	3:1	
E	3:1	3:1	3:1	3:1	3:1	3:1	3:1	3:1	3:1	3:1	3:1	3:1	3:1	3:1	3:1	3:1	3:1	3:1	3:1	3:1	3:1	3:1	3:1	
F	3:1	3:1	3:1	3:1	3:1	3:1	3:1	3:1	3:1	3:1	3:1	3:1	3:1	3:1	3:1	3:1	3:1	3:1	3:1	3:1	3:1	3:1	3:1	
G	3:1	3:1	3:1	3:1	3:1	3:1	3:1	3:1	3:1	3:1	3:1	3:1	3:1	3:1	3:1	3:1	3:1	3:1	3:1	3:1	3:1	3:1	3:1	
H	3:1	3:1	3:1	3:1	3:1	3:1	3:1	3:1	3:1	3:1	3:1	3:1	3:1	3:1	3:1	3:1	3:1	3:1	3:1	3:1	3:1	3:1	3:1	
I	1:1	1:1	1:1	1:1	1:1	1:1	1:1	1:1	1:1	1:1	1:1	1:1	1:1	1:1	1:1	1:1	1:1	1:1	1:1	1:1	1:1	1:1	1:1	
J	1:1	1:1	1:1	1:1	1:1	1:1	1:1	1:1	1:1	1:1	1:1	1:1	1:1	1:1	1:1	1:1	1:1	1:1	1:1	1:1	1:1	1:1	1:1	
K	1:1	1:1	1:1	1:1	1:1	1:1	1:1	1:1	1:1	1:1	1:1	1:1	1:1	1:1	1:1	1:1	1:1	1:1	1:1	1:1	1:1	1:1	1:1	
L	1:1	1:1	1:1	1:1	1:1	1:1	1:1	1:1	1:1	1:1	1:1	1:1	1:1	1:1	1:1	1:1	1:1	1:1	1:1	1:1	1:1	1:1	1:1	
M	1:1	1:1	1:1	1:1	1:1	1:1	1:1	1:1	1:1	1:1	1:1	1:1	1:1	1:1	1:1	1:1	1:1	1:1	1:1	1:1	1:1	1:1	1:1	
N	1:1	1:1	1:1	1:1	1:1	1:1	1:1	1:1	1:1	1:1	1:1	1:1	1:1	1:1	1:1	1:1	1:1	1:1	1:1	1:1	1:1	1:1	1:1	
O	1:1	1:1	1:1	1:1	1:1	1:1	1:1	1:1	1:1	1:1	1:1	1:1	1:1	1:1	1:1	1:1	1:1	1:1	1:1	1:1	1:1	1:1	1:1	
P	1:1	1:1	1:1	1:1	1:1	1:1	1:1	1:1	1:1	1:1	1:1	1:1	1:1	1:1	1:1	1:1	1:1	1:1	1:1	1:1	1:1	1:1	1:1	

Figure 4.1 Layout of the 384 well plate containing the reaction mixtures. The amines (top), electrophiles (middle), and stoichiometries (bottom) were arranged such that each well contains a unique combination of amine, electrophile, and stoichiometry.

After the plate preparation procedure described above, which takes a total of 30 min, two 384 well plates are generated. Each plate contains 384 unique reaction mixtures with a final concentration of 50 mM of each electrophile, 50 mM (1:1 stoichiometry) or 150 mM (3:1 stoichiometry) of each amine, and 50 mM (NaBH_4 and NaCNBH_3) or 75 mM ($\text{NaBH}(\text{OAc})_3$) for the reducing agent. The difference between the two plates is that one plate also contains one equivalent (50 mM) of acetic acid. This procedure was performed for each reducing agent generating a total of five 384 well plates (1,920 unique reactions). Only five well plates were generated because the addition of acetic acid was not tested for the NaCNBH_3 reactions for fear of releasing hydrogen cyanide.

After the pinning procedure, which is described below, each of the five 384 well plates was sealed with a foil seal (AlumaSeal II, EXCEL Scientific) and allowed to sit at room temperature for 42 hours. This was done to evaluate if additional reaction time would promote product formation for the slower reactions, particularly the ones involving the ketones. Counting reaction time as an additional variable, a total of ten unique 384 well plates (3,840 reactions) were evaluated in this study.

4.2.2 DESI Slide Preparation

To enable analysis by DESI, the reaction mixtures were transferred from the 384 well plate to a flat surface. This surface, called a DESI slide, consists of a PTFE membrane (Zitex G-115, Saint-Gobain Performance Plastics) which is glued to a glass support. The glass support is custom fabricated (Abrisa Technologies) to have the same footprint (5.030 in long, 3.365 in wide, 0.08 in thick) as a standard microtiter plate so that it can fit correctly on the deck of the Biomek i7.

The reaction mixtures were transferred from the 384 well plate to the DESI slide using a pin tool, which consists of an array of 384 stainless steel, slotted pins (FP3NS50, V & P Scientific) that are machined to retain 50 nL of liquid after being dipped into a solution. The pins ride in a fixture (AFIX384FP3, V & P Scientific) which attaches to the 384 multichannel head of the Biomek i7. The pins were dipped into the 384 well plate containing the reaction mixtures, which “aspirates” 50 nL of each reaction mixture, and then the pins are touched to the surface of the DESI slide transferring 50 nL of each reaction mixture to the surface. One transfer using the pin tool creates 384 reaction mixture “spots” on the DESI slide, each of which is approximately 1 mm in diameter. Additional transfers can be made to the same DESI slide by slightly offsetting the

location of the pins relative to the DESI slide during each transfer. In this study, each 384 well plate was pinned four times onto the DESI slide generating four replicate spots of each reaction mixture. An additional copy of each DESI slide was also made for MS/MS analysis.

4.2.3 DESI-MS Conditions

DESI-MS data was collected using a Prosolia DESI 2D stage connected to a Thermo LTQ XL mass spectrometer. The DESI solvent (0.1 % formic acid in methanol) was supplied at a flowrate of 2.75 uL/min, and nitrogen was used as the DESI nebulizing gas at a pressure of 150 psi. Full scan mass spectra were collected over the m/z range of 50-700 in positive ion mode with a spray voltage of 5 kV. The automatic gain control (AGC) of the LTQ XL was turned on with a maximum injection time of 250 ms.

The DESI stage and the mass spectrometer were controlled using a custom software suite called CHRIS (CHemical Reaction Integrated Screening). This software will be discussed in greater detail in a future publication, but briefly, it allows for spot-to-spot acquisition of the data rather than a traditional DESI imaging approach which acquires data from the entire surface of the DESI slide. With an analysis time of ~1 sec per spot, 384 reaction mixtures can be analyzed in under seven minutes. In this study, data was acquired from each of the four replicates of the 384 reaction mixtures and from 384 “blank” spots, which were areas of the DESI slide that did not contain any reaction mixtures. These blank spots were used during the data analysis to calculate signal to noise ratios. In total, 1,920 spots were analyzed per DESI slide resulting in an analysis time of 32 min per slide.

4.2.4 Dilution of the 384 well plates for LC-MS and Direct Injection

After the pinning procedure, each 384 well plate was diluted 1000x in preparation for the LC-MS and direct injection experiments described below. This dilution was performed using the Biomek i7. In the first step of the dilution, 2 uL of each reaction mixture was transferred to a second 384 well plate (Analytical Sales & Services, max volume: 225 uL) containing 178 uL of methanol. After mixing, 5 uL from the second plate was transferred to a final plate containing 50 uL of water. After mixing, the final plate was sealed with a pre-scored, silicone cap mat to prevent evaporation.

4.2.5 LC-MS Conditions

LC-MS data was collected using a Dionex UltiMate 3000 UHPLC system (WPS-3000 autosampler, HPG-3200SD binary pump, TCC-3000 column oven, and SRD-3200 degasser) connected to a Thermo TSQ Quantum Access Max mass spectrometer. The column used was an XBridge BEH C18 with a particle size of 2.5 μm , and the column was held at 45 °C throughout. Mobile phase A was 0.1% formic acid in water, and mobile phase B was acetonitrile. A flowrate of 1 mL/min was used throughout, and the gradient was as follows: 5% B at 0.0 min; linear transition to 95% B until 2.0 min; held at 95% B until 2.5 min; linear transition back to 5% B until 3.0 min; held at 5% B until 3.75 min for equilibration. The needle wash solution was methanol:water (1:1). An injection volume of 5 μL was used, and the injection to injection cycle time for each sample was 5.1 minutes.

Full scan mass spectra were collected over the m/z range of 50-700 in positive ion mode with a scan time of 0.200 s. The source conditions were as follows: spray voltage: 5 kV; vaporizer temperature: 500 °C; sheath gas pressure: 60 (arbitrary units); ion sweep gas pressure: 1.5 (arbitrary units); aux gas pressure: 20 (arbitrary units); capillary temperature: 250 °C.

4.2.6 Direct Injection Conditions

The direct injections were performed using a Dionex UltiMate WPS-3000 autosampler and ISO-3100SD isocratic pump connected to a Thermo TSQ Quantum Access Max mass spectrometer. A flowrate of 100 $\mu\text{L}/\text{min}$ of methanol was used to carry each injection (5 μL) directly to the mass spectrometer. The needle wash solution was methanol:water (1:1), and the injection to injection cycle time for each sample was 1.4 minutes.

Full scan mass spectra were collected over the m/z range of 50-700 in positive ion mode with a scan time of 0.500 s. The source conditions were as follows: spray voltage: 5 kV; vaporizer temperature: 150 °C; sheath gas pressure: 20 (arbitrary units); ion sweep gas pressure: 1.0 (arbitrary units); aux gas pressure: 5 (arbitrary units); capillary temperature: 250 °C.

4.2.7 DESI-MS/MS Data Acquisition

DESI-MS/MS data was acquired for all major products which had a signal to noise ratio of at least 3:1. This data was acquired from an identical copy of each DESI slide using the CHRIS

software suite. During the full scan data acquisition, the CHRIS software records the XY coordinates of each spot on the DESI slide. This allows the user to return to that same location on a copy of the original slide to acquire MS/MS data. A copy was used rather than returning to the original DESI slide because reaction products are removed by the DESI spray during the original acquisition leaving less material for MS/MS analysis. CHRIS software automatically loads the appropriate instrument method as it transitions from spot to spot based on a user provided a list of m/z values and their corresponding XY coordinates.

The MS/MS acquisition took approximately 30 s per spot because product ion scans were acquired at three different relative collision energies (20% first, then 10%, and finally 30%) in three consecutive 10 s long segments to get a broad view of the fragmentation behavior of each molecule. Except for the scan type, the DESI and mass spectrometric conditions used for the MS/MS acquisition were the same as those used for the full scan acquisition.

4.2.8 CHRIS Data Analysis

The output of each full scan DESI experiment was a single RAW file containing the data for all 1,920 spots (384x4 reaction spots and 384 blank spots). In order to correlate the mass spectra in each RAW file with the corresponding reaction information, the CHRIS data analysis software was used. This software takes two inputs: the raw data and a plate layout file. The plate layout file is an Excel file provided by the user which contains the 384 well plate layout (Figure 4.1), all m/z values of interest (starting materials, products, intermediates, by-products, etc.), and the positions on the DESI slide where the 384 well plate was pinned.

During the data acquisition, the CHRIS software records the start and stop times for the acquisition of each spot. This allows CHRIS to correlate the mass spectra in the RAW file with each spot on the DESI slide. Using the information in the plate layout file, CHRIS then correlates each spot with the corresponding reaction conditions and m/z values. The output of the CHRIS data analysis software is a set of csv files which contain the max and average intensity for each m/z value for each replicate spot of each unique reaction condition.

4.2.9 Custom Python Scripts for Data Processing

Several Python scripts were created for this study to expedite the processing, analysis, and visualization of the large quantity of data generated. These scripts are included in Appendix A. A brief description of each script is provided below.

m/z Value Calculation

The m/z values for each starting material and expected products, intermediates, and by-products were calculated using a Python script. The output of this script is a csv file which contains the expected m/z values for each unique combination of amine and electrophile. This csv file is accessed by other scripts when reagent names and/or m/z values are needed.

DESI Data Processing Script

A Python script was written to perform statistical calculations on the data from each DESI slide and to condense the information from all ten DESI slides into one csv file. For each m/z value monitored for each unique reaction, the script averages the four replicates, calculates the standard deviation and relative standard deviation, calculates the average noise based on the signal from the 384 blank spots on each DESI slide, and finally calculates the signal to noise ratio. The output of this script is a csv file which contains the data from all ten DESI experiment. This csv file is accessed by other scripts to create visualizations of the data.

LC-MS and Direct Injection Data Processing Script

Each 384 well plate analyzed by LC-MS or direct injection generated a list of 384 RAW files. Each RAW file was then converted to a text file using `msconvert` from ProteoWizard.¹⁷ A Python script was written to parse each of these text files and extract the retention time, peak height, and peak area for each m/z value. The output of this script is a series of csv files which contain this information for all ten 384 well plates that were analyzed by LC-MS and direct injection. The script works for either LC-MS or direct injection data. Only the input and output paths need to be changed to import the correct data and send the output to the appropriate folder.

MS/MS Data Processing Script

The output of the CHRIS MS/MS data acquisition software was a list of RAW files, one for each m/z value analyzed. Each RAW file contained three different segments, one for each relative collision energy used. Each RAW file was converted to a text file using `msconvert`, and a Python script was then used to parse each text file and average the scans corresponding to each relative collision energy. This output of this script is a list of figures, each of which contains three subplots showing the averaged spectra for each relative collision energy.

4.3 Results and Discussion

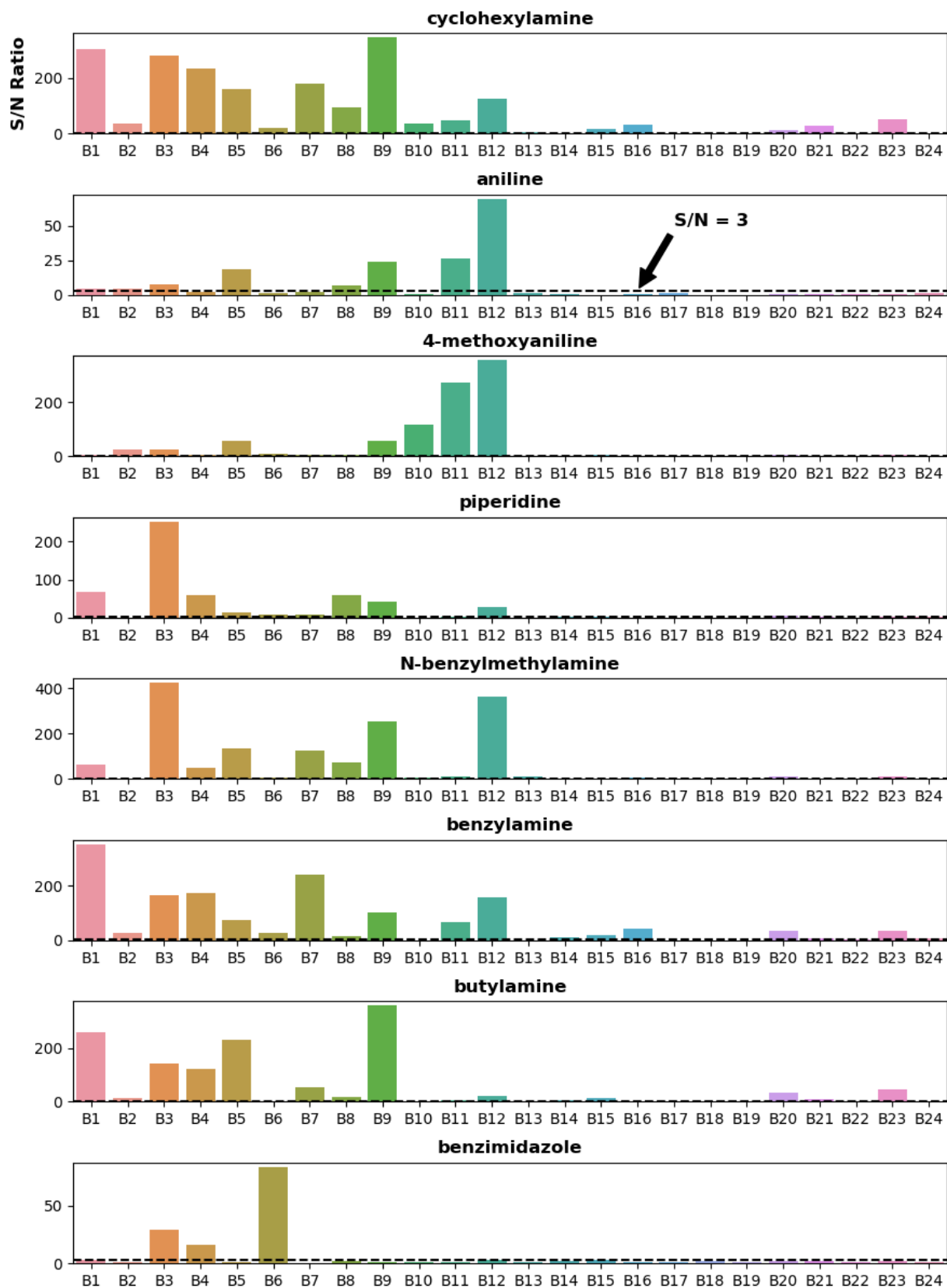
4.3.1 Amine and Electrophile Reactivity Trends

In total, 3,840 unique reactions were analyzed in this study. Figure 4.2 shows an overall summary of the DESI-MS results for these reactions broken down by amine and electrophile. The aliphatic primary amines (cyclohexylamine, benzylamine, and butylamine) have the highest number of successful reactions ($S/N > 3$) and in general higher signal to noise values indicating significant product formation. The aliphatic secondary amines (piperidine and *N*-benzylmethylamine) also have relatively high signal to noise values, but there are fewer successful reactions overall. The aromatic amines (aniline and 4-methoxyaniline) have few successful reactions and in general lower signal to noise values. Benzimidazole, an aromatic heterocycle, is the least reactive amine having the fewest number of successful reactions and low signal to noise values. These trends match the amine reactivity trends expected. In reductive amination reactions, aliphatic primary amines are the most reactive nucleophiles followed by aliphatic secondary amines with aromatic amines being the least reactive.

When examining the electrophile trends in Figure 4.2, one can immediately see that the aldehydes (B1-B12) produce many more successful reactions than the ketones (B13-B24). This is expected as aldehydes are much more electrophilic than ketones, which means that the formation of the imine intermediate (the rate limiting step) occurs much faster with aldehydes. Among the aldehydes, reagents with strong electron donating groups, such as 4-(dimethylamino)benzaldehyde (B8), have lower signal to noise ratios because the increased electron density at the aldehyde carbonyl discourages nucleophilic attack by the amine. On the contrary, aldehydes with strong

electron withdrawing groups, such 4-nitrobenzaldehyde (B1), which favor nucleophilic attack, have high signal to noise ratios.

Figure 4.2 The DESI-MS signal to noise ratio of the final, reduced product as a function of amine and electrophile. Each subplot represents a different amine, and the electrophiles (B1-B24) are represented on the x-axis. The dashed line represents a signal to noise of 3:1.



4.3.2 Effect of Reducing Agent, Reaction Time, Acid and Stoichiometry

Reductive amination reactions have several variables that can be adjusted which affect the outcome of the reaction. The variables explored in this study include the choice of reducing agent ($\text{NaBH}(\text{OAc})_3$, NaBH_4 , or NaCNBH_3), length of reaction time (0 or 42 hours), the presence or absence of a stoichiometric amount of acetic acid, and the stoichiometry of the amine.

Figure 4.3 shows how these variables impacted the number of successful reactions ($\text{S/N} > 3$) for the final, reduced product. NaCNBH_3 proved to be the least effective reducing agent for the aldehyde reactions but the most effective for the ketone reactions while NaBH_4 and $\text{NaBH}(\text{OAc})_3$ showed similar efficacy for both aldehydes and ketones. NaCNBH_3 and $\text{NaBH}(\text{OAc})_3$ are commonly used in reductive amination reactions because they are not strong enough to reduce the aldehyde or ketone starting material but are strong enough to reduce the much more electrophilic iminium intermediate. NaBH_4 is not commonly used in reductive amination reactions because it is strong enough to reduce the aldehyde or ketone starting material, which makes the fact that NaBH_4 and $\text{NaBH}(\text{OAc})_3$ showed similar efficacy surprising. This result highlights an advantage of high-throughput experimentation. Because the time and cost of running each individual reaction is reduced, unusual conditions, such as using NaBH_4 for reductive amination reactions, can be explored without wasting significant time or money.

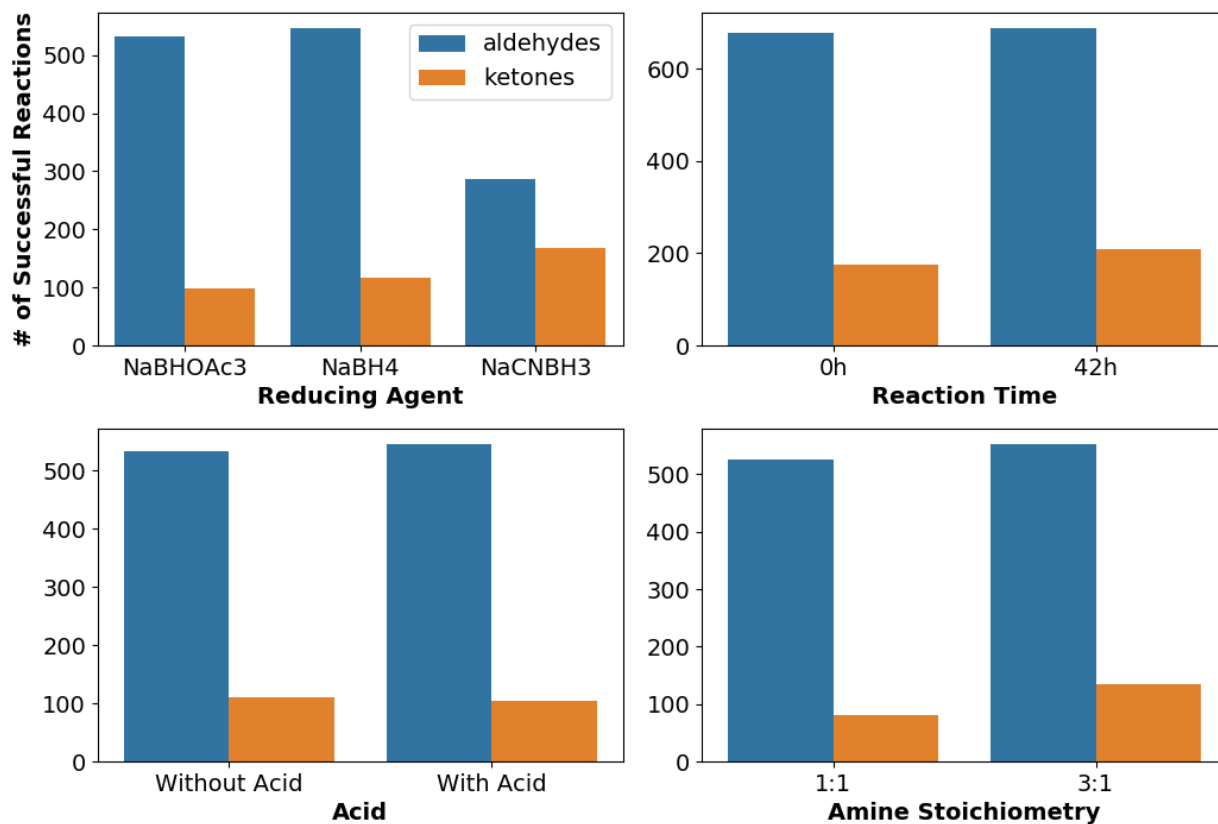


Figure 4.3 Effect of reducing agent, reaction time, addition of acetic acid, and stoichiometry on the number of successful reactions. A successful reaction is defined as having a signal to noise ration greater than 3:1 for the final, reduced product.

Increasing the reaction time to 42 hours resulted in a minor increase in the number of successful reactions for the ketones but made little difference in the aldehyde reactions. The aldehyde reactions are apparently fast enough to produce detectable amounts of product with no incubation period; however, one would expect that the increased reaction time would significantly increase the number of successful ketone reactions. Figure 4.4 shows that imine formation did increase significantly over time indicating that the increased reaction time did encourage imine formation. The lack of final, reduced product at 42 hours could be because the reaction mixtures were prepared in the open air. If enough water was present to degrade the reducing agent, there may not have been enough reducing agent left to reduce any imine intermediate that formed later in the course of the reaction.

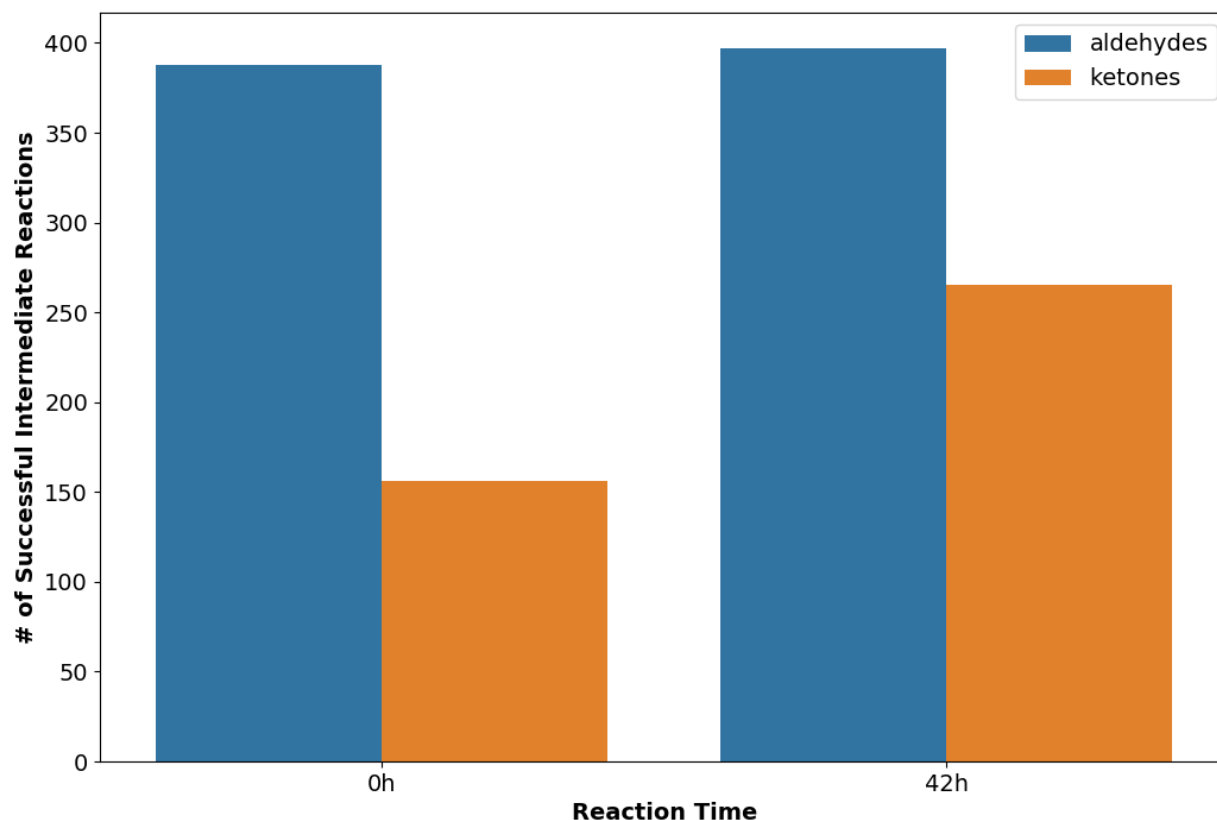


Figure 4.4 Effect of reaction time on the number of successful intermediate reactions. A successful intermediate reaction is defined as having a signal to noise ratio greater than 3:1 for the imine intermediate.

The presence or absence of acetic acid had little effect on the outcome of the reactions. The results of the NaCNBH_3 reactions are not factored into these numbers because there was no “With Acid” condition. Acid is not typically added to reductive amination reactions involving aldehydes because it could potentially accelerate the reduction of the aldehyde. Acetic acid is commonly added in a stoichiometric amount to reactions involving ketones when NaBH(OAc)_3 is used. The acid is added to accelerate the imine formation, which is slower with ketones. Since the presence of acid had no negative effect on the aldehyde reactions and no positive effect on the ketone reactions, perhaps the strength of the acid or the concentration used (1 equivalent) was insufficient.

Using a stoichiometry of 3:1 (amine:electrophile) vs. 1:1 resulted in a slight increase in the number of successful aldehyde reactions and a fairly significant increase in the number of successful ketone reactions. Reductive amination reactions are often carried out with an excess of the amine to favor the formation of the imine intermediate and to reduce by-product formation

(two additions of the electrophile to the amine). It appears that the slower ketone reactions did benefit from the favored imine formation provided by an excess of the amine.

4.3.3 Validation of DESI-MS Results with LC-MS and Direct Injection

Each of the ten 384 well plates was analyzed by DESI-MS, LC-MS and direct injection MS. The LC-MS and direct injection experiments were carried out in order to validate the results of the DESI-MS experiments. LC-MS is a technique that is used widely throughout industry to evaluate reaction mixtures. Direct injection is a simpler MS experiment where no chromatography is involved, so all of the reaction components are ionized together and appear in the same spectra, much like the DESI-MS spectra. The use of DESI-MS for reaction screening is a new concept developed by our group.¹⁴ If the results from more traditional techniques like LC-MS and direct injection correlate well with those from DESI-MS, it lends validity to the use of DESI-MS as tool for reaction screening.

Heat maps showing results from each of the three analytical techniques are shown in Figure 4.5. One can see that there is significant agreement among the experiments. All three techniques reveal that the ketones are much less reactive than the aldehydes. Aniline (A2), 4-methoxyaniline (A3), and benzimidazole (A8) are identified as being the least reactive amines, and 4-(dimethylamino)benzaldehyde (B8) is shown to be the least reactive aldehyde in all three experiments. The major difference among the three experiments is that LC-MS shows higher peak intensities for the products than DESI-MS or direct injection. This is expected as each component of the reaction is separated on the column prior to ionization in LC-MS. This results in less suppression of the product ionization by other components in the reaction mixture. DESI-MS and direct injection do not have any separation prior to ionization, so the product is subject to ion suppression.

Figure 4.5 Heat maps comparing the peak height of the final, reduced product analyzed by DESI-MS (Top), direct injection (Middle), and LC-MS (Bottom). Dark red indicates the areas of highest intensity, and dark blue indicates the areas of lowest intensity. This data was obtained from the NaBH₄, 0h, without acid 384 well plate.

4.3.4 Advantages of DESI-MS as a Reaction Screening Tool

The most obvious advantage that DESI-MS has as a reaction screening tool is its extremely short analysis time of 1 s per sample. Table 4.1 compares the time it takes to screen one 384 well plate of reaction mixtures using DESI-MS, direct injection, and LC-MS. A 384 well plate can be analyzed in 7 minutes using DESI-MS while the same plate takes 33 hours using LC-MS. This is based on an LC-MS cycle time of 5.1 minutes, which is relatively short compared to many gradients which often take 10 or 20 minutes. LC-MS cycle times can be shortened by using shorter columns with smaller particle sizes and higher flowrates, but even with a cycle time of 1.4 minutes, the same as that for direct injection, a 384 well plate still takes 9 hours to analyze.

Table 4.1 Comparison of the analysis time, solvent consumption, and sample consumption for each of the analysis techniques used in this study.

	Analysis Time (per 384 well plate)	Solvent Consumption (per 384 well plate)	Sample Consumption
DESI-MS	7 minutes	20 uL	50 nL
Direct Injection	9 hours	54 mL	2 uL
LC-MS	33 hours	2 L	2 uL

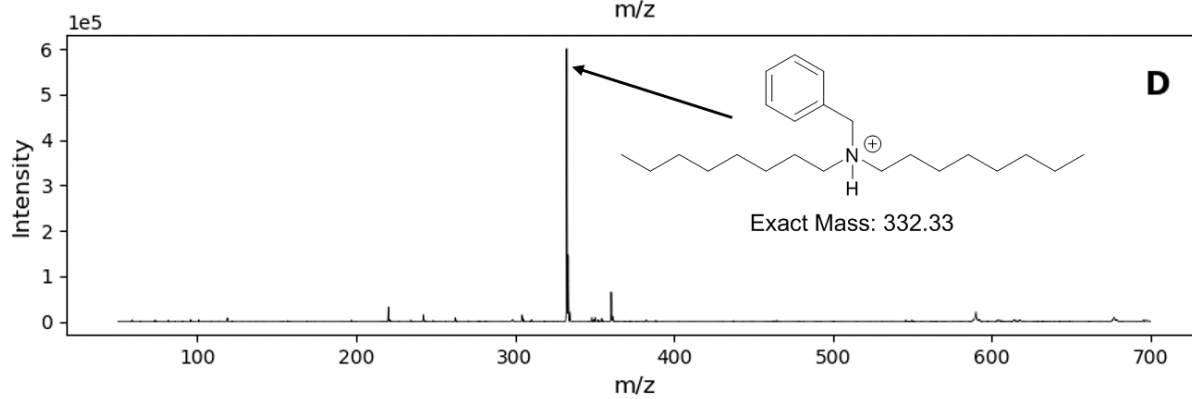
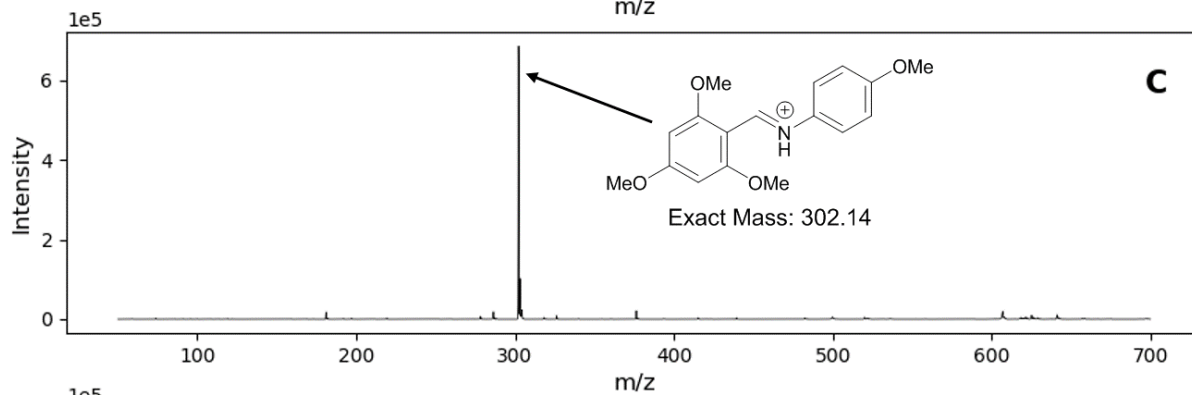
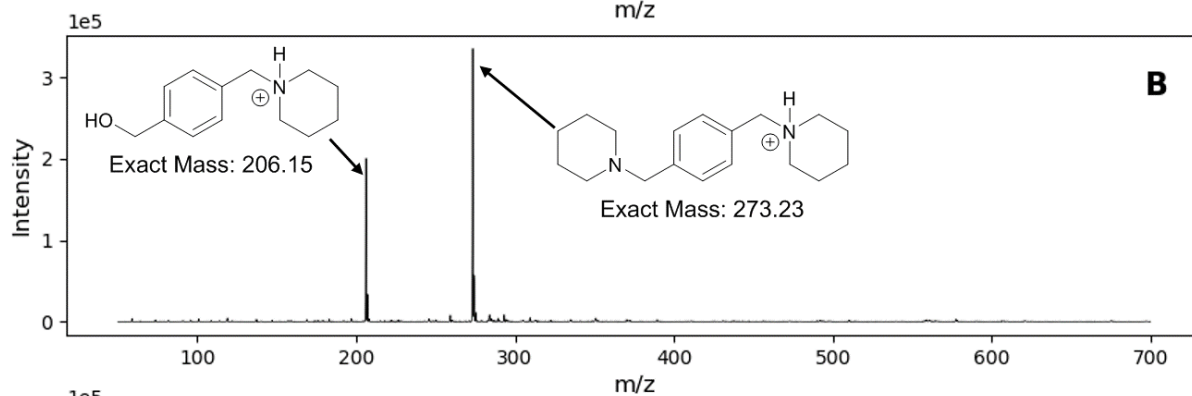
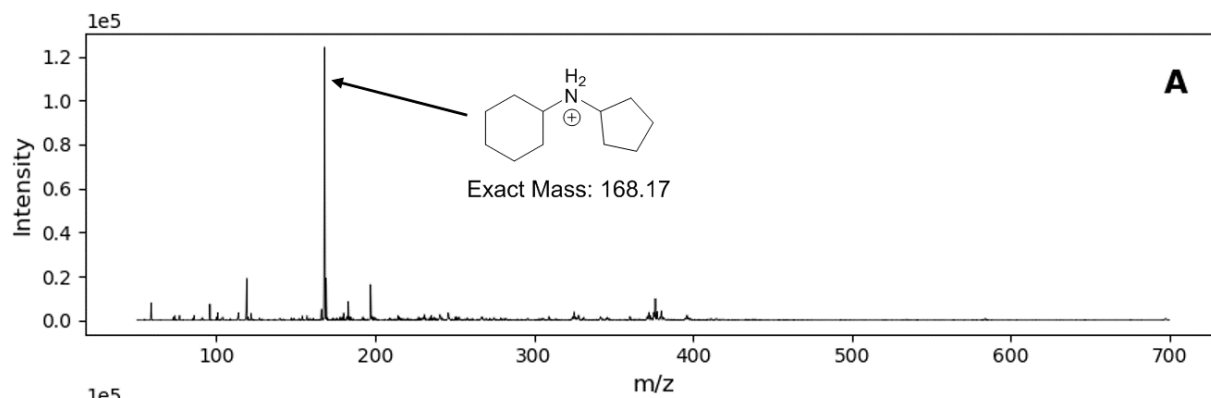
Table 4.1 also highlights the low solvent consumption of DESI-MS. Only 20 uL of DESI spray solvent are required to screen one 384 well plate. LC-MS requires 2 L of mobile phase (1 mL/min flowrate, 5.1 minute cycle time) to analyze the same plate. DESI-MS has a solvent consumption which is five orders of magnitude lower than LC-MS, which reduces costs and results in less chemical waste.

DESI-MS also has an advantage over LC-MS and direct injection in the amount of sample required. DESI-MS only requires 50 nL sample while in this experiment, LC-MS and direct injection required 2 uL. The reagents used in reaction screening are often very expensive and difficult to obtain in large amounts, so making reaction mixtures in small volumes lowers the costs associated with reaction screening. Since DESI-MS requires only 50 nL of sample, reaction mixtures can be made in extremely small volumes (<10 uL) while still being able to sample from them multiple times.

4.3.5 Example Mass Spectra

The desired product from reductive amination reactions is a single addition of the electrophile to the amine nucleophile; however, there are several common intermediates and by-products. Figure 4.6 contains mass spectra with examples of the various outcomes that were possible for the reactions in this study.

Figure 4.6 Example mass spectra from DESI-MS showing the various types of products, by-products, and intermediates monitored in this study. A) Reaction between **A1** and **B21** showing the final, reduced product. B) Reaction between **A4** and **B6** showing two additions of the amine to the dielectrophile as well as the reduced, single addition product. C) Reaction between **A3** and **B3** showing the imine intermediate. D) Reaction between **A6** and **B11** showing two additions of the electrophile to the amine.



4.3.6 Example MS/MS Spectra

MS/MS spectra were acquired for all products which had a signal to noise value greater than 3:1. An example MS/MS spectrum is shown in Figure 4.7. Little fragmentation is observed at normalized collision energies (NCE) of 10 and 20; however, at an NCE of 30, significant fragmentation is observed. The intensity is highest for the spectrum with an NCE of 20 because it was acquired first, followed by NCE 10 and finally and NCE 30. Material on the DESI slide is ablated away as the DESI spray passes over the spot, so the signal decreases over time. During MS/MS acquisition, the DESI spray rasters over the spot for 30 s to give enough time to acquire all three NCEs.

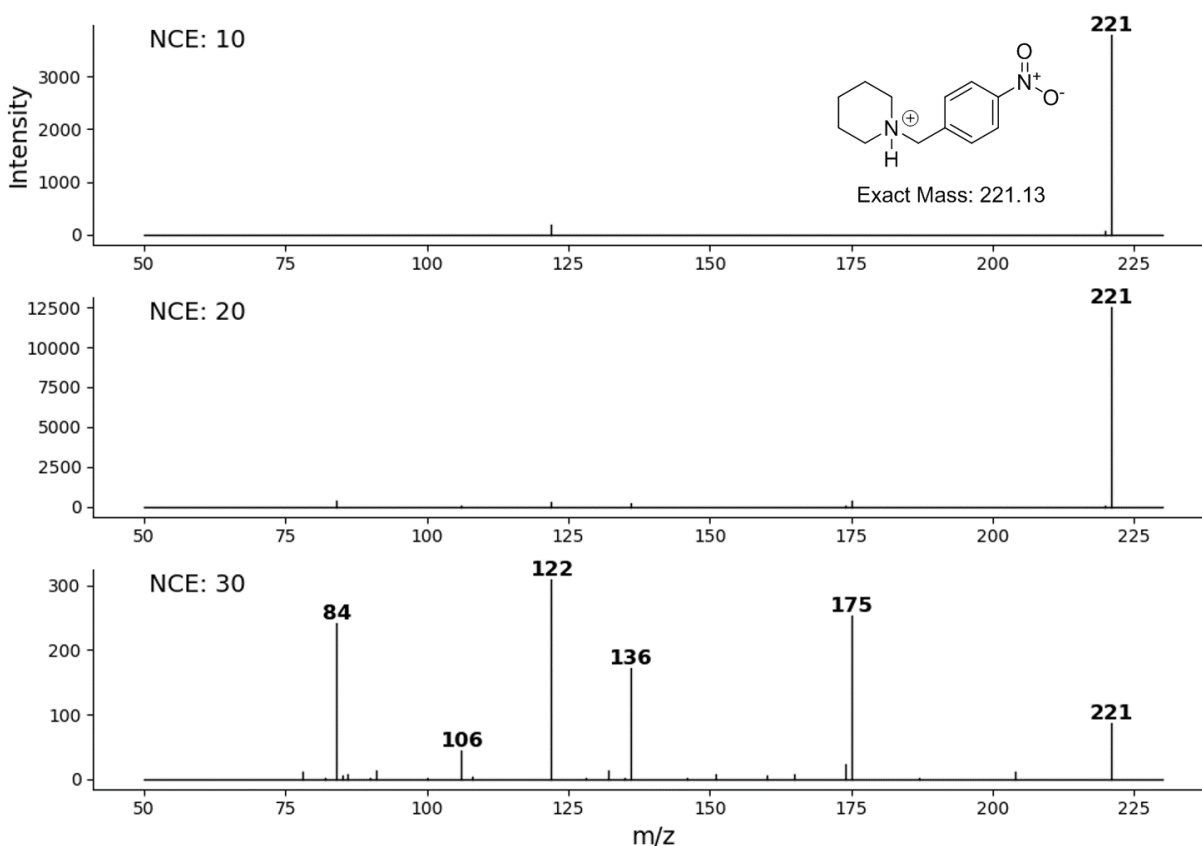


Figure 4.7 MS/MS spectra for the product of the reaction between **A4** and **B1**. The spectra were acquired at three different normalized collision energies (NCEs).

Figure 4.8 shows the interpreted spectrum for the product from Figure 4.7. MS/MS spectra were used to confirm the identity of the products, intermediates, and by-products monitored in this study.

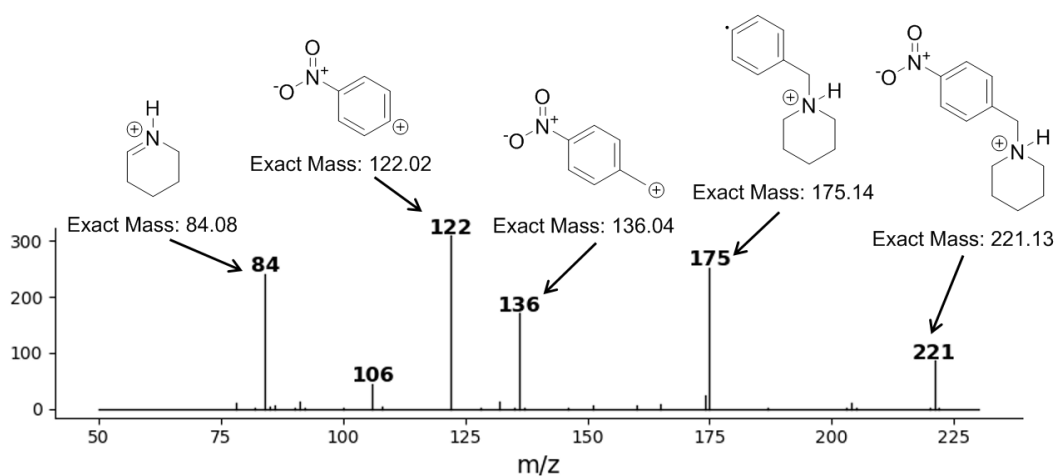


Figure 4.8 Interpreted MS/MS spectrum of the product of the reaction between **A4** and **B1**. This MS/MS spectrum is used to confirm the identity of the product.

4.4 Conclusions

In this study, a total of 3,840 unique reductive amination reactions were screened using a DESI-MS based high throughput reaction screening system. Using this system, 1,920 unique reactions were screened in a single day starting from commodity chemicals. Unusual reaction conditions were explored, such as using NaBH_4 as a reducing agent, which proved to be effective in producing product. HTE enables the evaluation of these high-risk reaction conditions because the costs associated with performing each individual reaction are significantly reduced. In addition to collecting DESI-MS data, all reactions were analyzed using traditional MS techniques such as LC-MS and direct injection. The results of the DESI-MS correlated well with the results from these more traditional techniques validating the effectiveness DESI-MS for reaction screening. MS/MS spectra were collected to confirm the identity of the peaks detected in the full scan spectra. A custom-built software suite was developed to control both the DESI stage and mass spectrometer allowing for the acquisition of both full scan and MS/MS data. This software also processes the raw data from each experiment and generates csv files from which the user can access the reaction data.

This system represents a breakthrough in organic reaction screening. With an analysis time of only 1 second per sample, a solvent consumption 20 μL per 384 well plate, and a sample consumption of only 50 nL , this system allows for the cost-effective screening of thousands of organic reactions per day.

APPENDIX A. CUSTOM PYTHON SCRIPTS

m/z Value Calculation Script

```
import pandas as pd
```

```
H = 1.0078
```

```
O = 15.9949
```

```
Na = 22.9898
```

```
amine_names = [  
    'cyclohexylamine',  
    'aniline',  
    '4-methoxyaniline',  
    'piperidine',  
    'N-benzylmethylamine',  
    'benzylamine',  
    'butylamine',  
    'benzimidazole'  
]
```

```
primary_amine_names = [  
    'cyclohexylamine',  
    'aniline',  
    '4-methoxyaniline',  
    'benzylamine',  
    'butylamine',  
]
```

```
amine_masses = [  
    99.1048,  
    93.0578,  
    123.0684,  
    85.0891,  
    121.0891,  
    107.0735,  
    73.0891,  
    118.0531  
]
```

```
primary_amine_masses = [  
    99.1048,  
    93.0578,  
    123.0684,  
    107.0735,  
]
```

```

73.0891,
]

aldehyde_names = [
    "4-nitrobenzaldehyde",
    "benzaldehyde",
    '2-4-6-trimethoxybenzaldehyde',
    "3-nitrobenzaldehyde",
    '4-hydroxybenzaldehyde',
    "terephthalaldehyde",
    "2-nitrobenzaldehyde",
    '4-(dimethylamino)benzaldehyde',
    '3-hydroxybenzaldehyde',
    'hexanal',
    'octanal',
    'decanal'
]

aldehyde_masses = [
    151.0269,
    106.0419,
    196.0736,
    151.0269,
    122.0368,
    134.0368,
    151.0269,
    149.0841,
    122.0368,
    100.0888,
    128.1201,
    156.1514
]

ketone_names = [
    'acetophenone',
    '4-hydroxyacetophenone',
    '4-5-dimethoxyindanone',
    '1-indanone',
    '3-pentanone',
    '2-4-dimethyl-3-pentanone',
    '2-2-4-4-tetramethyl-3-pentanone',
    '3-hydroxyacetophenone',
    'cyclopentanone',
    '3-5-heptanedione',
    '3-benzylidene-2-4-pentanedione',
    '4-hydroxybenzophenone'
]

```

```
]
```

```
ketone_masses = [  
    120.0575,  
    136.0524,  
    192.0786,  
    132.0575,  
    86.0732,  
    114.1045,  
    142.1358,  
    136.0524,  
    84.0575,  
    128.0837,  
    188.0837,  
    198.0681  
]
```

```
electrophile_names = aldehyde_names + ketone_names  
electrophile_masses = aldehyde_masses + ketone_masses  
column_names = ['amine m/z'] + electrophile_names  
row_names = ['electrophile m/z'] + amine_names  
df_products = pd.DataFrame(columns=column_names, index=row_names)
```

```
# calculations for amine starting material m/z values  
for i in range(len(amine_masses)):  
    sm_protonated = str(round(amine_masses[i] + H, 2))  
    sm_sodiated = str(round(amine_masses[i] + Na, 2))  
    df_products.loc[amine_names[i], 'amine m/z'] = sm_protonated + ',' + sm_sodiated
```

```
# calculations for electrophile starting material m/z values  
for i in range(len(electrophile_masses)):  
    sm_protonated = str(round(electrophile_masses[i] + H, 2))  
    sm_sodiated = str(round(electrophile_masses[i] + Na, 2))  
    sm_reduced_protonated = str(round(electrophile_masses[i] + H * 3, 2))  
    sm_reduced_sodiated = str(round(electrophile_masses[i] + H * 2 + Na, 2))  
    df_products.loc['electrophile m/z', electrophile_names[i]] = sm_protonated + ',' + sm_sodiated  
    + "," + sm_reduced_protonated + "," + sm_reduced_sodiated
```

```
# calculations for the protonated and sodiated products  
for i in range(len(amine_masses)):  
    for j in range(len(electrophile_masses)):  
        protonated = str(round(amine_masses[i] + electrophile_masses[j] - O + H, 2))  
        sodiated = str(round(amine_masses[i] + electrophile_masses[j] - O + Na, 2))  
        df_products.loc[amine_names[i], electrophile_names[j]] = protonated  
    # calculations for the double amine addition products for terephthalaldehyde, 3,5-  
    heptanedione, and 3-benzylidene-2,4-pentanedione
```

```

    if electrophile_names[j] == "terephthalaldehyde" or electrophile_names[j] == "3,5-
heptanedione" or electrophile_names[j] == '3-benzylidene-2,4-pentanedione':
        singly_charged = str(round(2 * amine_masses[i] + electrophile_masses[j] - 2 * O + H, 2))
        doubly_charged = str(round((2 * amine_masses[i] + electrophile_masses[j] - 2 * O + 2 *
H) / 2, 2))
        df_products.loc[amine_names[i], electrophile_names[j]] += "," + singly_charged + "," +
doubly_charged

# calculations for additional products
for i in range(len(electrophile_names)):
    for j in range(len(amine_names)):
        # imine intermediate
        im = str(round(amine_masses[j] + electrophile_masses[i] - O - H, 2))
        df_products.loc[amine_names[j], electrophile_names[i]] += "," + im
    for j in range(len(primary_amine_names)):
        # sodiated imine intermediate
        im_sodiated = str(round(primary_amine_masses[j] + electrophile_masses[i] - O - 2 * H + Na,
2))
        # double addition
        da = str(round(primary_amine_masses[j] + 2 * electrophile_masses[i] - 2 * O + H, 2))
        da_sodiated = str(round(primary_amine_masses[j] + 2 * electrophile_masses[i] - 2 * O + Na,
2))
        df_products.loc[primary_amine_names[j], electrophile_names[i]] += "," + im_sodiated + ","
+ da + "," + da_sodiated

df_products.to_csv("Reductive Amination/Reductive_Amination_Round_3_m-z_values.csv")

```

DESI Data Processing Script

```

import os
import pandas as pd
from RA_data_processing_functions import create_dataframe

path = "Reductive Amination/DESI/Data Folders/"
folders = [name for name in os.listdir(path)]
file_name_p = "/Products_intensities.csv"
file_name_sm = "/Starting_materials_intensities.csv"
df_mz_values = pd.read_csv("Reductive Amination/Reductive_Amination_Round_3_m-
z_values.csv", index_col=0)
pinning = "No ISTD"
df_list = []

for folder in folders:
    file_path_p = path + folder + file_name_p
    file_path_sm = path + folder + file_name_sm
    df_p = create_dataframe(file_path_p, pinning, df_mz_values, "p")

```

```

df_sm = create_dataframe(file_path_sm, pinning, df_mz_values, "sm")
df = pd.concat([df_p, df_sm])
df.drop(columns=["Pinning", "X", "Y", "Max", "Average"], inplace=True)
if "with_Acid" in folder:
    df["Acid"] = "With Acid"
else:
    df["Acid"] = "Without Acid"
if "NaBH4" in folder:
    df["RA"] = "NaBH4"
elif "NaCNBH3" in folder:
    df["RA"] = "NaCNBH3"
elif "NaBHOAc3" in folder:
    df["RA"] = "NaBHOAc3"
if "42h" in folder:
    df["Time"] = "42h"
else:
    df["Time"] = "0h"
columns = ["RA", "Time", "Acid"] + [col for col in df.columns.tolist() \
    if (col != "RA") and (col != "Time") and (col != "Acid")]
df = df[columns]
df_list.append(df)

```

```

df_all = pd.concat(df_list)
df_all.to_csv("Reductive Amination/DESI/RA_Round_3_Data_All.csv")

```

DESI Data Processing Script Functions

```

import numpy as np
import pandas as pd

```

```

def get_all_mz_values(df):
    mz_values = []
    for nucleophile in df.index:
        for electrophile in df.columns:
            if nucleophile == "electrophile m/z" and electrophile == "amine m/z":
                continue
            mz_list = df.loc[nucleophile, electrophile].split(",")
            for mz in mz_list:
                if float(mz) not in mz_values:
                    mz_values.append(float(mz))
    return mz_values

```

```

def get_noise(df, df_mz_values):
    mz_list_all = get_all_mz_values(df_mz_values)
    mz_list_all.sort()

```

```

df_blank = df[df["Pinning"] == "Blank"]

mz_list_blank = list(df_blank["m/z"].unique())
mz_list_blank.sort()

max_mean_list = []
max_median_list = []
average_mean_list = []
average_median_list = []
missing_mz_list = []

for mz in mz_list_all:
    if mz in mz_list_blank:
        df_blank_mz = df_blank[df_blank["m/z"] == mz]
        max_list = list(df_blank_mz["Max"])
        if len(max_list) < 384:
            difference = 384 - len(max_list)
            for i in range(difference):
                max_list.append(1)
            max_mean_list.append(np.mean(max_list))
            max_median_list.append(np.median(max_list))
            average_list = list(df_blank_mz["Average"])
            if len(average_list) < 384:
                difference = 384 - len(average_list)
                for i in range(difference):
                    average_list.append(1)
            average_mean_list.append(np.mean(average_list))
            average_median_list.append(np.median(average_list))
        else:
            missing_mz_list.append(mz)
            max_mean_list.append(1)
            max_median_list.append(1)
            average_mean_list.append(1)
            average_median_list.append(1)

noise = {}

for i in range(len(mz_list_all)):
    noise[mz_list_all[i]] = [
        max_mean_list[i],
        max_median_list[i],
        average_mean_list[i],
        average_median_list[i]
    ]

return noise

```

```

def calculate_values(df, mz, pinning, noise, product):
    df_mz_pinning = df[(df["m/z"] == mz) & (df["Pinning"] == pinning)]
    if not df_mz_pinning.empty:
        x_list = df_mz_pinning["X"].tolist()
        y_list = df_mz_pinning["Y"].tolist()
        new_row = df_mz_pinning.iloc[0].copy()
        new_row["Product"] = product
        for i in range(len(x_list)):
            new_row["X" + str(i + 1)] = x_list[i]
        for i in range(len(y_list)):
            new_row["Y" + str(i + 1)] = y_list[i]
        new_row["Noise Max"] = noise[mz][0]
        new_row["Noise Average"] = noise[mz][2]
        new_row[pinning + " Count"] = len(df_mz_pinning)
        new_row[pinning + " Max"] = df_mz_pinning["Max"].mean()
        new_row[pinning + " Max SD"] = df_mz_pinning["Max"].std()
        new_row[pinning + " Max RSD"] = df_mz_pinning["Max"].std() /
df_mz_pinning["Max"].mean() * 100
        new_row[pinning + " Average"] = df_mz_pinning["Average"].mean()
        new_row[pinning + " Average SD"] = df_mz_pinning["Average"].std()
        new_row[pinning + " Average RSD"] = df_mz_pinning["Average"].std() /
df_mz_pinning["Average"].mean() * 100
        new_row[pinning + " S/N Max"] = df_mz_pinning["Max"].mean() / noise[mz][0]
        new_row[pinning + " S/N Average"] = df_mz_pinning["Average"].mean() / noise[mz][2]
    else:
        # print(pinning + " " + str(mz) + " Empty Error")
        new_row = df.iloc[0].copy()
        new_row["Product"] = product
        new_row["m/z"] = mz
        new_row["Pinning"] = pinning
        new_row["Noise Max"] = noise[mz][0]
        new_row["Noise Average"] = noise[mz][2]
        new_row[pinning + " Count"] = 0
        new_row[pinning + " Max"] = 0
        new_row[pinning + " Max SD"] = 0
        new_row[pinning + " Max RSD"] = 0
        new_row[pinning + " Average"] = 0
        new_row[pinning + " Average SD"] = 0
        new_row[pinning + " Average RSD"] = 0
        new_row[pinning + " S/N Max"] = 0
        new_row[pinning + " S/N Average"] = 0
    new_df = new_row.to_frame().T
    return new_df

```

```

def create_dataframe(file_path, pinning, df_mz_values, sm_p):

```

```

df = pd.read_csv(file_path, sep="\t")

stoichiometries = df["Amine Stoichiometry"].unique().tolist()

noise = get_noise(df, df_mz_values)

rows_list = []

for nucleophile in df_mz_values.index[1:]:
    df_nucleophile = df[df["starting_materials"] == nucleophile]
    for electrophile in df_mz_values.columns[1:]:
        df_nucleophile_electrophile = df_nucleophile[df_nucleophile["starting_materials.1"] ==
electrophile]
        for sto in stoichiometries:
            df_nucleophile_electrophile_sto =
df_nucleophile_electrophile[df_nucleophile_electrophile["Amine Stoichiometry"] == sto]
            if sm_p == "sm":
                product_masses_str = df_mz_values.loc[nucleophile, "amine m/z"] + "," +
df_mz_values.loc["electrophile m/z", electrophile]
                # print(product_masses_str)
            elif sm_p == "p":
                product_masses_str = df_mz_values.loc[nucleophile, electrophile]
                product_masses = [float(x) for x in product_masses_str.split(",")]
                if sm_p == "p":
                    product_masses.sort()
                if not df_nucleophile_electrophile_sto.empty:
                    if len(product_masses) == 3:
                        new_row = calculate_values(df_nucleophile_electrophile_sto, product_masses[0],
pinning, noise, "Intermediate Protonated")
                        rows_list.append(new_row)
                        new_row = calculate_values(df_nucleophile_electrophile_sto, product_masses[1],
pinning, noise, "Protonated")
                        rows_list.append(new_row)
                        new_row = calculate_values(df_nucleophile_electrophile_sto, product_masses[2],
pinning, noise, "Sodiated")
                        rows_list.append(new_row)
                    elif len(product_masses) == 5:
                        new_row = calculate_values(df_nucleophile_electrophile_sto, product_masses[0],
pinning, noise, "Double Amine Addition 2+")
                        rows_list.append(new_row)
                        new_row = calculate_values(df_nucleophile_electrophile_sto, product_masses[1],
pinning, noise, "Intermediate Protonated")
                        rows_list.append(new_row)
                        new_row = calculate_values(df_nucleophile_electrophile_sto, product_masses[2],
pinning, noise, "Protonated")
                        rows_list.append(new_row)

```

```

        new_row = calculate_values(df_nucleophile_electrophile_sto, product_masses[3],
pinning, noise, "Sodiated")
        rows_list.append(new_row)
        new_row = calculate_values(df_nucleophile_electrophile_sto, product_masses[4],
pinning, noise, "Double Amine Addition 1+")
        rows_list.append(new_row)
        elif len(product_masses) == 6 and sm_p == "p":
            new_row = calculate_values(df_nucleophile_electrophile_sto, product_masses[0],
pinning, noise, "Intermediate Protonated")
            rows_list.append(new_row)
            new_row = calculate_values(df_nucleophile_electrophile_sto, product_masses[1],
pinning, noise, "Protonated")
            rows_list.append(new_row)
            new_row = calculate_values(df_nucleophile_electrophile_sto, product_masses[2],
pinning, noise, "Intermediate Sodiated")
            rows_list.append(new_row)
            new_row = calculate_values(df_nucleophile_electrophile_sto, product_masses[3],
pinning, noise, "Sodiated")
            rows_list.append(new_row)
            new_row = calculate_values(df_nucleophile_electrophile_sto, product_masses[4],
pinning, noise, "Double Electrophile Addition Protonated")
            rows_list.append(new_row)
            new_row = calculate_values(df_nucleophile_electrophile_sto, product_masses[5],
pinning, noise, "Double Electrophile Addition Sodiated")
            rows_list.append(new_row)
        elif len(product_masses) == 6 and sm_p == "sm":
            new_row = calculate_values(df_nucleophile_electrophile_sto, product_masses[0],
pinning, noise, "Amine Protonated")
            rows_list.append(new_row)
            new_row = calculate_values(df_nucleophile_electrophile_sto, product_masses[1],
pinning, noise, "Amine Sodiated")
            rows_list.append(new_row)
            new_row = calculate_values(df_nucleophile_electrophile_sto, product_masses[2],
pinning, noise, "Electrophile Protonated")
            rows_list.append(new_row)
            new_row = calculate_values(df_nucleophile_electrophile_sto, product_masses[3],
pinning, noise, "Electrophile Sodiated")
            rows_list.append(new_row)
            new_row = calculate_values(df_nucleophile_electrophile_sto, product_masses[4],
pinning, noise, "Reduced Electrophile Protonated")
            rows_list.append(new_row)
            new_row = calculate_values(df_nucleophile_electrophile_sto, product_masses[5],
pinning, noise, "Reduced Electrophile Sodiated")
            rows_list.append(new_row)
        elif len(product_masses) == 8:

```

```

        new_row = calculate_values(df_nucleophile_electrophile_sto, product_masses[0],
pinning, noise, "Double Amine Addition 2+")
        rows_list.append(new_row)
        new_row = calculate_values(df_nucleophile_electrophile_sto, product_masses[1],
pinning, noise, "Intermediate Protonated")
        rows_list.append(new_row)
        new_row = calculate_values(df_nucleophile_electrophile_sto, product_masses[2],
pinning, noise, "Protonated")
        rows_list.append(new_row)
        new_row = calculate_values(df_nucleophile_electrophile_sto, product_masses[3],
pinning, noise, "Intermediate Sodiated")
        rows_list.append(new_row)
        new_row = calculate_values(df_nucleophile_electrophile_sto, product_masses[4],
pinning, noise, "Sodiated")
        rows_list.append(new_row)
        new_row = calculate_values(df_nucleophile_electrophile_sto, product_masses[5],
pinning, noise, "Double Amine Addition 1+")
        rows_list.append(new_row)
        new_row = calculate_values(df_nucleophile_electrophile_sto, product_masses[6],
pinning, noise, "Double Electrophile Addition Protonated")
        rows_list.append(new_row)
        new_row = calculate_values(df_nucleophile_electrophile_sto, product_masses[7],
pinning, noise, "Double Electrophile Addition Sodiated")
        rows_list.append(new_row)
    else:
        print("Product Length Error")
        print(nucleophile)
        print(electrophile)
    else:
        print("Empty Frame Error")
        print(nucleophile)
        print(electrophile)
        print(sto)
new_df = pd.concat(rows_list, sort=False)
return new_df

```

LC-MS and Direct Injection Data Processing Script

```

import re
from pathlib import Path
import pandas as pd
import numpy as np
import os

def get_data(ion, m_z_list, intensity_list, retention_time):
    eic = []

```

```

low = ion - 0.5
high = ion + 0.5
for i in range(len(m_z_list)):
    hit_list = []
    for j in range(len(m_z_list[i])):
        if m_z_list[i][j] > low and m_z_list[i][j] < high:
            hit_list.append(intensity_list[i][j])
    if hit_list == []:
        eic.append(0.0)
    else:
        eic.append(max(hit_list))
height = max(eic)
RT = retention_time[eic.index(height)]
area = np.trapz(eic, retention_time)
return [RT, height, area]

```

```

path = "Reductive Amination/Flow Injection/Data Folders/"
folders = [name for name in os.listdir(path)]

```

```

for folder in folders:
    destdir = Path(path + folder)
    files = [p for p in destdir.iterdir() if p.is_file()]
    noise_destdir = Path(path + folder + "/Water Injections")
    noise_files = [p for p in noise_destdir.iterdir() if p.is_file()]

```

```

if len(files) != 384:
    print("Incorrect Number of Files!")
else:

```

```

    noise_data = { }
    for j in range(len(noise_files)):
        noise_m_z_list = []
        noise_intensity_list = []

```

```

    prevline = ""
    line_type = ""

```

```

    with noise_files[j].open() as f:
        for line in f:
            line = line.rstrip()

```

```

            if re.search("binary", line) and re.search("m/z array", prevline):
                m_z = [float(x) for x in line.split(" ")[12:]]
                noise_m_z_list.append(m_z)
                line_type = "m/z array"
            elif re.search("binary", line) and re.search("time array", prevline):
                noise_retention_time = [float(x) for x in line.split(" ")[12:]]

```

```

        line_type = "retention time array"

        if re.search("binary", line) and re.search("intensity array", prevline) and line_type ==
"m/z array":
            intensity = [float(x) for x in line.split(" ")[12:]]
            noise_intensity_list.append(intensity)

        prevline = line

        noise_data[j] = [noise_m_z_list, noise_intensity_list, noise_retention_time]

amine_names_unique = [
    'cyclohexylamine',
    'aniline',
    '4-methoxyaniline',
    'piperidine',
    'N-benzylmethylamine',
    'benzylamine',
    'butylamine',
    'benzimidazole',
    'cyclohexylamine 1:1',
    'aniline 1:1',
    '4-methoxyaniline 1:1',
    'piperidine 1:1',
    'N-benzylmethylamine 1:1',
    'benzylamine 1:1',
    'butylamine 1:1',
    'benzimidazole 1:1'
]

df = pd.read_csv("Reductive Amination/Reductive_Amination_Round_3_m-z_values.csv",
index_col=0)

electrophile_names = df.columns[1:]

reagent_names = []
for amine in amine_names_unique:
    for electrophile in electrophile_names:
        reagent_names.append([amine, electrophile])

df_amine_RT = pd.DataFrame(columns=electrophile_names, index=amine_names_unique)
df_amine_height = pd.DataFrame(columns=electrophile_names,
index=amine_names_unique)
df_amine_area = pd.DataFrame(columns=electrophile_names, index=amine_names_unique)
df_protonated_RT = pd.DataFrame(columns=electrophile_names,
index=amine_names_unique)

```

```

df_protonated_height = pd.DataFrame(columns=electrophile_names,
index=amine_names_unique)
df_protonated_area = pd.DataFrame(columns=electrophile_names,
index=amine_names_unique)
df_intermediate_RT = pd.DataFrame(columns=electrophile_names,
index=amine_names_unique)
df_intermediate_height = pd.DataFrame(columns=electrophile_names,
index=amine_names_unique)
df_intermediate_area = pd.DataFrame(columns=electrophile_names,
index=amine_names_unique)
df_protonated_yp_height = pd.DataFrame(columns=electrophile_names,
index=amine_names_unique)
df_protonated_yp_area = pd.DataFrame(columns=electrophile_names,
index=amine_names_unique)
df_intermediate_yp_height = pd.DataFrame(columns=electrophile_names,
index=amine_names_unique)
df_intermediate_yp_area = pd.DataFrame(columns=electrophile_names,
index=amine_names_unique)
df_amine_noise_RT = pd.DataFrame(columns=electrophile_names,
index=amine_names_unique)
df_amine_noise_height = pd.DataFrame(columns=electrophile_names,
index=amine_names_unique)
df_amine_noise_area = pd.DataFrame(columns=electrophile_names,
index=amine_names_unique)
df_protonated_noise_RT = pd.DataFrame(columns=electrophile_names,
index=amine_names_unique)
df_protonated_noise_height = pd.DataFrame(columns=electrophile_names,
index=amine_names_unique)
df_protonated_noise_area = pd.DataFrame(columns=electrophile_names,
index=amine_names_unique)
df_intermediate_noise_RT = pd.DataFrame(columns=electrophile_names,
index=amine_names_unique)
df_intermediate_noise_height = pd.DataFrame(columns=electrophile_names,
index=amine_names_unique)
df_intermediate_noise_area = pd.DataFrame(columns=electrophile_names,
index=amine_names_unique)
df_amine_SN_height = pd.DataFrame(columns=electrophile_names,
index=amine_names_unique)
df_amine_SN_area = pd.DataFrame(columns=electrophile_names,
index=amine_names_unique)
df_protonated_SN_height = pd.DataFrame(columns=electrophile_names,
index=amine_names_unique)
df_protonated_SN_area = pd.DataFrame(columns=electrophile_names,
index=amine_names_unique)
df_intermediate_SN_height = pd.DataFrame(columns=electrophile_names,
index=amine_names_unique)

```

```
df_intermediate_SN_area = pd.DataFrame(columns=electrophile_names,  
index=amine_names_unique)
```

```
for i in range(len(files)):  
    if i < 192:  
        A = reagent_names[i][0]  
    else:  
        A = reagent_names[i][0][:-4]  
  
    amine_mz = float(df.loc[A, "amine m/z"].split(",")[0])  
    product_mz_list = df.loc[A, reagent_names[i][1]].split(",")  
    product_mz_list.sort()  
  
    if len(product_mz_list) == 3:  
        intermediate_mz = float(product_mz_list[0])  
        protonated_mz = float(product_mz_list[1])  
    elif len(product_mz_list) == 5:  
        intermediate_mz = float(product_mz_list[1])  
        protonated_mz = float(product_mz_list[2])  
    elif len(product_mz_list) == 6:  
        intermediate_mz = float(product_mz_list[0])  
        protonated_mz = float(product_mz_list[1])  
    elif len(product_mz_list) == 8:  
        intermediate_mz = float(product_mz_list[1])  
        protonated_mz = float(product_mz_list[2])  
  
    m_z_list = []  
    intensity_list = []  
  
    prevline = ""  
    line_type = ""  
  
    with files[i].open() as f:  
        for line in f:  
            line = line.rstrip()  
  
            if re.search("binary", line) and re.search("m/z array", prevline):  
                m_z = [float(x) for x in line.split(" ")[12:]]  
                m_z_list.append(m_z)  
                line_type = "m/z array"  
            elif re.search("binary", line) and re.search("time array", prevline):  
                retention_time = [float(x) for x in line.split(" ")[12:]]  
                line_type = "retention time array"
```

```

        if re.search("binary", line) and re.search("intensity array", prevline) and line_type ==
"m/z array":
            intensity = [float(x) for x in line.split(" ")[12:]]
            intensity_list.append(intensity)

        prevline = line

        amine_data = get_data(amine_mz, m_z_list, intensity_list, retention_time)
        protonated_data = get_data(protonated_mz, m_z_list, intensity_list, retention_time)
        intermediate_data = get_data(intermediate_mz, m_z_list, intensity_list, retention_time)

        amine_noise_data = []
        for key in noise_data:
            amine_noise_data.append(get_data(amine_mz, noise_data[key][0], noise_data[key][1],
noise_data[key][2]))
        protonated_noise_data = []
        for key in noise_data:
            protonated_noise_data.append(get_data(protonated_mz, noise_data[key][0],
noise_data[key][1], noise_data[key][2]))
        intermediate_noise_data = []
        for key in noise_data:
            intermediate_noise_data.append(get_data(intermediate_mz, noise_data[key][0],
noise_data[key][1], noise_data[key][2]))

        amine_noise_average_RT = np.mean(amine_noise_data, axis=0)[0]
        amine_noise_average_height = np.mean(amine_noise_data, axis=0)[1]
        amine_noise_average_area = np.mean(amine_noise_data, axis=0)[2]
        protonated_noise_average_RT = np.mean(protonated_noise_data, axis=0)[0]
        protonated_noise_average_height = np.mean(protonated_noise_data, axis=0)[1]
        protonated_noise_average_area = np.mean(protonated_noise_data, axis=0)[2]
        intermediate_noise_average_RT = np.mean(intermediate_noise_data, axis=0)[0]
        intermediate_noise_average_height = np.mean(intermediate_noise_data, axis=0)[1]
        intermediate_noise_average_area = np.mean(intermediate_noise_data, axis=0)[2]

        df_amine_noise_RT.loc[reagent_names[i][0], reagent_names[i][1]] =
amine_noise_average_RT
        df_amine_noise_height.loc[reagent_names[i][0], reagent_names[i][1]] =
amine_noise_average_height
        df_amine_noise_area.loc[reagent_names[i][0], reagent_names[i][1]] =
amine_noise_average_area
        df_protonated_noise_RT.loc[reagent_names[i][0], reagent_names[i][1]] =
protonated_noise_average_RT
        df_protonated_noise_height.loc[reagent_names[i][0], reagent_names[i][1]] =
protonated_noise_average_height
        df_protonated_noise_area.loc[reagent_names[i][0], reagent_names[i][1]] =
protonated_noise_average_area

```

```

df_intermediate_noise_RT.loc[reagent_names[i][0], reagent_names[i][1]] =
intermediate_noise_average_RT
df_intermediate_noise_height.loc[reagent_names[i][0], reagent_names[i][1]] =
intermediate_noise_average_height
df_intermediate_noise_area.loc[reagent_names[i][0], reagent_names[i][1]] =
intermediate_noise_average_area

```

```

df_amine_RT.loc[reagent_names[i][0], reagent_names[i][1]] = amine_data[0]
df_amine_height.loc[reagent_names[i][0], reagent_names[i][1]] = amine_data[1]
df_amine_area.loc[reagent_names[i][0], reagent_names[i][1]] = amine_data[2]
df_protonated_RT.loc[reagent_names[i][0], reagent_names[i][1]] = protonated_data[0]
df_protonated_height.loc[reagent_names[i][0], reagent_names[i][1]] = protonated_data[1]
df_protonated_area.loc[reagent_names[i][0], reagent_names[i][1]] = protonated_data[2]
df_intermediate_RT.loc[reagent_names[i][0], reagent_names[i][1]] =
intermediate_data[0]
df_intermediate_height.loc[reagent_names[i][0], reagent_names[i][1]] =
intermediate_data[1]
df_intermediate_area.loc[reagent_names[i][0], reagent_names[i][1]] =
intermediate_data[2]
df_protonated_yp_height.loc[reagent_names[i][0], reagent_names[i][1]] =
protonated_data[1] / (protonated_data[1] + amine_data[1])
df_protonated_yp_area.loc[reagent_names[i][0], reagent_names[i][1]] =
protonated_data[2] / (protonated_data[2] + amine_data[2])
df_intermediate_yp_height.loc[reagent_names[i][0], reagent_names[i][1]] =
intermediate_data[1] / (intermediate_data[1] + amine_data[1])
df_intermediate_yp_area.loc[reagent_names[i][0], reagent_names[i][1]] =
intermediate_data[2] / (intermediate_data[2] + amine_data[2])

```

```

df_amine_SN_height.loc[reagent_names[i][0], reagent_names[i][1]] = amine_data[1] /
amine_noise_average_height
df_amine_SN_area.loc[reagent_names[i][0], reagent_names[i][1]] = amine_data[2] /
amine_noise_average_area
df_protonated_SN_height.loc[reagent_names[i][0], reagent_names[i][1]] =
protonated_data[1] / protonated_noise_average_height
df_protonated_SN_area.loc[reagent_names[i][0], reagent_names[i][1]] =
protonated_data[2] / protonated_noise_average_area
df_intermediate_SN_height.loc[reagent_names[i][0], reagent_names[i][1]] =
intermediate_data[1] / intermediate_noise_average_height
df_intermediate_SN_area.loc[reagent_names[i][0], reagent_names[i][1]] =
intermediate_data[2] / intermediate_noise_average_area

```

if "NaBH4" in folder:

RA = "NaBH4"

elif "NaBHOAc3" in folder:

RA = "NaBHOAc3"

elif "NaCNBH3" in folder:

```

RA = "NaCNBH3"

if "with_Acid" in folder:
    acid = "_with_Acid"
else:
    acid = "_without_Acid"

if "42h" in folder:
    time = "_42h"
else:
    time = "_0h"

df_amine_noise_RT.to_csv("Reductive Amination/Flow Injection/Heat Maps/" + RA + acid
+ time + "_amine_RT.csv")
df_amine_noise_height.to_csv("Reductive Amination/Flow Injection/Heat Maps/" + RA +
acid + time + "_amine_height.csv")
df_amine_noise_area.to_csv("Reductive Amination/Flow Injection/Heat Maps/" + RA + acid
+ time + "_amine_area.csv")
df_protonated_noise_RT.to_csv("Reductive Amination/Flow Injection/Heat Maps/" + RA +
acid + time + "_protonated_RT.csv")
df_protonated_noise_height.to_csv("Reductive Amination/Flow Injection/Heat Maps/" +
RA + acid + time + "_protonated_height.csv")
df_protonated_noise_area.to_csv("Reductive Amination/Flow Injection/Heat Maps/" + RA +
acid + time + "_protonated_area.csv")
df_intermediate_noise_RT.to_csv("Reductive Amination/Flow Injection/Heat Maps/" + RA
+ acid + time + "_intermediate_RT.csv")
df_intermediate_noise_height.to_csv("Reductive Amination/Flow Injection/Heat Maps/" +
RA + acid + time + "_intermediate_height.csv")
df_intermediate_noise_area.to_csv("Reductive Amination/Flow Injection/Heat Maps/" + RA
+ acid + time + "_intermediate_area.csv")
df_amine_RT.to_csv("Reductive Amination/Flow Injection/Heat Maps/" + RA + acid + time
+ "_amine_RT.csv")
df_amine_height.to_csv("Reductive Amination/Flow Injection/Heat Maps/" + RA + acid +
time + "_amine_height.csv")
df_amine_area.to_csv("Reductive Amination/Flow Injection/Heat Maps/" + RA + acid +
time + "_amine_area.csv")
df_protonated_RT.to_csv("Reductive Amination/Flow Injection/Heat Maps/" + RA + acid +
time + "_protonated_RT.csv")
df_protonated_height.to_csv("Reductive Amination/Flow Injection/Heat Maps/" + RA + acid
+ time + "_protonated_height.csv")
df_protonated_area.to_csv("Reductive Amination/Flow Injection/Heat Maps/" + RA + acid
+ time + "_protonated_area.csv")
df_intermediate_RT.to_csv("Reductive Amination/Flow Injection/Heat Maps/" + RA + acid
+ time + "_intermediate_RT.csv")
df_intermediate_height.to_csv("Reductive Amination/Flow Injection/Heat Maps/" + RA +
acid + time + "_intermediate_height.csv")

```

```

df_intermediate_area.to_csv("Reductive Amination/Flow Injection/Heat Maps/" + RA + acid
+ time + "_intermediate_area.csv")
df_protonated_yp_height.to_csv("Reductive Amination/Flow Injection/Heat Maps/" + RA +
acid + time + "_protonated_yp_height.csv")
df_protonated_yp_area.to_csv("Reductive Amination/Flow Injection/Heat Maps/" + RA +
acid + time + "_protonated_yp_area.csv")
df_intermediate_yp_height.to_csv("Reductive Amination/Flow Injection/Heat Maps/" + RA
+ acid + time + "_intermediate_yp_height.csv")
df_intermediate_yp_area.to_csv("Reductive Amination/Flow Injection/Heat Maps/" + RA +
acid + time + "_intermediate_yp_area.csv")
df_amine_SN_height.to_csv("Reductive Amination/Flow Injection/Heat Maps/" + RA + acid
+ time + "_amine_SN_height.csv")
df_amine_SN_area.to_csv("Reductive Amination/Flow Injection/Heat Maps/" + RA + acid
+ time + "_amine_SN_area.csv")
df_protonated_SN_height.to_csv("Reductive Amination/Flow Injection/Heat Maps/" + RA +
acid + time + "_protonated_SN_height.csv")
df_protonated_SN_area.to_csv("Reductive Amination/Flow Injection/Heat Maps/" + RA +
acid + time + "_protonated_SN_area.csv")
df_intermediate_SN_height.to_csv("Reductive Amination/Flow Injection/Heat Maps/" + RA
+ acid + time + "_intermediate_SN_height.csv")
df_intermediate_SN_area.to_csv("Reductive Amination/Flow Injection/Heat Maps/" + RA +
acid + time + "_intermediate_SN_area.csv")

```

MS/MS Data Processing Script

```

import re
from pathlib import Path
from matplotlib import pyplot as plt
import pandas as pd
import numpy as np
import os

def plot_single_NCE(NCE):
    plt.figure(figsize=(10,7.5))
    ax = plt.subplot()
    (markers, stemlines, baseline) = plt.stem(range(50, precursor + 10),
averaged_binned_data[NCE][:precursor + 10 - 50])
    plt.setp(baseline, linestyle="-", color="black", linewidth=1)
    plt.setp(markers, marker=" ")
    plt.setp(stemlines, color="black", linewidth=1)
    plt.xlabel("m/z", fontsize=14)
    plt.ylabel("Intensity", fontsize=14)

    y_max = max(averaged_binned_data[NCE])
    y_offset = y_max * 0.02

```

```

for j in range(50, precursor + 10):
    if (averaged_binned_data[NCE][j - 50] / y_max) >= 0.1:
        plt.annotate(str(j), xy=(j, averaged_binned_data[NCE][j - 50] + y_offset),
            fontsize=12, fontweight='bold', ha='center')

plt.annotate("NCE: " + NCE[:-2], xy=(0.05, 0.9), xycoords="axes fraction", fontsize=14)

ax.spines["right"].set_visible(False)
ax.spines["top"].set_visible(False)

plt.title("Precursor m/z: " + str(precursor) + "; Spot Coordinates: (" + x + ", " + y + ")",
    fontsize=16)
plt.tight_layout()
plt.savefig(folder + "/Figures/NCE_" + NCE[:-2] + "/" + "mz" + str(precursor) + "_" +
    file_name[:-4] + "_NCE_" + NCE + ".png")

df_p = pd.read_csv("MS-MS/X_Y_protonated_SN_3.csv")
df_i = pd.read_csv("MS-MS/X_Y_intermediate_SN_3.csv")
df_p["X1"] = df_p["X1"].astype(str)
df_p["Y1"] = df_p["Y1"].astype(str)
df_p["XY"] = df_p["X1"] + "," + df_p["Y1"]
df_i["X2"] = df_i["X2"].astype(str)
df_i["Y2"] = df_i["Y2"].astype(str)
df_i["XY"] = df_i["X2"] + "," + df_i["Y2"]

path = "MS-MS/MS-MS_Test/MS-MS Data Folders/"
folders = [name for name in os.listdir(path)]

for d in folders:
    folder = path + d + "/Converted"
    subfolders = [name for name in os.listdir(folder)]
    if "Figures" not in subfolders:
        os.mkdir(folder + "/Figures")
    subfolders_2 = [name for name in os.listdir(subfolders)]
    if "NCE_10_20_30" not in subfolders_2:
        os.mkdir(folder + "/Figures/NCE_10_20_30")
    if "NCE_10" not in subfolders_2:
        os.mkdir(folder + "/Figures/NCE_10")
    if "NCE_20" not in subfolders_2:
        os.mkdir(folder + "/Figures/NCE_20")
    if "NCE_30" not in subfolders_2:
        os.mkdir(folder + "/Figures/NCE_30")
    destdir = Path(folder)
    files = [p for p in destdir.iterdir() if p.is_file()]
    for i in range(len(files)):
        file_name = str(files[i]).split("\\")[-1]

```

```

file_number = file_name.split("_")[-1][-4]
precursor = int(file_name.split("_")[-2])
y = file_name.split("_")[-3]
x = file_name.split("_")[-4]
xy = x + "," + y

if "protonated" in d.lower():
    if xy not in df_p["XY"].tolist():
        continue
if "intermediate" in d.lower():
    if xy not in df_i["XY"].tolist():
        continue

data = {
    "10.0": {"mz": [], "intensity": []},
    "20.0": {"mz": [], "intensity": []},
    "30.0": {"mz": [], "intensity": []}
}

prevline = ""
line_type = ""

with files[i].open() as f:
    for line in f:
        line = line.rstrip()

        if re.search("collision energy", line):
            CE = line.split(" ")[17][-1]

            if re.search("binary:", line) and re.search("m/z array", prevline):
                data[CE]["mz"].append([float(x) for x in line.split(" ")[12:]])
                line_type = "m/z array"

            if re.search("binary:", line) and re.search("intensity array", prevline) and line_type ==
"m/z array":
                data[CE]["intensity"].append([float(x) for x in line.split(" ")[12:]])

            prevline = line

binned_data = {
    "10.0": [],
    "20.0": [],
    "30.0": []
}

for key in data:

```

```

for i in range(len(data[key]["mz"])):
    binned_spectrum = []
    for j in range(50, 701):
        hit_list = []
        for mz in data[key]["mz"][i]:
            if mz > (j - 0.25) and mz < (j + 0.75):
                hit_list.append(data[key]["intensity"][i][data[key]["mz"][i].index(mz)])
        if hit_list == []:
            binned_spectrum.append(0.0)
        else:
            binned_spectrum.append(max(hit_list))
    binned_data[key].append(binned_spectrum)

averaged_binned_data = {}

for key in binned_data:
    averaged_binned_data[key] = np.average(binned_data[key], axis=0)

plt.figure(figsize=(10,7.5))

keys = list(averaged_binned_data.keys())

for i in range(len(keys)):
    ax = plt.subplot(3, 1, i + 1)
    (markers, stemlines, baseline) = plt.stem(range(50, precursor + 10),
    averaged_binned_data[keys[i]][:precursor + 10 - 50])
    plt.setp(baseline, linestyle="-", color="black", linewidth=1)
    plt.setp(markers, marker=" ")
    plt.setp(stemlines, color="black", linewidth=1)
    if i == 2:
        plt.xlabel("m/z", fontsize=14)
    else:
        plt.xlabel("")
    if i == 0:
        plt.ylabel("Intensity", fontsize=14)
    else:
        plt.ylabel("")

    y_max = max(averaged_binned_data[keys[i]])
    y_offset = y_max * 0.02

    for j in range(50, precursor + 10):
        if (averaged_binned_data[keys[i]][j - 50] / y_max) >= 0.1:
            plt.annotate(str(j), xy=(j, averaged_binned_data[keys[i]][j - 50] + y_offset),
            fontsize=12, fontweight='bold', ha='center')

```

```
plt.annotate("NCE: " + keys[i][: -2], xy=(0.05, 0.9), xycoords="axes fraction", fontsize=14)

ax.spines["right"].set_visible(False)
ax.spines["top"].set_visible(False)

plt.tight_layout()
plt.subplots_adjust(top=0.9)
plt.suptitle("Precursor m/z: " + str(precursor) + "; Spot Coordinates: (" + x + ", " + y + ")",
            fontsize=16)
plt.savefig(folder + "/Figures/NCE_10_20_30/" + "mz" + str(precursor) + "_" + file_name[: -
4] + "_NCE_10_20_30.png")

for key in keys:
    plot_single_NCE(key)

plt.close("all")
```

REFERENCES

1. Babiak, J.; Lucotch, B.; Russo, A.; Heydt, L.; Williams, S.; McCaully, R., The trials and tribulations of a robotic screening core. *The Journal of Automatic Chemistry* **1995**, *17* (2), 55-58.
2. Skehan, P., Dealing with the data deluge in high throughput screening. *Journal of Automated Methods and Management in Chemistry* **2000**, *22* (5), 145-148.
3. Blakemore, D. C.; Castro, L.; Churcher, I.; Rees, D. C.; Thomas, A. W.; Wilson, D. M.; Wood, A., Organic synthesis provides opportunities to transform drug discovery. *Nature Chemistry* **2018**, *10* (4), 383-394.
4. Fan, J.-B.; Yeakley, J. M.; Bibikova, M.; Chudin, E.; Wickham, E.; Chen, J.; Doucet, D.; Rigault, P.; Zhang, B.; Shen, R.; McBride, C.; Li, H.-R.; Fu, X.-D.; Oliphant, A.; Barker, D. L.; Chee, M. S., A versatile assay for high-throughput gene expression profiling on universal array matrices. *Genome Res* **2004**, *14* (5), 878-885.
5. Liu, Y.; Li, G., A power-free, parallel loading microfluidic reactor array for biochemical screening. *Scientific Reports* **2018**, *8* (1), 13664.
6. Saleski, T. E.; Kerner, A. R.; Chung, M. T.; Jackman, C. M.; Khasbaatar, A.; Kurabayashi, K.; Lin, X. N., Syntrophic co-culture amplification of production phenotype for high-throughput screening of microbial strain libraries. *bioRxiv* **2019**, 518639.
7. D'Agostino, V. G.; Sighel, D.; Zucal, C.; Bonomo, I.; Micaelli, M.; Lolli, G.; Provenzani, A.; Quattrone, A.; Adami, V., Screening Approaches for Targeting Ribonucleoprotein Complexes: A New Dimension for Drug Discovery. *SLAS DISCOVERY: Advancing Life Sciences R&D* **2019**, *24* (3), 314-331.
8. Hilfiker, R.; Berghausen, J.; Blatter, F.; Burkhard, A.; De Paul, S. M.; Freiermuth, B.; Geoffroy, A.; Hofmeier, U.; Marcolli, C.; Siebenhaar, B.; Szelagiewicz, M.; Vit, A.; von Raumer, M., Polymorphism - integrated approach from high-throughput screening to crystallization optimization. *Journal of Thermal Analysis and Calorimetry* **2003**, *73* (2), 429-440.
9. Morissette, S. L.; Almarsson, Ö.; Peterson, M. L.; Remenar, J. F.; Read, M. J.; Lemmo, A. V.; Ellis, S.; Cima, M. J.; Gardner, C. R., High-throughput crystallization: polymorphs, salts, co-crystals and solvates of pharmaceutical solids. *Advanced Drug Delivery Reviews* **2004**, *56* (3), 275-300.
10. Isbrandt, E. S.; Sullivan, R. J.; Newman, S. G., High Throughput Strategies for the Discovery and Optimization of Catalytic Reactions. *Angewandte Chemie International Edition* **2019**, *58* (22), 7180-7191.

11. Mattes, D. S.; Streit, B.; Bhandari, D. R.; Greifenstein, J.; Foertsch, T. C.; Münch, S. W.; Ridder, B.; v. Bojničić-Kninski, C.; Nesterov-Mueller, A.; Spengler, B.; Schepers, U.; Bräse, S.; Loeffler, F. F.; Breitling, F., Combinatorial Synthesis of Peptoid Arrays via Laser-Based Stacking of Multiple Polymer Nanolayers. *Macromolecular Rapid Communications* **2019**, *40* (6), 1800533.
12. Zhu, H.; Huang, G., High-throughput paper spray mass spectrometry via induced voltage. *Rapid Communications in Mass Spectrometry* **2019**, *33* (4), 392-398.
13. Wleklinski, M.; Loren, B. P.; Ferreira, C. R.; Jaman, Z.; Avramova, L.; Sobreira, T. J. P.; Thompson, D. H.; Cooks, R. G., High throughput reaction screening using desorption electrospray ionization mass spectrometry. *Chemical Science* **2018**.
14. Wleklinski, M.; Loren, B. P.; Ferreira, C. R.; Jaman, Z.; Avramova, L.; Sobreira, T. J. P.; Thompson, D. H.; Cooks, R. G., High throughput reaction screening using desorption electrospray ionization mass spectrometry. *Chemical Science* **2018**, *9* (6), 1647-1653.
15. Cooks, R. G.; Ouyang, Z.; Takats, Z.; Wiseman, J. M., Ambient Mass Spectrometry. *Science* **2006**, *311* (5767), 1566-1570.
16. Szilagyi, B.; Koswara, A.; Loren, B. P.; Ferreira, C. R.; Thompson, D. H.; Nagy, Z. K., Piezoelectric-based high performance spray solvent delivery system for desorption electrospray ionization mass spectrometry: Systematic design and case studies for high throughput screening of N-alkylation reactions. *Chemical Engineering Science* **2019**, *195*, 1010-1020.
17. Chambers, M. C.; Maclean, B.; Burke, R.; Amodei, D.; Ruderman, D. L.; Neumann, S.; Gatto, L.; Fischer, B.; Pratt, B.; Egertson, J.; Hoff, K.; Kessner, D.; Tasman, N.; Shulman, N.; Frewen, B.; Baker, T. A.; Brusniak, M.-Y.; Paulse, C.; Creasy, D.; Flashner, L.; Kani, K.; Moulding, C.; Seymour, S. L.; Nuwaysir, L. M.; Lefebvre, B.; Kuhlmann, F.; Roark, J.; Rainer, P.; Detlev, S.; Hemenway, T.; Huhmer, A.; Langridge, J.; Connolly, B.; Chadick, T.; Holly, K.; Eckels, J.; Deutsch, E. W.; Moritz, R. L.; Katz, J. E.; Agus, D. B.; MacCoss, M.; Tabb, D. L.; Mallick, P., A cross-platform toolkit for mass spectrometry and proteomics. *Nature Biotechnology* **2012**, *30* (10), 918-920.
18. Shevlin, M., Practical High-Throughput Experimentation for Chemists. *ACS Medicinal Chemistry Letters* **2017**, *8* (6), 601-607.
19. Zinia, J.; Ahmed, M.; Samyukta, S.; Larisa, A.; H., T. D., High Throughput Experimentation and Continuous Flow Validation of Suzuki–Miyaura Cross-Coupling Reactions. *Chemistry – A European Journal* **2018**, *24* (38), 9546-9554.
20. Selekman, J. A.; Qiu, J.; Tran, K.; Stevens, J.; Rosso, V.; Simmons, E.; Xiao, Y.; Janey, J., High-Throughput Automation in Chemical Process Development. *Annual Review of Chemical and Biomolecular Engineering* **2017**, *8* (1), 525-547.

21. Ichiishi, N.; Caldwell, J. P.; Lin, M.; Zhong, W.; Zhu, X.; Streckfuss, E.; Kim, H.-Y.; Parish, C. A.; Krska, S. W., Protecting group free radical C–H trifluoromethylation of peptides. *Chemical Science* **2018**, *9* (17), 4168-4175.
22. Macarron, R.; Banks, M. N.; Bojanic, D.; Burns, D. J.; Cirovic, D. A.; Garyantes, T.; Green, D. V. S.; Hertzberg, R. P.; Janzen, W. P.; Paslay, J. W.; Schopfer, U.; Sittampalam, G. S., Impact of high-throughput screening in biomedical research. *Nature Reviews Drug Discovery* **2011**, *10*, 188.
23. Liu, M.; Chen, K.; Christian, D.; Fatima, T.; Pissarnitski, N.; Streckfuss, E.; Zhang, C.; Xia, L.; Borges, S.; Shi, Z.; Vachal, P.; Tata, J.; Athanasopoulos, J., High-Throughput Purification Platform in Support of Drug Discovery. *ACS Combinatorial Science* **2012**, *14* (1), 51-59.
24. Chen, P., Electrospray Ionization Tandem Mass Spectrometry in High-Throughput Screening of Homogeneous Catalysts. *Angewandte Chemie International Edition* **2003**, *42* (25), 2832-2847.
25. Buitrago Santanilla, A.; Regalado, E. L.; Pereira, T.; Shevlin, M.; Bateman, K.; Campeau, L.-C.; Schneeweis, J.; Berritt, S.; Shi, Z.-C.; Nantermet, P.; Liu, Y.; Helmy, R.; Welch, C. J.; Vachal, P.; Davies, I. W.; Cernak, T.; Dreher, S. D., Nanomole-scale high-throughput chemistry for the synthesis of complex molecules. *Science* **2015**, *347* (6217), 49-53.
26. Troshin, K.; Hartwig, J. F., Snap deconvolution: An informatics approach to high-throughput discovery of catalytic reactions. *Science* **2017**, *357* (6347), 175-181.
27. Kim, H.; Min, K. I.; Inoue, K.; Im, D. J.; Kim, D. P.; Yoshida, J., Submillisecond organic synthesis: Outpacing Fries rearrangement through microfluidic rapid mixing. *Science* **2016**, *352* (6286), 691-694.
28. Snead, D. R.; Jamison, T. F., A three-minute synthesis and purification of ibuprofen: pushing the limits of continuous-flow processing. *Angew Chem Int Ed Engl* **2015**, *54* (3), 983-7.
29. Takáts, Z.; Wiseman, J. M.; Gologan, B.; Cooks, R. G., Mass Spectrometry Sampling Under Ambient Conditions with Desorption Electrospray Ionization. *Science* **2004**, *306* (5695), 471-473.
30. Costa, A. B.; Graham Cooks, R., Simulated splashes: Elucidating the mechanism of desorption electrospray ionization mass spectrometry. *Chemical Physics Letters* **2008**, *464* (1), 1-8.
31. Xin, Y.; M., B. R.; Graham, C. R., Organic Reactions in Microdroplets: Reaction Acceleration Revealed by Mass Spectrometry. *Angewandte Chemie International Edition* **2016**, *55* (42), 12960-12972.

32. Goldstein, S. W.; Bill, A.; Dhuguru, J.; Ghoneim, O., Nucleophilic Aromatic Substitution—Addition and Identification of an Amine. *Journal of Chemical Education* **2017**, *94* (9), 1388-1390.
33. Scales, S.; Johnson, S.; Hu, Q.; Do, Q.-Q.; Richardson, P.; Wang, F.; Braganza, J.; Ren, S.; Wan, Y.; Zheng, B.; Faizi, D.; McAlpine, I., Studies on the Regioselective Nucleophilic Aromatic Substitution (S_NAr) Reaction of 2-Substituted 3,5-Dichloropyrazines. *Organic Letters* **2013**, *15* (9), 2156-2159.
34. Roughley, S. D.; Jordan, A. M., The Medicinal Chemist's Toolbox: An Analysis of Reactions Used in the Pursuit of Drug Candidates. *Journal of Medicinal Chemistry* **2011**, *54* (10), 3451-3479.
35. Cvijetić, I. N.; Verbić, T. Ž.; Ernesto de Resende, P.; Stapleton, P.; Gibbons, S.; Juranić, I. O.; Drakulić, B. J.; Zloh, M., Design, synthesis and biological evaluation of novel aryldiketo acids with enhanced antibacterial activity against multidrug resistant bacterial strains. *European Journal of Medicinal Chemistry* **2018**, *143*, 1474-1488.
36. Trump, R. P.; Blanc, J.-B. E.; Stewart, E. L.; Brown, P. J.; Caivano, M.; Gray, D. W.; Hoekstra, W. J.; Willson, T. M.; Han, B.; Turnbull, P., Design and Synthesis of an Array of Selective Androgen Receptor Modulators. *Journal of Combinatorial Chemistry* **2007**, *9* (1), 107-114.
37. Chen, L.; Fu, W.; Feng, C.; Qu, R.; Tong, L.; Zheng, L.; Fang, B.; Qiu, Y.; Hu, J.; Cai, Y.; Feng, J.; Xie, H.; Ding, J.; Liu, Z.; Liang, G., Structure-based design and synthesis of 2,4-diaminopyrimidines as EGFR L858R/T790M selective inhibitors for NSCLC. *European Journal of Medicinal Chemistry* **2017**, *140*, 510-527.
38. Phuangswai, O.; Beswick, P.; Ratanabunyong, S.; Tabtimmai, L.; Suphakun, P.; Obounchoey, P.; Srisook, P.; Horata, N.; Chuckowree, I.; Hannongbua, S.; Ward, S. E.; Choowongkamon, K.; Gleeson, M. P., Evaluation of the anti-malarial activity and cytotoxicity of 2,4-diamino-pyrimidine-based kinase inhibitors. *European Journal of Medicinal Chemistry* **2016**, *124*, 896-905.
39. La Pietra, V.; Sartini, S.; Botta, L.; Antonelli, A.; Ferrari, S. M.; Fallahi, P.; Moriconi, A.; Coviello, V.; Quattrini, L.; Ke, Y.-Y.; Hsing-Pang, H.; Da Settimo, F.; Novellino, E.; La Motta, C.; Marinelli, L., Challenging clinically unresponsive medullary thyroid cancer: Discovery and pharmacological activity of novel RET inhibitors. *European Journal of Medicinal Chemistry* **2018**, *150*, 491-505.
40. Li, L.; Lv, K.; Yang, Y.; Sun, J.; Tao, Z.; Wang, A.; Wang, B.; Wang, H.; Geng, Y.; Liu, M.; Guo, H.; Lu, Y., Identification of N-Benzyl 3,5-Dinitrobenzamides Derived from PBTZ169 as Antitubercular Agents. *ACS Medicinal Chemistry Letters* **2018**, *9* (7), 741-745.
41. Gazitúa, M.; Tapia, R. A.; Contreras, R.; Campodónico, P. R., Effect of the nature of the nucleophile and solvent on an S_NAr reaction. *New Journal of Chemistry* **2018**, *42* (1), 260-264.

42. Kwan, E. E.; Zeng, Y.; Besser, H. A.; Jacobsen, E. N., Concerted nucleophilic aromatic substitutions. *Nature Chemistry* **2018**, *10* (9), 917-923.
43. Bunnett, J. F.; Zahler, R. E., Aromatic Nucleophilic Substitution Reactions. *Chemical Reviews* **1951**, *49* (2), 273-412.
44. Um, I.-H.; Hong, J.-Y.; Kim, J.-J.; Chae, O.-M.; Bae, S.-K., Regioselectivity and the Nature of the Reaction Mechanism in Nucleophilic Substitution Reactions of 2,4-Dinitrophenyl X-Substituted Benzenesulfonates with Primary Amines. *The Journal of Organic Chemistry* **2003**, *68* (13), 5180-5185.
45. Ormazabal-Toledo, R.; Santos, J. G.; Ríos, P.; Castro, E. A.; Campodónico, P. R.; Contreras, R., Hydrogen Bond Contribution to Preferential Solvation in S_NAr Reactions. *The Journal of Physical Chemistry B* **2013**, *117* (19), 5908-5915.
46. Ormazábal-Toledo, R.; Contreras, R.; Tapia, R. A.; Campodónico, P. R., Specific nucleophile–electrophile interactions in nucleophilic aromatic substitutions. *Organic & Biomolecular Chemistry* **2013**, *11* (14), 2302-2309.
47. Gazitúa, M.; Tapia, R. A.; Contreras, R.; Campodónico, P. R., Mechanistic pathways of aromatic nucleophilic substitution in conventional solvents and ionic liquids. *New Journal of Chemistry* **2014**, *38* (6), 2611-2618.
48. Len, C.; Bruniaux, S.; Delbecq, F.; Parmar, V., Palladium-Catalyzed Suzuki–Miyaura Cross-Coupling in Continuous Flow. *Catalysts* **2017**, *7* (5), 146.
49. Falcone, C. E.; Jaman, Z.; Wleklinski, M.; Koswara, A.; Thompson, D. H.; Cooks, R. G., Reaction screening and optimization of continuous-flow atropine synthesis by preparative electrospray mass spectrometry. *Analyst* **2017**, *142* (15), 2836-2845.
50. Loren, B. P.; Wleklinski, M.; Koswara, A.; Yammine, K.; Hu, Y.; Nagy, Z. K.; Thompson, D. H.; Cooks, R. G., Mass spectrometric directed system for the continuous-flow synthesis and purification of diphenhydramine. *Chemical Science* **2017**, *8* (6), 4363-4370.
51. Ewan, H. S.; Iyer, K.; Hyun, S.-H.; Wleklinski, M.; Cooks, R. G.; Thompson, D. H., Multistep Flow Synthesis of Diazepam Guided by Droplet-Accelerated Reaction Screening with Mechanistic Insights from Rapid Mass Spectrometry Analysis. *Organic Process Research & Development* **2017**, *21* (10), 1566-1570.
52. Wleklinski, M.; Falcone, C. E.; Loren, B. P.; Jaman, Z.; Iyer, K.; Ewan, H. S.; Hyun, S.-H.; Thompson, D. H.; Cooks, R. G., Can Accelerated Reactions in Droplets Guide Chemistry at Scale? *European Journal of Organic Chemistry* **2016**, *2016* (33), 5480-5484.
53. Örkényi, R.; Éles, J.; Faigl, F.; Vincze, P.; Prechl, A.; Szakács, Z.; Kóti, J.; Greiner, I., Continuous Synthesis and Purification by Coupling a Multistep Flow Reaction with Centrifugal Partition Chromatography. *Angewandte Chemie International Edition* **2017**, *56* (30), 8742-8745.

54. Jessop, P. G.; Jessop, D. A.; Fu, D.; Phan, L., Solvatochromic parameters for solvents of interest in green chemistry. *Green Chemistry* **2012**, *14* (5), 1245-1259.
55. Forlani, L., Are weak interactions responsible for kinetic catalytic behaviour in SNAr reactions? *Journal of Physical Organic Chemistry* **1999**, *12* (6), 417-424.
56. Miao, Z.; Chen, H., Direct Analysis of Liquid Samples by Desorption Electrospray Ionization-Mass Spectrometry (DESI-MS). *Journal of the American Society for Mass Spectrometry* **2009**, *20* (1), 10-19.
57. Badu-Tawiah, A.; Bland, C.; Campbell, D. I.; Cooks, R. G., Non-Aqueous Spray Solvents and Solubility Effects in Desorption Electrospray Ionization. *Journal of the American Society for Mass Spectrometry* **2010**, *21* (4), 572-579.
58. Crampton, M. R.; Emokpae, T. A.; Howard, J. A. K.; Isanbor, C.; Mondal, R., Leaving group effects on the mechanism of aromatic nucleophilic substitution (SNAr) reactions of some phenyl 2,4,6-trinitrophenyl ethers with aniline in acetonitrile. *Journal of Physical Organic Chemistry* **2004**, *17* (1), 65-70.
59. Fong, R. C.; Scheirer, W. J.; Cox, D. D., Using human brain activity to guide machine learning. *Scientific Reports* **2018**, *8* (1), 5397.
60. Borji, A., Negative results in computer vision: A perspective. *Image and Vision Computing* **2018**, *69*, 1-8.
61. Abdel-Magid, A. F.; Mehrman, S. J., A Review on the Use of Sodium Triacetoxyborohydride in the Reductive Amination of Ketones and Aldehydes. *Organic Process Research & Development* **2006**, *10* (5), 971-1031.
62. Sawicki, J. W.; Bogdan, A. R.; Searle, P. A.; Talaty, N.; Djuric, S. W., Rapid analytical characterization of high-throughput chemistry screens utilizing desorption electrospray ionization mass spectrometry. *Reaction Chemistry & Engineering* **2019**, *4* (9), 1589-1594.



Contents lists available at ScienceDirect

Talanta

journal homepage: www.elsevier.com/locate/talanta



Direct ion generation from swabs[☆]

Alan K. Jarmusch¹, Valentina Pirro¹, David L. Logsdon, R. Graham Cooks*

Department of Chemistry and Center for Analytical Instrumentation Development, Purdue University, West Lafayette, IN 47907, United States



ARTICLE INFO

Keywords:

Ambient ionization
Electrospray
Mass spectrometry
Medical swabs
In vivo sampling
Point-of-care testing

ABSTRACT

Medical swabs are used for biofluid and tissue sampling in clinical applications. The use of medical swabs as electrospray ionization probes for direct mass spectrometric analysis is a novel and potentially widely applicable development. Here we discuss ion generation, characterize ionization behavior via microscopic videography and describe some illustrative examples of applications.

1. Introduction

New methods of ion generation which simplify analysis and reduce cost are needed for the next generation of mass spectrometry applications, e.g. point of care medicine and in situ drug testing. During the fifteen-year development of ambient ionization methods, over 80 techniques have been reported [1], and these address the need for ion generation under native atmospheric conditions (temperature, humidity, pressure) and with minimal to no sample preparation. A continuing trend, first seen in desorption electrospray ionization (DESI), is the integration of sampling and ionization into a single device. This has resulted in such new methods as rapid evaporative ionization [2], the *masSpec Pen* [3], liquid microjunction surface sampling probe [4,5], probe electrospray ionization (PESI) [6–8], touch spray (TS) [9,10], paper spray (PS) [11–13], and coated blade spray (CBS) [14–17]. Techniques like PS and CBS are examples of substrate-spray technologies [17]. As recently stated by Gómez-Ríos et al., the operational principle consists of supplying liquid to wicking materials, such as paper strips, and then applying a high electrical field to generate gaseous ions from sharp features of the material via electrospray ionization (ESI) or ESI-like mechanisms [17]. The conditions under which ESI occurs have been well characterized [18–20], even though a universal mechanism of ionization remains to be detailed. The basic criterion is the establishment of a strong electric field that overcomes the surface tension of the analyte-containing solution. A number of parameters influence this criterion including solvent surface tension, solvent conductivity, solvent flow rate, voltage applied to the electrospray emitter, radius of electrospray emitter, distance from the electrospray emitter to

ground. The desired result of parameter selection is the generation of a Taylor cone and a stable cone-jet mode electrospray plume. The electrospray plume expels analyte-containing charged primary solvent droplets that undergo evaporation and Coulombic fission beyond the Rayleigh limit and yield gas-phase analyte ions [18–20].

In 2014, we developed swab touch spray (STS) as another example of substrate-spray ambient ionization. In this method, a sample, either solid or liquid, is transferred to a swab tip by gentle touch; ions are subsequently generated upon application of solvent to the swab tip and of a high voltage directly to the swab handle [21–26]. Swabs are ubiquitous, easy-to-use, and inexpensive sampling devices which are used widely in clinical microbiology, cytology, DNA testing, and forensics. Applications that are best tailored for STS are those relying on in vivo, rapid, minimally invasive sampling of minute amounts of sample (e.g. biofluid and tissue), and for which swabs are already the preferred means of sampling. Swab tips are usually made of cotton, rayon, polyester or foam in fused shapes of different dimensions. Medical swabs are designed to reduce bleeding at touch and invasiveness of sampling, to reach superficial wounds or deep body orifices, to achieve high absorption capacity, and to transfer quantitative volumes of fluids. Hence, the potential utility of generating ions directly from medical swabs for rapid and direct MS analysis is substantial and can be done without altering the swab design (i.e. shape, dimension, material) that is already fit for purpose. This makes swabs unconventional ESI emitters with irregular geometries and uncommon dimensions (i.e. overall swab radii are on the order of mm – typical ESI emitters radii are μm).

A number of STS applications have been reported already in the literature including the detection of microbial lipids from cultures [21],

[☆] This article is dedicated to Purnendu K (Sandy) Dasgupta in celebration of his versatility in analytical science and his ingenuity in instrumentation development.

* Correspondence to: 560 Oval Drive, West Lafayette, IN 47907, United States.

E-mail address: cooks@purdue.edu (R.G. Cooks).

¹ Equal contribution.

<https://doi.org/10.1016/j.talanta.2018.02.105>

Received 24 December 2017; Received in revised form 25 February 2018; Accepted 26 February 2018
Available online 12 March 2018

0039-9140/ © 2018 Elsevier B.V. All rights reserved.

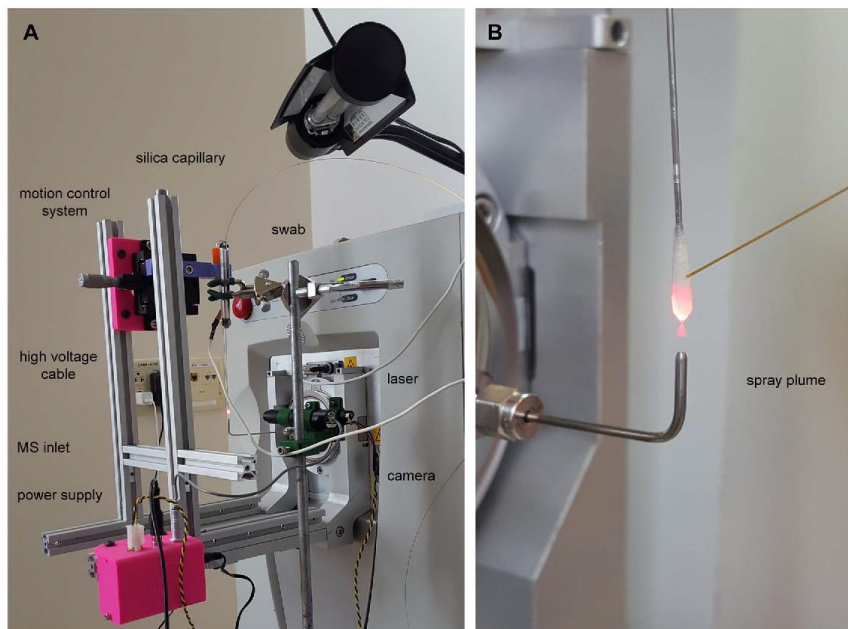


Fig. 1. (A) Image of the custom source interface. (B) Photograph of electro spray generated from swab, red laser pointer was used to illuminate the electro spray plume.

illicit drug detection in oral fluid [22], nicotine detection in meconium [24], detection of gunshot residues from human skin [25], detection of chemical warfare agents from surfaces [26] and intraoperative assessment of surgical brain tumor margins [23]. Analyses in the reported methods were qualitative and relied on limits of detection to establish the presence of target analytes (e.g. illicit drugs in biofluids [22]) or relative spectral changes to assess positive outcomes (e.g. presence of cancerous tissue [23]). Swabs were used dry to sample biofluids and tissue in vivo [21,23–25], or conditioned with solvents and then used to sample analytes from dry surfaces [26]. The aforementioned applications used a variety of slightly different methods each of which suggested electro spray ionization behavior. Ionization in STS is believed to occur similarly to that in PS ionization, i.e. ions are generated from a porous surface via electro spray-like mechanisms [12]; however, characterization of ionization behavior in response to operating conditions and details of mechanism in STS have not been studied. With the aim of improving STS performance (i.e. reproducibility of signal generation, signal intensity, and signal stability), we sought to better characterize the parameters which impact ion generation; an aspect of STS that was not discussed in previous articles. In this study, we provide the first visual evidence of electro spray-like behavior in STS and describe the parameters which influence ion generation from commercially-available swabs composed of different materials. Microscopic videography of the spray plume revealed multiple, known, electro spray ionization modes to be present in STS. The parameters which influence STS, the visual observations, and the data are illustrative in this report.

2. Materials and methods

2.1. Medical swabs

Most of the experiments were performed using sterile medical swabs, model 160 C, provided by Copan Diagnostics (Murrieta, CA). The swabs have an aluminum handle and rayon tip of largest diameter

of ~ 2.4 mm (Fig. S1). The swabs are packaged in individual tubes for easy transport and storage. They are mounted in a plastic cap that serves as a convenient holder. Each tube and cap assembly is sealed with a tamper proof label for assurance of sterility and chain of custody. Additional swabs manufactured by Puritan Medical Products (Guilford, ME) were also tested, specifically models 25-800 C50, 25-800 R50 (Fig. S1), and 25-801 D50. These swabs have a flexible aluminum handle and a tip made of cotton, rayon, and polyester, respectively. Tips are of fused shape with largest diameter of ~ 1.8 mm. Swabs having an electrostatic dissipative (ESD) plastic handle (model TX750E, Texwipe, Kernersville, NC) were tested (Fig. S1). These swabs have a conical tip in polyurethane with ~ 0.8 mm in diameter at the apex. Lastly, a 10- μ L Mitra[®] microsampler device (Neoteryx, Torrance CA) was tested. This device has a swab tip that allows for accurate and precise collection of biofluids using VAMS[™] technology, and a plastic handle. All the swabs tested are commercialized for purposes other than MS analysis. They have been used with no modification from their commercial form.

2.2. Chemicals

Most of the experiments were performed by spraying pure organic solvents — ranging from hexanes to N,N-dimethylformamide (DMF) — using different swabs and electro spray conditions. Table S1 summarizes all the solvents tested, their surface tension, viscosity, dielectric constant, and density. All solvents were HPLC grade ($\geq 99.9\%$ pure) and were purchased from Sigma-Aldrich (Minneapolis, MN). A few binary and ternary mixtures of solvents were also tested (Table S2). Formic acid (LC-MS grade, Fisher Scientific, Belgium) at 0.1% v/v and the non-ionic surfactant octyl β -D-glucopyranoside ($\geq 98\%$ pure, Sigma Aldrich) were tested as solvent modifiers.

2.3. Microscopic videography

For each swab tested and each electro spray condition used, videos

Table 1
Electrospray ionization conditions for touch spray with medical swabs.

Solvent	Positive Ionization Mode				Negative Ionization Mode			
	Onset Voltage (kV)	Spray Mode	Surfactant ^a	Solvent Flow Rate (μL/min)	Onset Voltage (kV)	Spray Mode	Surfactant	Solvent Flow Rate (μL/min)
Acetone	5.5 ± 0.5	Cone jet	n/a ^{**}	35 ± 3	5.75 ± 0.5	Cone jet	n/a	35 ± 3
ACN	6.0 ± 0.5	Cone jet	Insoluble	15 ± 3	> 5.75	Pulsating	Insoluble	> 18
Chloroform	5.5 ± 0.5	Cone jet; pulsating	n/a	8 ± 3	> 6.0	Pulsating alternated with ramified Jet	n/a	> 5
Dichloromethane	> 5.0	Pulsating	n/a	> 5	> 5.5	Pulsating	n/a	> 5
DMP	6.25 ± 0.5	Cone jet	nsd ^{***}	5 ± 3	> 5.75	Pulsating; discharging	nsd	–
Ethanol	5.5 ± 0.5	Cone jet	nsd	20 ± 3	6.0 ± 0.5	Cone Jet	nsd	25 ± 3
Ethyl acetate	5.5 ± 0.5	Cone jet	n/a	25 ± 3	> 5.75	Pulsating; discharging	nsd	–
Isopropyl alcohol	5.5 ± 0.5	Cone jet	n/a	15 ± 3	6.0 ± 0.5	Cone jet	nsd	20 ± 3
Hexanes	> 5.0	Pulsating	nsd	> 35	> 5.0	Pulsating	nsd	> 35
Methanol	5.5 ± 0.5	Cone jet	nsd	15 ± 3	6.5 ± 0.5	Ramified jet alternated with cone jet	nsd	18 ± 3

^a Octyl β-D-glucopyranoside (Conc ≤ 250 ppm).

^{**} n/a = not tested.

^{***} nsd = not significantly different.

of the spray plume were recorded to observe the electrospray behavior. A Watec WAT-704R camera was used to acquire the videos; the software Cyberlink PowerDirector v.14 (www.cyberlink.com) was used to record them; Adobe Premier Pro CC (www.adobe.com) was used for video editing when necessary. The spray plume was illuminated with a red laser pointer as shown in Fig. 1.

2.4. Mass spectrometry

All experiments were performed using a linear ion trap mass spectrometer (LTQ, Thermo Scientific, San Jose, CA). High voltage was applied to the swab handle using a custom high voltage cable, the instrument high voltage supply, and a copper clip. Solvent was applied continuously on the swab tip via a fused-silica capillary (i.d. 250 μm, o.d. 360 μm) using an external syringe pump. A customized interface that locks directly to the mass spectrometer was built to affix the swab in a vertical position in front of the instrument (Fig. 1). The swab was oriented vertically with the tip directly above the MS inlet capillary, which was bent 90° upwards. The swab was positioned 5–8 mm above the inlet. A precision motion control system was used to adjust the position of the swab whenever necessary. The syringe pump flow rate was set at 50 μL/min for about 30 s, accounting for the dead volume and wetting the swab tip. Once the swab tip was visibly wet, high voltage was applied to the metallic handle. Solvent flow rates and voltages were adjusted to observe changes in the electrospray behavior. High voltages were ramped between 4 and 7 kV (upper limit of the instrument power supply), both in negative and positive ionization mode. Solvent flow rates ranged from 5 and 100 μL/min. Mass spectral data were acquired in full scan or using MSⁿ as needed. All data were acquired with the automatic gain control activated. Capillary inlet temperature was set at 275 °C.

3. Results and discussion

3.1. Electrospray formation

Typically, ESI occurs from capillary tubing through which analyte-containing solvent is pumped and high voltage is applied. STS differs in that electrospray occurs from solvent on the surface of the swab tip. Initially, solvent is pumped onto the porous swab material. Visual saturation of the swab material was observed after the application of 10–40 μL depending on the particular swab tested. After saturation, an excess of solvent resulted in an observed droplet suspended at the apex of the swab tip. The droplet of excess solvent remained suspended and eventually dripped when no voltage was applied to the swab. When a

high voltage was applied to the handle of the swab, ideally a conductive material, the suspended droplet elongated. The elongation reduces the diameter from which droplets are produced which in turn increases the electric field strength to allow it to exceed the solvent surface tension and generate an electrospray (Video S1). Electrospray from suspended, dripping, and levitating droplets has previously been reported and explained using similar droplet elongation mechanisms [18–20]. The electric field was generated between the swab and the inlet of the mass spectrometer positioned underneath the swab (Fig. 1). Electric field strength was manipulated in our experimental apparatus by changing the high voltage applied to the swab handle and the distance between the swab and the inlet. It was empirically determined that a swab-to-inlet distance of 5–8 mm resulted in consistent spray for the tested conditions and materials.

Supplementary material related to this article can be found online at <http://dx.doi.org/10.1016/j.talanta.2018.02.105>.

We initially tested swabs with metallic handles and hemispherical swab tips. The limitations imposed by the availability of commercial swabs constrained the exploration of the swab geometry and materials at this stage. For all solvents tested, the onset voltages required for the generation of a Taylor cone were higher than those typically used in TS, PESI, PS and CBS experiments (≤ 4.0 kV), because of the hemispherical shape of the swab as well as the large diameter of the tip (> 1.5 mm; in the presence of solvent the smaller size of the individual elements of the tip do not affect field strength). Table 1 summarizes the results for Copan swabs; however, no significant differences were observed when using the Puritan swabs that had a slightly smaller tip. The onset voltages (V_{on}) ranged between 4.5 kV and 6.5 kV. The manufacturing irregularities in the swab tips (e.g. distortion of the tip geometry and different sizes of the tip itself), prohibited reporting of a single onset voltage for a specific combination of solvents and swabs, instead we provided a fairly narrow range of voltages (± 0.5 kV on average) which would result in the generation of a stable spray plume, as assessed using microscopy videography (Tables 1 and S2). Generally, higher voltages were necessary to spray solvents with greater surface tension (e.g. $V_{onMeOH} < V_{onACN}$). Higher voltages were also necessary for negative ESI compared to positive ESI, matching previous observations [18–20]. Mixing solvents with low surface tension and solvents with high surface tension decreased the onset voltage (Table S2); this is one approach to improving spray performance albeit this process is often nonlinear and difficult to predict. Addition of deionized water to more than 5% in pure organic solvents, both for positive and negative ionization modes, resulted in electric discharges. This is likely attributable to the high surface tension of water. For the analysis of water-containing specimens (e.g. oral fluid), drying the swab prior to

ionization was necessary [22]. Conductivity of the spray solution was not tested, but it does certainly influence ion generation via electro-spray. The addition of non-ionic surfactant octyl β -D-glucopyranoside (≤ 250 ppm) did not lower the onset voltages significantly, against expectation.

The solvent flow rate varied greatly across the swabs and conditions tested (Tables 1 and S2); however, flow rates were reasonably consistent in replicate measurements for the same set of parameters (e.g. swab, polarity, spray voltage). Average variation was $\pm 3 \mu\text{L}/\text{min}$ and was largely the results of swab manufacturing irregularities. The ideal solvent flow rate achieves a balance with electrospray consumption which is dependent on a few factors including emitter diameter and electric field strength. A stable Taylor cone and electrospray plume was observed when the correct solvent flow rate was applied. The electrospray plume lasted as long as solvent and high voltage was applied. Deviations from a balanced state between solvent supply and consumption resulted in spray instabilities as discussed later. As expected, we observed that higher flow rates were necessary to spray using higher voltages. Higher flow rates were necessary to spray in negative ionization mode compared to positive ionization mode. Lower flow rates were necessary to spray solvents with higher surface tension and viscosity (e.g. 5–10 $\mu\text{L}/\text{min}$ for DMF vs. 20–25 $\mu\text{L}/\text{min}$ for ethanol using Copan swabs). No stable spray plume could be generated using pure hexane or chloroform regardless of the flow rate used as not enough solvent could be accumulated to the swab tip due to rapid evaporation (Table 1).

The fluid dynamics occurring at the swab-solvent interface, as well as adsorption kinetics with the swab, is interesting and might influence the observed signal. STS is an extraction-based technology sought to be directly coupled with MS for rapid analysis of complex matrices. We observed such extractive behavior in the decay of target analytes signal over time (Fig. S2 and Fig. 2A). Interestingly, when adding internal standards to the spray solvent used to wet the swab tip, we observed signal suppression of target analytes that was proportional to the concentration of the internal standard in the spraying solvent. Fig. 2B shows approximately a 25-fold increase in cocaine signal when the concentration of internal standard cocaine- d_3 in the spraying solvent was reduced 25 fold. Cocaine was added to blank oral fluid at 250 ppb and 10 μL were pipetted on the swab tip. Cocaine- d_3 was added to the spraying solvent (acetonitrile 0.1% formic acid) at 250, 50, and 10 ppb. Experiments were repeated three times for each cocaine- d_3 concentration level.

Swabs with non-conductive plastic and wood handles were not tested; theoretical onset voltages would have exceeded that of the instrument power supply (± 7 kV). However, this limitation can be overcome by simply applying the high voltage to a metallic needle that touches the swab tip rather than to the handle itself, as shown in Fig. S3. We foresee no significant differences in electrospray behavior when using this alternative strategy. On the other hand, this adaptation is important as more and more commercial swabs have plastic handles to minimize production costs; there is greater selection of swab shapes and materials to be tested when non-conductive handle swabs are considered. Electrostatic dissipative (ESD) plastic handle swabs were tested as an intermediate material between non-conductive (e.g. wood) and conductive (e.g. aluminum) handles. The high voltage was applied directly to the ESD handle. An electrospray plume was observed in positive ion mode, but higher voltages (≥ 6.0 kV) were required due to the increased resistance of the material; no stable spray plume could be generated in negative ion mode regardless of the condition tested (Fig. S). The ESD swabs performed significantly worse than swabs with conductive handles in terms of electrospray stability and signal intensity and will not be discussed further.

3.2. Electrospray modes

Electrospray formation was observed macroscopically in most of the

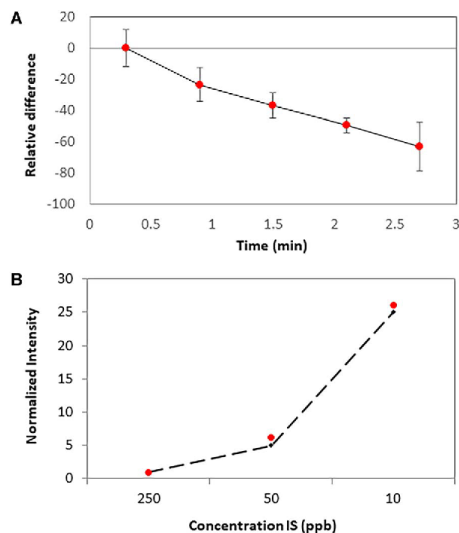


Fig. 2. (A) Relative difference in ion counts for cocaine (250 ppb spiked in oral fluid; 10 μL transferred on the swab tip) over spraying time. Counts for the transition m/z 304 \rightarrow 182 \rightarrow 150 were normalized to the counts of the internal standard cocaine- d_3 transition, m/z 307 \rightarrow 185 \rightarrow 153. (B) Red circles, ratio between the intensity of cocaine and cocaine- d_3 spiked in the spraying solvent at concentrations of 250 ppb, 50 ppb, and 10 ppb. Counts for the transition m/z 304 \rightarrow 182 \rightarrow 150 were normalized to the counts of the internal standard cocaine- d_3 transition m/z 307 \rightarrow 185 \rightarrow 153. Black diamonds, nominal ratio between the concentration of cocaine and the concentration of cocaine- d_3 . (For interpretation of the references to color in this figure legend, the reader is referred to the web version of this article.)

conditions tested, Fig. 1, but microscopic videography revealed parameter-dependent electrospray modes (i.e. pulsating mode, stable cone-jet, ramified cone-jet) displayed in Fig. 3. It is known that different electrospray modes result in different droplet characteristics, such as size and velocity distributions, ion yields [19], effective signal and reproducibility. The major parameters that resulted in observable changes in electrospray behavior were the solvent properties - which include conductivity and surface tension - solvent flow rate, and electric field strength. Note that each electrospray condition was tested multiple times using different swabs of the same type to assess repeatability. Hundreds of swabs were tested overall; approximately 5% of them had to be disregarded because manufacturing defects inhibited the formation of an electrospray regardless of the condition tested.

For all the pure solvents tested, except for hexane, chloroform, and dichloromethane, a stable cone-jet was observed in positive ionization mode (Fig. 3A, Table 1). Conversely, most of the pure solvents did not form a stable cone-jet in negative ionization mode with applied high voltages up to -7 kV; exceptions being ethanol (Fig. 3D), acetone, and isopropyl alcohol (Table 1). No measurement of droplet size distribution was performed in this study, but we anticipate large primary droplets compared to that of nanospray given the large emitter diameter. We hypothesize that, as in the case of PS [12], swab electrospray produces variable droplet sizes because the electrospray generated was difficult to maintain at equilibrium due to the irregularities of the swab tip, potential asymmetries of the electric field at the tip, and small fluctuations of solvent consumption occurring even under conditions of balanced flow rate. If excessive solvent was delivered to the swab tip, one observed the rapid enlargement of the Taylor cone and the spray plume (Fig. S5A-C), but eventually excess solvent would drip from the swab tip; whereas if the solvent flow rate was too low, one observed rapid shrinkage of the Taylor cone and the spray plume, with overall

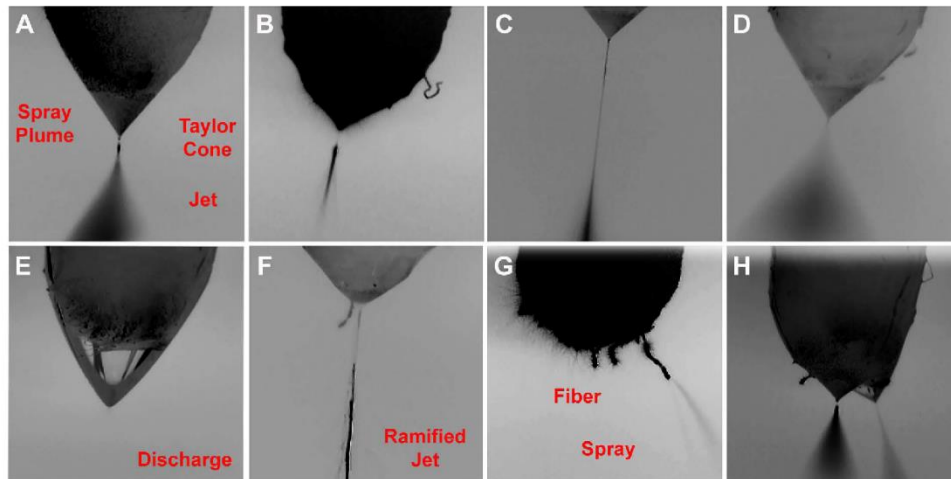


Fig. 3. Photographs of electro spray generated from Copan rayon swabs, red laser pointer was used to illuminate the electro spray plume. (A) Ethanol doped with 0.25 mg/mL of octyl β -D-glucopyranoside, voltage + 5.5 kV. (B) Ethanol, voltage + 5.5 kV. (C) Isopropyl alcohol, voltage + 6.0 kV. (D) Ethanol doped with 0.25 mg/mL of octyl β -D-glucopyranoside, voltage – 6.25 kV. (E) DMF, voltage – 6.5 kV. (F) Acetone-ACN 1:1 v/v, voltage – 6.5 kV. (G) Acetone, voltage + 5.5 kV. (H) Acetone, voltage + 5.5 kV.

decrease of signal intensity, until reaching complete dryness of the swab (Fig. S5D-F). Under conditions of solvent depletion, the spray mode, and consequently the ions that were generated, changed; the higher currents produced suggested the formation of corona discharge.

The electro spray jet mode was also observed. The meniscus of the liquid-air interface was nearly always a Taylor cone from which a stable jet of liquid was emitted which eventually broke into primary droplets. The jet distance was reproducible and dependent on the solvent system

more than on the applied high voltage. The longest jet was observed when spraying isopropyl alcohol (Fig. 3C). Ionization was the most stable and efficient in the cone-jet mode. Relative deviation of absolute counts over spraying time was less than 15% under stable conditions. Spray currents were < 0.3 μ A and mass spectra were dominated by protonated species. Even in this mode, absolute ion counts were generally one order of magnitude lower than those generated when spraying the same solutions by nanoESI using pulled borosilica

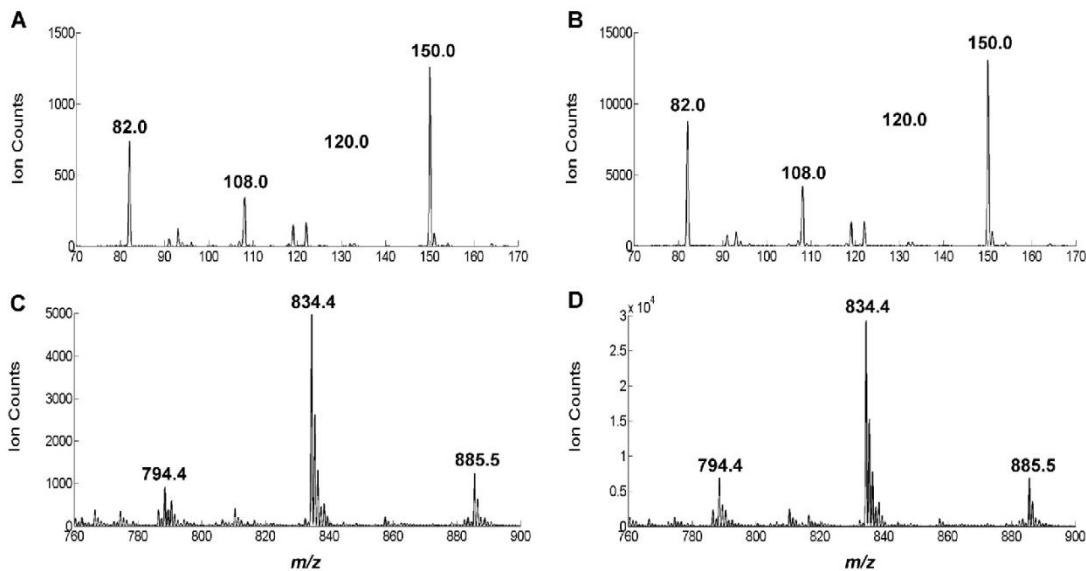


Fig. 4. **Top:** Cocaine solution in acetonitrile 0.1% formic acid, 250 ppb. (+) MS^3 sequential product ion scan m/z 304.1 \rightarrow 182.0 \rightarrow O acquired using STS- MS^3 (A) and nESI- MS^3 (B). **Bottom:** Mouse brain tissue extract in ACN-DMF-EtOH 45:5:50% v/v, 1 mg/mL. (–) Full scan mass spectrum acquired using STS-MS (C) and nESI-MS (D). The solutions were prepared in the solvent system reported above at the specified concentrations. Ten μ L were transferred into a nESI glass capillary and electro sprayed using + 1.0 kV for cocaine detection and – 2.0 kV for lipid profiling; 100 μ L were then aspirated with a syringe and electro sprayed by pumping the solution on a blank Copan swab at 25 μ L/min and applying + 6.5 kV for cocaine detection and – 6.5 kV for lipid profiling. Other MS instrument settings were kept constant.

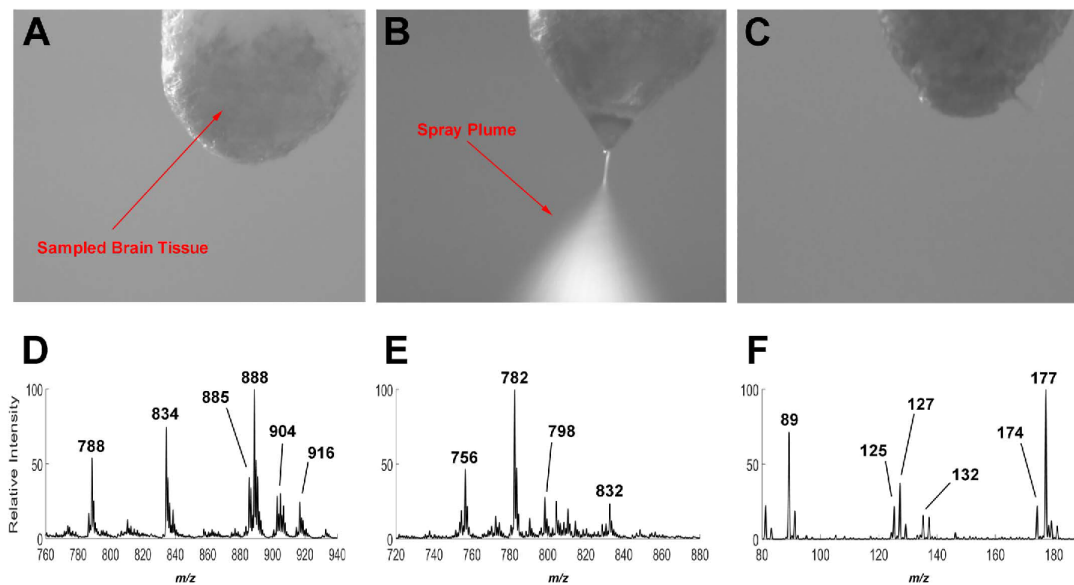


Fig. 5. Video frames showing a Copan rayon swab, red laser pointer was used to illuminate the electro spray plume. (A) Frame time, 0.00 min: photograph of the swab tip immediately after sampling ex vivo a specimen of thawed human brain tissue (IRB # 1410342262). Tissue quantity transferred on the swab, 3.1 mg; pathological diagnosis: low-tumor infiltrated tissue, mixed grey and white matter. (B) Frame time, 2.42 min: photograph of the electro spray plume generated using ACN-DMF-EtOH 45:5:50% as solvent system and -6.5 kV of high voltage. (C) Frame time, 7.00 min: photograph of the swab tip after spraying for approximately 5 min. Note, the camera was slightly moved between frame A and B to better illuminate the spray plume. Full scan mass spectra acquired using STS-MS (average over 10 s of acquisition): (D) Negative ion mode, m/z 760–940; (E) Positive ion mode, m/z 720–880; (F) Negative ion mode, m/z 80–200. For ion attributions see references [23,28].

capillaries with tip diameters of ~ 5 μm (Fig. 4). Background spectra were dependent on the swab material (e.g. polyester, rayon, cotton) and the solvent system used (Fig. S6 and S7). Positive background ions occurred mostly in the low mass range except for acetone and acetonitrile where ions over the m/z 600–1000 overwhelmed the spectrum and were associated with polymers likely found in the swab material or in the adhesive used to fix the swab tip to the handle. Negative background ions occurred predominantly in the low mass range (m/z 200–350) and most were identified as solvent cluster peaks, and fatty acids.

The swab tips were not affected by the application of solvent and high voltage and appeared almost unmodified after the experiment (Fig. 5). We observed no clogging on the MS inlet capillary even when analyzing biological samples. The stiffness and crevasses of the porous tip material help to hold viscous and solid samples (e.g. oral fluid, bacteria colonies, brain matter) [21–23].

The addition of solvent modifiers, such as formic acid, did not alter the spray behavior; whereas the addition of octyl β -D-glucopyranoside, a non-ionic surfactant, significantly widened the spray plume, as visible in Fig. 3A compared to Fig. 3B which displays the spray plumes for ethanol doped with the non-ionic surfactant (250 ppm, Fig. 3A) versus pure ethanol (Fig. 3B). Wider plumes did not consistently provide higher spectral counts, but the signal tended to be more reproducible and less dependent on the positioning of the swab relative to the MS inlet, and therefore is a desirable feature.

Occasionally, the formation of two Taylor cones (Fig. 3H) was observed, i.e. multi-jet mode. The multi-jet mode was unstable, spraying simultaneously and merging into a single larger plume before dividing once again. Lastly, given the non-optimized composition and materials of the swabs, we occasionally observed plumes formed from individual fibers that extended from the bulk of the swab tip, as is visible in Fig. 3G. These sprays yielded few detectable ions and were hard to

sample by the mass spectrometer. In these cases, the swabs were disregarded and the experiments repeated. Other unstable spray modes were observed in negative ionization mode, a condition in which the formation of a stable cone-jet was more difficult to achieve. For methanol, acetonitrile, and chloroform, we observed pulsating and ramified jet modes (Fig. 3F) that resulted in higher currents (between 0.6 and 1.5 μA on average) and into low-to-no MS signal at any position in the spray. In these cases, we observed that even minor differences in the dimension of the Taylor cone could change the spray mode. It was common to see the spray mode rapidly alternate between cone, pulsing, and ramified jet (Video S2) which deeply affected the spectral signal (Fig. S8). Discharge occurred using pure DMF (Fig. 4E) with currents up to tens of μA . Mixing large percentages of ethanol or acetone to miscible solvents with high surface tension like DMF proved a successful strategy to decrease the overall surface tension of the solvent system and allow for the generation of a stable cone-jet and the production of analytically useful ions (Table S2). Such a strategy was recently used to analyze fresh human brain tissue sampled with the swabs and detect ions of glycerophospholipids (mostly deprotonated ions and chlorinated adducts in negative ion mode; protonated, sodiated and potassium adducts in positive ion mode) and oncometabolites that are diagnostic for brain cancers [23]. The solvent system consisted of ACN-DMF-EtOH 45:5:50% v/v. The mass spectra were information-rich and correlated ($r = 0.90$) with those typically acquired using DESI with ACN-DMF 50:50% v/v [27], a combination of solvents that did not generate a stable cone-jet using the swabs.

Supplementary material related to this article can be found online at <http://dx.doi.org/10.1016/j.talanta.2018.02.105>.

4. Conclusions

Swabs have desirable features as sampling probes for direct ambient

MS analysis, i.e. simplicity, moderate cost, and biocompatibility. The prospective applications of STS include those in which point of care testing, in vivo and minimally invasive sampling are paramount, e.g. therapeutic drug monitoring, workplace and roadside drug testing, and antidoping control. Alternatively, storage and transportation of the swabs in sealed tubes is convenient for laboratory testing of dried samples. Sample quantities transferred on the tip are small (e.g. a few mg of tissue [23], a few μL of oral fluid [21]) albeit not controllable with the swab designs tested so far. Analysis time is rapid (seconds to minutes) though depending on the MS data acquisition mode, the number of analytes to be detected and the dwell time for each analyte. Limits of detection reached down to part per billion [21–26]. The ion current generated is sufficient to couple STS to different mass analyzers (ion traps, triple quadrupoles, Orbitraps, and miniature ion traps have been tested so far) and to adapt data acquisition towards fragmentation or accurate mass measurements. The generation of ions is continuous and can facilitate the development of multiplexed methods for large scale screening of compounds either in a data dependent or data independent fashion, keeping in mind that the signal intensity is the result of an extraction process from a matrix and that the signal is exhausted over time, constraining the period of ion acquisition to minutes. Toxicological and chemical warfare investigations, roadside and workplace drug testing, and anti-doping controls, are examples of applications whose efficacy is highly dependent on an untargeted analytical screening protocol. These cases could be ideal for the utilization of STS-MS. Low solvent consumption, no need for gas assistance or heating or for enclosed chambers for desorption/ionization make STS amenable to point of care testing. Naturally, a methodology based on direct ion generation from a complex matrix may have weak points, including matrix effects, incomplete recovery, decreased quantitative performance or co-extractive interferences some of which can be partially overcome using MS^n and ion mobility strategies.

It is worth considering that the fact that generation of ions directly from swabs may be relatively surprising, given their non-traditional shapes and sizes; however, good quality signal and stable sprays were usual. Our observations provide the initial evidence that ion generation occurs via ESI-like mechanisms. The mode of ESI was highly dependent on the conditions used. Electrospray parameters had to be optimized for different solvents and swab types in order to find stable conditions, and microscopic videography is essential for the optimization process, which once established could be applied routinely. Under such conditions, data were highly reproducible provided only that manufacturing defects in the swabs did not inhibit ionization, a relatively rare event. This issue currently limits the automation and throughput of STS-MS but it stems largely from the use of swabs designed to fit purposes other than ESI probes for MS analysis. The variety of solvents from which a stable electrospray plume was formed broadens the range of molecules that can be detected and hence the applicability of STS in medicine and forensics. Droplet size measurements, electric field and fluid transport simulations are additional experiments that should provide a more detailed characterization of swab electrospray. Such knowledge can guide the design of swabs specifically tailored for MS analysis. Swab shape and dimension can be adapted to improve spray formation and stability, and possibly ameliorate the negative effect of water on the electrospray for the analysis of biofluids. Material selection, porosity, and functionalization can be modified selectively to improve swab-analyte affinity and analyte recovery, and reduce chemical noise, a strategy that is largely and successfully applied to the technology of CBS; commercial ESI probes can be designed to accommodate a swab as emitter and to multiplex for high throughput.

Acknowledgements

The authors acknowledge financial support from the Purdue University Center for Cancer Research, and Copan Diagnostics and Puritan Medical Products for providing some of the swabs used in this

study. The authors thank Dr. Zane Baird for building the custom STS interface and Adam Hollerbach for discussions.

Conflict of interest

Authors declare no conflict of interest.

Appendix A. Supporting information

Supplementary data associated with this article can be found in the online version at <http://dx.doi.org/10.1016/j.talanta.2018.02.105>.

References

- [1] R. Javanshad, A.R. Venter, Ambient ionization mass spectrometry: real-time, proximal sample processing and ionization, *Anal. Methods* 9 (2017) 4896–4907.
- [2] J. Balog, L. Sasi-Szabó, J. Kinross, M.R. Lewis, L.J. Muirhead, K. Veselkov, R. Mirnezami, B. Dezső, L. Damjanovich, A. Darzi, J.K. Nicholson, Z. Takáts, Intraoperative tissue identification using rapid evaporative ionization mass spectrometry, *Sci. Transl. Med.* 5 (2013) 194ra93.
- [3] J. Zhang, J. Rector, J.Q. Lin, J.H. Young, M. Sans, N. Katta, N. Giese, W. Yu, C. Nagi, J. Suliburk, J. Liu, A. Bensussan, R.J. DeHoog, K.Y. Garza, B. Ludolph, A.G. Sorace, A. Syed, A. Zahediavash, T.E. Milner, L.S. Eberlin, Nondestructive tissue analysis for ex vivo and in vivo cancer diagnosis using a handheld mass spectrometry system, *Sci. Transl. Med.* 9 (2017) ean3968.
- [4] V. Kertesz, M.J. Ford, G.J. Van Berkel, Automation of a surface sampling probe/electrospray mass spectrometry system, *Anal. Chem.* 77 (2005) 7183–7189.
- [5] G.J. Van Berkel, V. Kertesz, R.C. King, High-throughput mode liquid microjunction surface sampling probe, *Anal. Chem.* 81 (2009) 7096–7101.
- [6] K. Zaltsu, Y. Hayashi, T. Murata, T. Ohara, K. Nakagiri, M. Kusano, H. Nakajima, T. Nakajima, T. Ishikawa, H. Tsuchihashi, A. Ishii, Intact endogenous metabolite analysis of mice liver by probe electrospray ionization/triple quadrupole tandem mass spectrometry and its preliminary application to in vivo real-time analysis, *Anal. Chem.* 88 (2015) 3556–3561.
- [7] Y. Hayashi, K. Zaltsu, T. Murata, T. Ohara, S. Moreau, M. Kusano, H. Tanihata, H. Tsuchihashi, A. Ishii, T. Ishikawa, Intact metabolite profiling of mouse brain by probe electrospray ionization/triple quadrupole tandem mass spectrometry (PESI/MS/MS) and its potential use for local distribution analysis of the brain, *Anal. Chim. Acta* 983 (2017) 160–165.
- [8] F.M. Chen, L.Y. Lin, J. Zhang, Z.Y. He, K. Uchiyama, J.M. Lin, Single-cell analysis using drop-on-demand inkjet printing and probe electrospray ionization mass spectrometry, *Anal. Chem.* 88 (2016) (4364–4366).
- [9] K.S. Kerian, A.K. Jarmusch, R.G. Cooks, Touch spray mass spectrometry for in situ analysis of complex samples, *Analyst* 139 (2014) 2714–2720.
- [10] K.S. Kerian, A.K. Jarmusch, V. Pirro, M.O. Koch, T.A. Masterson, L. Cheng, R.G. Cooks, Differentiation of prostate cancer from normal tissue in radical prostatectomy specimens by desorption electrospray ionization and touch spray ionization mass spectrometry, *Analyst* 140 (2014) 1090–1098.
- [11] H. Wang, N.E. Manicke, Q. Yang, L. Zheng, R. Shi, R.G. Cooks, Z. Ouyang, Direct analysis of biological tissue by paper spray mass spectrometry, *Anal. Chem.* 83 (2011) 1197–1201.
- [12] R.D. Espy, A.R. Mullahadi, Z. Ouyang, R.G. Cooks, Spray mechanism in paper spray ionization, *Int. J. Mass Spectrom.* 325–327 (2012) 167–171.
- [13] I. Pereira, M.F. Rodrigues, A.R. Chaves, B.G. Vaz, Molecularly imprinted polymer (MIP) membrane assisted direct spray ionization mass spectrometry for agrochemicals screening in foodstuffs, *Talanta* 178 (2018) 507–514.
- [14] G.A. Gómez-Ríos, M. Tascon, N. Reyes-Garcés, E. Boyaci, J. Poole, J. Pawliszyn, Quantitative analysis of biofluid spots by coated blade spray mass spectrometry, a new approach to rapid screening, *Sci. Rep.* 7 (2017) 16104.
- [15] M. Tascon, G.A. Gómez-Ríos, N. Reyes-Garcés, J. Poole, E. Boyaci, J. Pawliszyn, High-throughput screening and quantitation of target compounds in biofluids by coated blade spray-mass spectrometry, *Anal. Chem.* 89 (2017) 8421–8428.
- [16] G.A. Gómez-Ríos, J. Pawliszyn, Development of coated blade spray ionization mass spectrometry for the quantitation of target analytes present in complex matrices, *Angew. Chem. Int. Ed. Engl.* 53 (2014) 14503–14507.
- [17] G.A. Gómez-Ríos, M. Tascon, J. Pawliszyn, Coated blade spray: shifting the paradigm of direct sample introduction to MS, *Bioanalysis* 10 (2018) 257–271.
- [18] N.B. Cech, C.G. Enke, Practical implications of some recent studies in electrospray ionization fundamentals, *Mass Spectrom. Rev.* 20 (2001) 362–387.
- [19] P. Nemes, I. Marginean, A. Vertes, Spraying mode effect on droplet formation and ion chemistry in electrosprays, *Anal. Chem.* 79 (2007) 3105–3116.
- [20] R.B. Cole, *Electrospray Ionization Mass Spectrometry: Fundamentals, Instrumentation, and Applications*, Wiley, 1997.
- [21] A.K. Jarmusch, V. Pirro, K.S. Kerian, R.G. Cooks, Detection of strep throat causing bacterium directly from medical swabs by touch spray-mass spectrometry, *Analyst* 139 (2014) 4785–4789.
- [22] V. Pirro, A.K. Jarmusch, M. Vincenti, R.G. Cooks, Direct drug analysis from oral fluid using medical swab touch spray mass spectrometry, *Anal. Chim. Acta* 861 (2015) 47–54.
- [23] V. Pirro, R.S. Llor, A.K. Jarmusch, A.M. Alfaro, A.A. Cohen-Gadol, E.M. Hattab, R.G. Cooks, Analysis of human gliomas by swab touch spray-mass spectrometry:

- applications to intraoperative assessment of surgical margins and presence of oncometabolites, *Analyst* 142 (2017) 4058–4066.
- [24] B.C. Yang, F. Wang, X. Yang, W. Zou, J.C. Wang, Y. Zou, F.Y. Liu, H. Liu, O.P. Huang, Medical swab touch spray-mass spectrometry for newborn screening of nicotine and cotinine in meconium, *J. Mass Spectrom.* 51 (2016) 1237–1242.
- [25] P.W. Fedick, R.M. Bain, Swab touch spray mass spectrometry for rapid analysis of organic gunshot residue from human hand and various surfaces using commercial and fieldable mass spectrometry systems, *Forensic Chem.* 5 (2017) 53–57.
- [26] D.T. Snyder, L.J. Szalwinski, R.L. Schrader, V. Pirro, R. Hilger, R.G. Cooks, Precursor and neutral loss scans in an RF scanning linear quadrupole ion trap, *J. Am. Soc. Mass Spectrom.* (2018) In press.
- [27] V. Pirro, C.M. Alfaro, A.K. Jarmusch, E.M. Hattab, A.A. Cohen-Gadol, R.G. Cooks, Intraoperative assessment of tumor margins during glioma resection by desorption electrospray ionization-mass spectrometry, *Proc. Natl. Acad. Sci. USA* 114 (2017) 6700–6705.
- [28] A.K. Jarmusch, C.M. Alfaro, V. Pirro, E.M. Hattab, A.A. Cohen-Gadol, R.G. Cooks, Differential lipid profiles of normal human brain matter and glioma by positive and negative mode desorption electrospray ionization – mass spectrometry imaging, *PLoS One* 11 (2016) e0163180.



Cite this: *Analyst*, 2018, **143**, 232

Sizing sub-diffraction limit electrosprayed droplets by structured illumination microscopy†

Adam Hollerbach,^a David Logsdon,^a Kiran Iyer,^a Anyin Li,^a J. Andy Schaber^b and R. Graham Cooks^{b*}

Electrosprayed droplets are widely studied for their role in the formation of ions at atmospheric pressure. Most droplet measurement methods used today employ light scattering to infer information about an electrospayed droplet's size. However, these methods fail to measure droplets smaller than about 400 nm in diameter due to constraints imposed by the diffraction limit of light. To overcome this limitation, a super resolution fluorescence microscopy-based method for determining the sizes of electrospayed droplets has been developed. Solutions containing rhodamine B and different amounts of glycerol were paper sprayed and nanoelectrosprayed onto conductive microscope coverslips using a single, high voltage pulse. Images of the deposited droplets were collected using a super resolution microscope operating in 3D structured illumination microscopy mode (3D-SIM). The sizes of droplets were measured using a modified circular Hough transformation program in Matlab. On average, the diameters of paper sprayed droplets were between 500 nm and 2 μm while almost all nanoelectrosprayed droplets were smaller than 1 μm. The center of a paper spray plume exhibited larger droplets than those at the periphery, likely due to greater Coulombic repulsive forces acting on the smaller droplets to drive them outwards. The periphery also likely contained progeny droplets in addition to smaller parent droplets. It was possible to alter the sizes of nanoelectrosprayed droplets in several ways, including by changing the solvent composition and voltage applied to the emitter. Droplets consisting of high concentrations of glycerol were larger than droplets containing high concentrations of methanol, presumably due to the high surface tension of glycerol. Correspondingly, droplets became smaller when the voltage applied to the emitter was increased, likely due to the ability to overcome the surface tension of the solvent more easily. The smallest detectable droplets confidently measured with this method were 200 nm in diameter. This method demonstrates a new way of measuring the sizes of electrospayed droplets with half the diameter of conventional droplet size measurement methods. Through further optimization, it may be possible to measure the sizes of electrospayed droplets as small as the theoretical resolution limit of SIM (~100 nm).

Received 1st August 2017,
Accepted 8th November 2017
DOI: 10.1039/c7an01278k
rsc.li/analyst

Introduction

Electrospray ionization (ESI), also known as electrohydrodynamic (EHD) spraying, is widely used for creating charged droplets, ions, and aerosols at atmospheric pressure.^{1–5} Recently, much attention has been devoted to understanding the physical and chemical properties of electrospayed droplets in mass spectrometry. It is well known that small droplets provide increased analyte ionization efficiencies^{6–8} and salt tolerances,^{9,10} which in turn have aided in the development of

low flow rate ionization techniques such as nanoelectrospray^{11,12} and picoelectrospray ionization.¹³ Other experiments have used both neutral and charged droplets as microvessels to accelerate different types of chemical reactions.^{14–19} Possessing a fundamental understanding of droplet size is required to further explore and understand the utility of small droplets.

Several different types of instruments have been developed for determining the sizes of electrospayed droplets and aerosols,^{20,21} including aerodynamic particle sizers,^{22–24} differential mobility spectrometers,^{24–27} and phase-Doppler anemometers (PDA).^{28–34} PDA is arguably the most widely used for directly analyzing electrospayed droplets larger than the diffraction limit of light. In PDA, a droplet travels through an interference pattern created by two lasers and scatters light at a beat frequency proportional to its velocity.³⁵ Multiple detectors are used to detect phase differences in the beat frequency. These differences, along with spatial elements of the experi-

^aChemistry Department, Purdue University, West Lafayette, IN, USA.

E-mail: cooks@purdue.edu

^bBioscience Imaging Facility, Bindley Bioscience Center, Purdue University, West Lafayette, IN, USA

†Electronic supplementary information (ESI) available. See DOI: 10.1039/c7an01278k

mental arrangement, are used to calculate the droplet's diameter. PDA has been used to measure the sizes and velocities of both conventionally electrospayed³⁰ and paper sprayed droplets.³² Additionally, Beauchamp *et al.* used a modified PDA setup to measure the size and charge of a droplet over the droplet's lifetime.³⁶ Their results showed that droplets shrank in size primarily due to solvent evaporation while Coulombic fission events were the primary cause of charge loss.

One of the first experiments to measure sub-diffraction limit sized electrospay droplets was performed by Chen *et al.*²⁵ In this study, electrospayed droplets containing sucrose were charge reduced and allowed to undergo complete desolvation, resulting in the formation of sucrose aggregates. A scanning mobility particle sizer was used to measure the sizes of the sucrose aggregates, which indirectly provided size measurements of the droplets which produced those aggregates. Using this method, information about droplets as small as 4 nm in diameter was inferred. Davidson *et al.* recently used this method to show that large droplets exhibit a much greater amount of nonspecific protein aggregation than small droplets due to the total number of protein molecules present in different sized droplets.²⁷ Williams and coworkers¹⁰ generated very small droplets and showed that this removed deleterious effects of buffers by reducing the number of salt ions in any one droplet, even though the number of droplets containing analyte decreased sharply.

Studies performed over fifteen years ago by Ku *et al.* demonstrated that transmission electron microscopy (TEM) can be used to measure the sizes of electrospayed droplets.³⁷ The authors electrospayed glycerol containing high concentrations of sodium iodide onto a TEM grid and subsequently froze the deposited droplets before insertion into the TEM chamber. Most of the droplets sprayed from a 100 μm I.D. fused silica capillary were between 200 and 500 nm in diameter. While their results agreed well with comparative aerodynamic particle sizer measurements performed on larger droplets, the authors noted that droplets consisting primarily of glycerol may not reflect the true size distributions of droplets consisting of more conventional organic spray solvents.

Presented here is the first super resolution fluorescence microscopy-based method for measuring sub-diffraction limit sized charged droplets. These experiments were performed to measure: (1) electrospayed droplets smaller than the diffraction limit of light, (2) droplets with a wide range of sizes, and (3) the radial distribution of droplets in an electrospay plume. To the best of our knowledge, no current technique can simultaneously address all three of these tasks using relatively simple and easy to access instrumentation. Since super resolution fluorescence microscopy is commercially available, 3D structured illumination microscopy (3D-SIM) was selected as the technique for performing all these tasks. Droplets produced from both paper spray and nanoelectrospray ionization sources were imaged and compared. A custom algorithm in Matlab was developed and used to measure the sizes of deposited droplets down to 200 nm in diameter. The technique facilitates a deeper understanding of the droplet size distri-

butions produced by different electrospay ionization sources while providing a simple, intuitive means to do so.

Experimental details

Microscopy

Super resolution images of droplets were acquired using a Nikon Ti-E super resolution microscope (Nikon Instruments Inc., NY, USA). The microscope was operated in 3D structured illumination microscopy (SIM) mode to obtain resolution twice that obtainable by conventional microscopes.³⁸ Briefly, SIM is performed by placing a grid possessing a known pattern in front of a sample and illuminating both. This will cause images to contain interference patterns in the form of moiré fringes. By translating and rotating the grid, different orientations of the moiré fringes can be obtained. Each moiré fringe orientation contains high spatial frequency information about the original sample and can be deconvolved with all the other images to produce a resolution-enhanced image. In the experiments performed here, the light source was a 561 nm laser. It was possible to achieve a total magnification of 250 \times by combining a 100 \times , oil-based objective (Nikon Apo TIRF 100 \times /1.49, Nikon Instruments Inc., NY, USA) with a supplemental 2.5 \times focusing lens located between the objective and a CCD detector (Model iXon Ultra 897, Andor, Belfast, UK) (Fig. 1). The microscope's 2D motorized stage was used to image different sections of the microscope slide. The field of view of each section was 32.8 \times 32.8 mm. Images of droplet residues were brought into focus using Nikon's 'Perfect Focus' usually followed by a small z-offset adjustment. The electron multiplier on the camera was turned off to minimize background noise. To compensate for the reduction in signal, a high concentration of fluorescent compound was used. Droplet agglomeration studies were performed on a Nikon TiS inverted confocal microscope (Nikon Instruments Inc., NY, USA) which utilized a 60 \times objective (Plan Apo VC 60 \times Oil DIC N2, Nikon Instruments Inc., NY, USA) and a CCD camera (QuantEM:512SC, Photometrics, AZ, USA) operating at 15 fps.

Chemicals and materials

Spray solutions consisted of 100 μM rhodamine B in glycerol and 9 : 1 methanol : glycerol. Rhodamine B and glycerol were purchased from Sigma (MO, USA) and methanol from Fisher Chemical (NJ, USA). Paper spray triangles were cut from Whatman #1 paper using regular scissors. Nanoelectrospray emitters with outer diameters of between 5 and 20 μm were pulled from borosilicate glass capillaries (0.86 mm i.d., Sutter Instruments, CA, USA) using a micropipette puller (Model P-97, Sutter Instruments, CA, USA). Tip outer diameters were measured by eye using a Kronos light microscope fitted with a scale bar. The error in all tip outer diameters was ± 0.5 μm . In all nanoelectrospray experiments, a 0.51 mm platinum 10% iridium wire (California Fine Wire Company, CA, USA) supplied voltage to the solutions. Grounded indium-tin-oxide (ITO) microscope coverslips (~ 0.16 mm thickness, NanoCS,

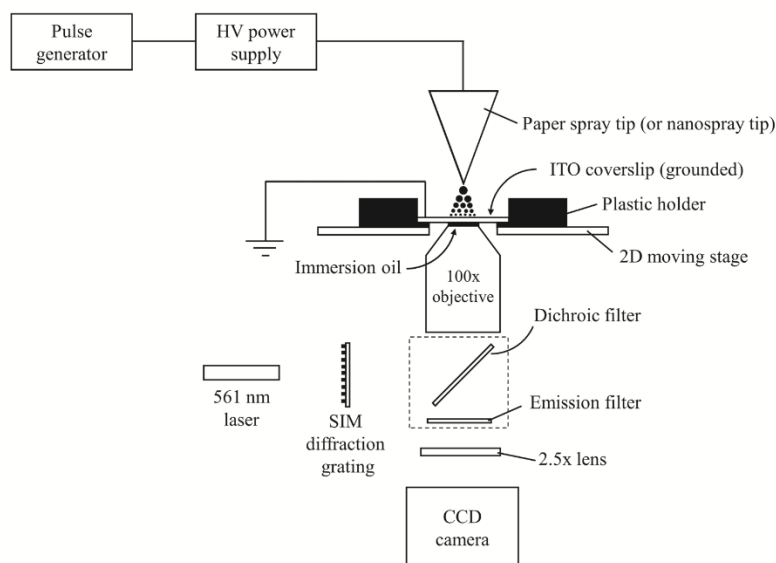


Fig. 1 Schematic of the experimental setup used for measuring the sizes of electrospayed droplets by 3D structured illumination microscopy.

NY, USA) were placed into contact with the objective and used as droplet deposition surfaces. Each ITO slide was sonicated in acetone and methanol to remove organic residue contaminants and stored in a desiccator prior to analysis. The fluorescent nanoparticles (Spherotech, IL, USA) used in this study possessed nominal diameters of 0.25, 0.53, and 0.84 μm . The particles were made from polystyrene and contained Nile red as the indicator dye. Each nanoparticle standard was diluted 1000 \times in water and stored in an amber vial to minimize degradation. Manufacturer reported distributions of the nanoparticles are described later.

Electrospray ionization

Both paper sprayed and nanoelectrosprayed droplets were analyzed in this study. A single electrospay pulse was used instead of continuous sprays to decrease the number of droplets produced and minimize the chances of droplet agglomeration on the surface. High voltage pulses were produced from a high voltage power supply (Model 610E-G-CE, Trek Inc., NJ, USA) connected to a waveform generator (Model AFG 3022, Tektronix, OR, USA). The voltages used for nanoelectrospray and paper spray were 3 and 5 kV, respectively. The distance between the tip of the emitter and the surface was varied between three and seven millimeters to obtain different droplet size distributions. The duration of the high voltage pulses was varied between 10 and 30 ms. Pulses longer than 30 ms were not used because significant droplet agglomeration tended to occur. A video of a 500 ms pulse was taken to showcase the extent of droplet agglomeration when using long pulses (Video 1[†]). The pulse in this experiment was generated

using a piezoelectric discharge gun (Zerostat3, Tedpella, CA). The spray emitters were mounted on a precision stage and could be moved from the initial measurement site with sub-100 micron precision. Initial tip-to-surface distance measurements were performed by placing the tip of the spray emitter level with the top of the microscope slide holder, which was 2.8 ± 0.1 mm away from the microscope slide surface. This measurement was done by eye. The spray emitter was then moved to a desired value. Even if the initial distance measurement was slightly in error, the differences between any distances measured after the initial one were small.

Results and discussion

Initial electrospay experiments were performed using paper spray ionization. Fig. 2a and b show two super resolution images of droplets produced after paper spraying glycerol for 10 and 30 ms, respectively. Glycerol was used to ensure droplets did not evaporate after being deposited. Both images were acquired on the same day and represent droplets located at the center of the spray plume. The tip-to-surface distance was 3–4 mm in each experiment. For any given location on the microscope slide, the 10 ms spray pulse showed between 3 and 30 deposited droplets, while the 30 ms spray pulse showed upwards of 125 deposited droplets. Most droplets showed a high degree of circularity. Non-circular droplets or suspected agglomerates (e.g. Fig. 2b arrow) were avoided as much as possible to prevent incorrect size measurements. It is important to note that the circles in the images shown here rep-

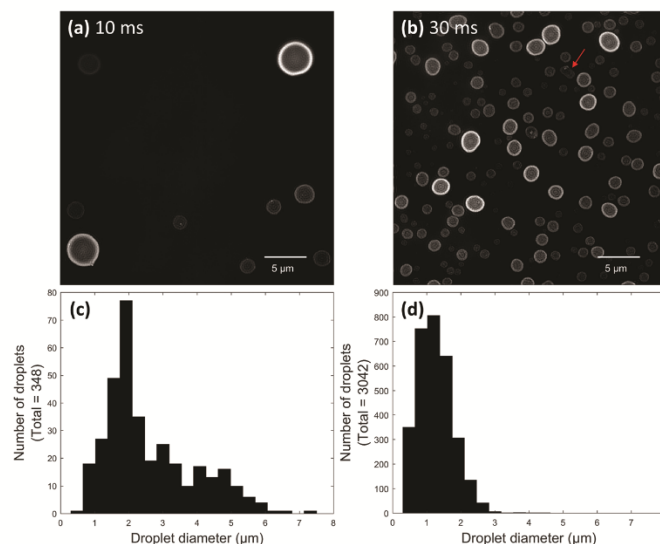


Fig. 2 Super resolution images of paper sprayed glycerol droplets collected after spraying for (a) 10 ms and (b) 30 ms at a 3.0 ± 0.5 mm distance. Droplet size distributions for each pulse experiment were obtained by combining droplets from several different areas of the respective image [(c) 10 ms, (d) 30 ms]. The arrow in 3b points to two droplets which have agglomerated.

resent the circular cross sections of the parts of the droplets directly in contact with the microscope slide. Individual droplet size distributions were generated for both pulse duration experiments by acquiring several frames at each pulse duration and added together to give a distribution for the respective pulse duration (Fig. 2c and d). For example, 55 frames were acquired for the 10 ms pulse duration experiment. These 55 frames were added together to give a distribution for the 10 ms pulse experiment. Then, in the 30 ms pulse experiment, droplets were collected on a new microscope slide and 20 frames were acquired. These 20 frames were added together to give a distribution for the 30 ms pulse experiment. The total number of frames acquired depended on the average number of droplets per image. Since each frame in the 10 ms experiment contained 6 droplets on average compared to the 159 droplets per frame in the 30 ms experiment, more frames were acquired for the 10 ms experiment to give a more representative distribution.

After comparing the two paper spray pulse duration experiments, most droplets were found to possess diameters between about 500 nm and 2 μm . Some droplets greater than 5 μm in diameter were also observed for the 10 ms pulse. The sizes of the glycerol-containing droplets measured here compare reasonably well to PDA studies of droplets containing 1 : 1 water : methanol which were paper sprayed using 3–4 mm probe distances.³² This seems to suggest that surface wetting did not cause the size measurements of droplets on the microscope slide surface to be significantly different than the corresponding air-based measurements. Interestingly, droplets pro-

duced by the 30 ms pulse seemed to be slightly smaller on average compared to droplets produced by the 10 ms pulse. This difference might be artefactual because a significantly lower overall number of droplets were produced from the 10 ms pulse, which limited the total number of droplets that could be counted for this pulse duration. Alternatively, droplets generated using shorter pulses might simply be slightly larger than droplets generated by longer pulses. This hypothesis could be extended to mean there is a difference between droplet sizes in pulsed and continuous electrospays. This topic will be explored in detail in the future.

All super resolution images were analyzed by a modified spot detection algorithm in Matlab. The detection process is demonstrated here using an image of paper sprayed glycerol droplets (30 ms pulse). Raw intensity images obtained from the microscope (Fig. 3a) were normalized until spots were easily distinguishable from the background (Fig. 3b). The normalization values for each image were manually chosen based on the intensity distribution of the droplets in each frame. Droplets which were spherical, sufficiently bright, and within specific size ranges were detected by a circular Hough transformation (*imfindcircles* function) in Matlab. Circular Hough transformations essentially work by iteratively constructing circles of different diameters around a circle in an image and then using a voting procedure to determine which circle fits the best. Droplets which were either non-spherical or low in intensity were not considered. When the droplets in an image possessed a narrow range of sizes, only a single transformation was used for analysis. If an image contained droplets with a

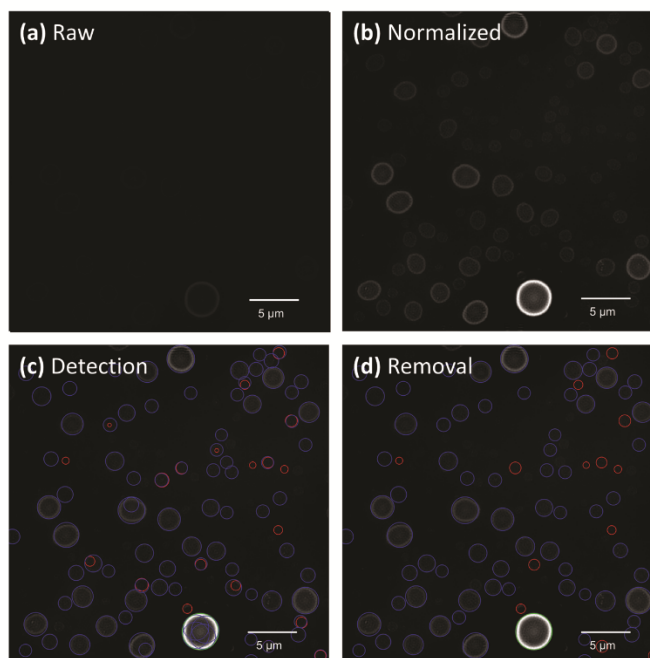


Fig. 3 Example workflow of the data processing algorithm showing (a) a raw intensity image obtained from the microscope, (b) the same image after normalization, (c) the image after applying a droplet detection algorithm, and (d) the image after applying a circle overlap removal algorithm. The image shown is of paper sprayed glycerol droplets collected for 30 ms at a 3.5 ± 0.5 mm tip-to-surface distance. Red circles indicate the detection of droplets with relatively small radii using one Hough transformation while blue circles indicate larger droplets detected by a separate Hough transformation. A third Hough transformation was used to show the detection of the largest droplet in the image, which is highlighted in bright green.

wide range of sizes, the range was subdivided into smaller size ranges and multiple Hough transformations were used (Fig. 3c). This was done to help the algorithm detect both low intensity and closely spaced droplets as well as provide the most accurate size measurements possible. An example of using a different number of transformations on an image of paper sprayed droplets is given in the ESI (Fig. S1†). The figure shows that using a larger number of transformations is required to accurately size large ranges of droplet sizes. However, when multiple transformations were employed, the transformations used to analyze small droplets routinely and incorrectly assigned small droplets to areas inside or around the peripheries of larger droplets. An overlap removal tool was used to eliminate these incorrect assignments by first determining if two or more circles overlapped by a user-defined number of pixels, which was almost always 1 pixel. If any circles did overlap, the algorithm then kept the circle possessing the most votes and deleted all the smaller ones (Fig. 3d). A few correctly identified droplets were usually discarded in the overlap removal process. It is important to note that the program was only used to detect droplets larger than 200 nanometers to prevent the detection of background noise even

though the theoretical resolution limit for SIM is about 100 nm.³⁸

To test the algorithm's accuracy, standard fluorescent nanoparticles with different nominal diameters (0.25, 0.53, and 0.84 μm) were prepared on separate microscope slides and analyzed (Fig. S2†). The algorithm measured nanoparticle diameters of 0.27 ± 0.04 μm, 0.53 ± 0.07 μm, and 0.89 ± 0.10 μm (mean \pm 1 std. dev). Photographs of the manufacturer's specifications are given in the ESI† for the 0.25 and 0.53 μm nominal diameter nanoparticles (Fig. S3 and S4†). A value of 0.84 ± 0.02 μm was given by the manufacturer for the largest set of nanoparticles tested, but no distribution was provided. As can be seen from Fig. S2–S4,† the distributions of nanoparticle diameters measured using this method are well within manufacturer specifications. Additionally, most images were resized prior to analysis. This was done to improve the detection algorithm's accuracy and ability to detect small droplets. The effect of resizing an image by factors of one, two, and three is given in the ESI† using an image of 0.84 μm diameter nanoparticles (Fig. S5†). A greater number of droplets was detected in resized images compared to non-resized; however, resized images usually required longer analysis times.

As stated earlier, all images were normalized prior to analysis depending on the intensity distribution of the droplets in the image. This was done primarily to allow the user interpreting the data to visualize all the droplets present in an image and select appropriate processing parameters, such as transformation sensitivities. However, since every image required a slightly different set of normalization values, an experiment was performed to test the effect of normalizing an image on the accuracy of the program. An image containing $0.53\ \mu\text{m}$ nominal diameter nanoparticles was analyzed using various normalization values (Fig. S6†). Depending on the normalization values chosen, images could be made brighter or darker by changing the higher or lower normalization value, respectively (Fig. S6a–S6e†). A single Hough transformation with an optimized sensitivity factor was used to analyze each image. As can be seen, roughly the same number of particles were detected in each image (Fig. S6f–S6j†) and the droplet size distributions acquired at each set of normalization values showed that the accuracy of the algorithm was independent of the normalization values when optimal conditions were selected (Fig. S6k–S6o†). The default normalization values outputted by the microscope software, demonstrated in Fig. S6c† in this example, were typically used for analysis.

Many electro spray solutions are prepared using some amount of organic solvent to reduce the surface tension of the spray solution and to help dissolve analytes. The effect of organic composition on droplet size was evaluated by paper spraying a $100\ \mu\text{M}$ solution of rhodamine B in 9 : 1 methanol : glycerol for 30 ms at a $3.5 \pm 0.5\ \text{mm}$ tip-to-surface distance.

A low concentration of glycerol was used in the spray solvent to help droplets maintain their shape when they landed on the surface. Images of the center and periphery of a paper spray plume were acquired from different parts of the same slide (Fig. 4a and b). Clear differences could be seen in the images. The center of the spray plume contained a wide range of droplet sizes, many of which were larger than $1.5\ \mu\text{m}$ in diameter (Fig. 4c). It is possible that some of the largest droplets in the paper spray plume center were agglomerated, though once again, the diameters measured here still compared well with PDA results, even though the PDA results were acquired using 1 : 1 water : methanol. In contrast, almost all the droplets at the periphery of the paper spray plume were smaller than $1.5\ \mu\text{m}$ in diameter (Fig. 4d). Interestingly, the largest bin in Fig. 4d contained droplets ranging from ~ 0.23 to $0.45\ \mu\text{m}$ in diameter (Fig. 4d arrow). The unexpected height of this bin seems to indicate the presence of a second distribution of sub-200 nm diameter droplets. This would be consistent with PDA measurements of paper spray droplet sizes,³² however, droplets at still smaller sizes would be too small to accurately measure using this method in its current state.

3D SIM was also used to analyze droplets produced by nanoelectrospray ionization. An initial study was performed to evaluate the effect of glycerol concentration on droplet size. Experiments were performed using solutions of 1 mM rhodamine B in three different ratios of methanol and glycerol: 4 : 1, 1 : 1, and 1 : 4. Each solution was loaded into a $5\ \mu\text{m}$ sized nanoelectrospray tip and deposited onto a coverslip from a 3 mm distance using a 20 ms pulse duration. After acquiring

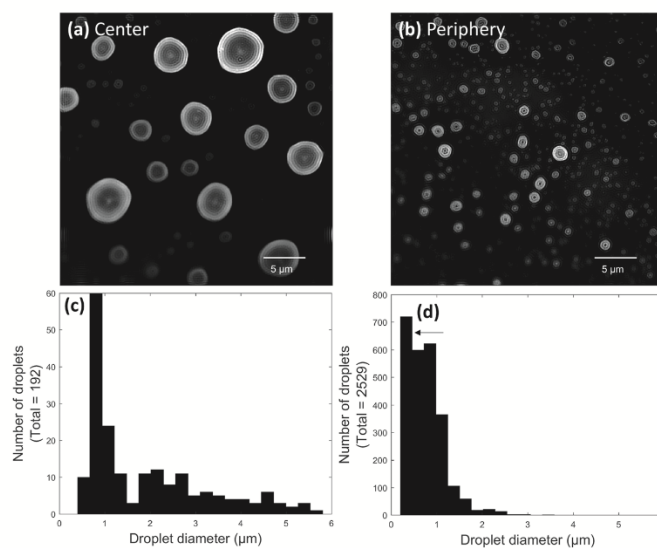


Fig. 4 Super resolution images of paper sprayed droplets containing 9 : 1 methanol : glycerol imaged at the (a) center and (b) periphery of the spray plume. Combined histograms of several different frames acquired at the spray plume's (c) center and (d) periphery. The droplets were generated at a $3.5 \pm 0.5\ \text{mm}$ tip-to-surface distance using a 30 ms pulse length.

images using the different glycerol concentrations, it was possible to see clear differences in droplet sizes (Fig. 5a–c). Smaller droplets were observed with higher concentrations of methanol, and conversely, larger droplets were observed with higher concentrations of glycerol. This makes sense since glycerol has a much higher surface tension than methanol and should produce larger droplets. Droplet size distributions were generated for each solvent composition using 28, 20, and 29 frames for the 4 : 1, 1 : 1, and 1 : 4 methanol : glycerol solvent ratios, respectively. As can be seen, the solution containing a high amount of methanol exhibited a maximum near 300 nm (Fig. 5d) while the solution containing a high glycerol content exhibited a maximum near 870 nm (Fig. 5f). Interestingly, the 1 : 1 methanol : glycerol solution exhibited a bimodal distribution of droplet diameters with maxima at approximately 195 and 550 nm (Fig. 5e). It is possible that the maximum at 195 nm was the result of progeny droplets created from Coulombic explosion events. However, it should be noted that the experiment is not entirely accurate for droplets smaller than about 200 nm in diameter in its current state, and thus further optimization is needed to fully validate this bimodal effect.

Glycerol was used in these experiments to minimize the effect of droplet evaporation after deposition. A study was performed to test if any significant droplet evaporation occurred over the course of an experiment. In one experiment, the sizes of nanosprayed droplets in one frame were monitored as a function of time while the laser constantly illuminated the droplets (Fig. S7,† blue trace). As can be seen, the average droplet diameter decreased when droplets were constantly exposed to the laser. However, glycerol should not evaporate at room temperature and pressure. This result likely suggests that photobleaching contributes to the degradation of sample intensity during continuous laser illumination. In a second experiment, another time study was performed for nanosprayed droplets, except this time the laser was only turned on during image acquisition (Fig. S7,† red trace). The average droplet diameter in this experiment did not seem to change significantly for 5 minutes, suggesting that the droplets were not greatly affected by photobleaching or solvent evaporation. The second experiment is more representative of how all the experiments presented herein were performed as the laser does not constantly illuminate the entire slide all at once, only a small section. It should be noted that the only data analysis parameters adjusted in these experiments were the normalization values.

Another set of nanoelectrospray ionization experiments was performed to evaluate how the voltage applied to a nanoelectrospray emitter affects droplet size. A 1 mM solution of rhodamine B in 9 : 1 methanol : glycerol was loaded into a 5 μm nanoelectrospray emitter and sprayed from a 3 mm distance using a 20 ms pulse. The same emitter was used for all voltage experiments. Voltages of 1.5, 2.0, 2.5, and 3.0 kV were tested. Interestingly, the average droplet diameter shrank with increasing voltage (Fig. 6). Droplets produced from a 1.5 kV pulse showed a rather broad distribution centered at about

Another set of nanoelectrospray ionization experiments was performed to evaluate how the voltage applied to a nanoelectrospray emitter affects droplet size. A 1 mM solution of rhodamine B in 9 : 1 methanol : glycerol was loaded into a 5 μm nanoelectrospray emitter and sprayed from a 3 mm distance using a 20 ms pulse. The same emitter was used for all voltage experiments. Voltages of 1.5, 2.0, 2.5, and 3.0 kV were tested. Interestingly, the average droplet diameter shrank with increasing voltage (Fig. 6). Droplets produced from a 1.5 kV pulse showed a rather broad distribution centered at about

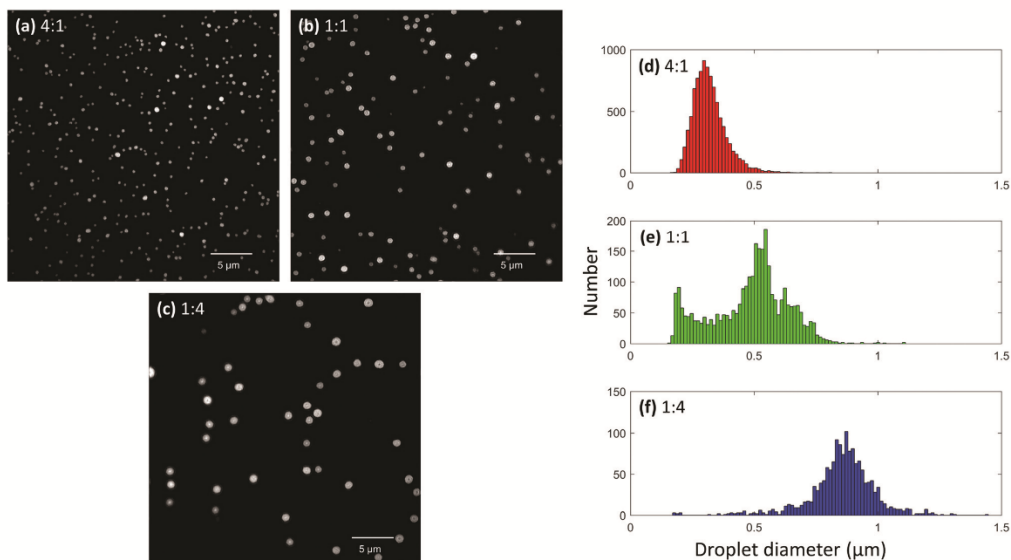


Fig. 5 Super resolution microscopy images of nanoelectrosprayed droplets containing 1 mM rhodamine B and (a) 4 : 1, (b) 1 : 1, and (c) 1 : 4 ratios of methanol : glycerol. Corresponding droplet diameter distributions of (d) 4 : 1, (e) 1 : 1, and (f) 1 : 4 ratios of methanol : glycerol. Each experiment was performed using a 5 μm o.d. tip, a 3.0 ± 0.5 mm distance, and a 20 ms pulse duration.

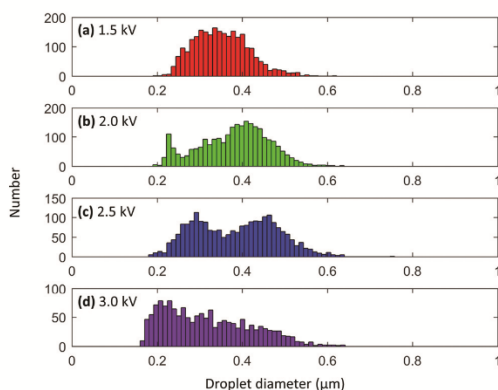


Fig. 6 Nano-electrosprayed droplet size distributions obtained using voltages of (a) 1.5 kV, (b) 2.0 kV, (c) 2.5 kV, and (d) 3.0 kV. Droplets were nano-electrosprayed from a 1 mM solution of rhodamine B in 9:1 methanol:glycerol from a 3.0 ± 0.5 mm distance using a 20 ms pulse duration. All voltage experiments were performed using the same 5 μ m o.d. nano-electrospray emitter.

335 nm (Fig. 6a). As the voltage was increased to 2.0 kV, a bimodal distribution of droplets appeared with maxima a smaller at 227 and a larger maximum at 410 nm (Fig. 6b). Although the maximum at 227 nm is again likely caused by the presence of progeny droplets, the maximum at 410 nm was unexpectedly larger than the maximum obtained for the 1.5 kV experiment. When the voltage was increased to 2.5 kV, the average droplet diameter again decreased and showed maxima of relatively equal heights at 292 and 463 nm (Fig. 6c). A final voltage of 3 kV yielded droplets centered around 220 nm in diameter (Fig. 6d). These results were somewhat unexpected because higher voltages tend to deplete solution more quickly than lower voltages, meaning that flow rate is surely increased with increasing voltage. A flow rate study was conducted using 5, 10, and 20 μ m o.d. nano-electrospray tips and showed that droplet sizes do increase with increasing flow rate (Fig. S8†). However, the set of voltage data shown here seems to suggest that the decrease in droplet size due to higher voltages is more prominent than the increase in droplet size that is gained from an increase in flow rate. The decrease in droplet size can be rationalized by considering that the use of higher voltages allows the surface tension of the solution to be overcome more easily than with lower voltages, which produces smaller initial sized droplets.

Conclusions

The experiments described here have demonstrated that super resolution fluorescence microscopy can be used to measure the sizes of electrosprayed droplets with improved resolution over conventional methods, down to 200 nm. Despite the addition of glycerol, the results measured for paper sprayed

droplets, between 0.5–2 μ m, matched reasonably well with the results measured without glycerol. The droplets produced by nano-electrospray ionization were almost all smaller than 1 μ m in diameter. Nano-electrosprayed droplets increased in size with a corresponding increase in glycerol concentration due to an increase in average solution surface tension. Droplets decreased in size with an increase in applied voltage, suggesting that the decrease in droplet size due to a high voltage overcoming the surface tension of the solution is more prominent than the increase in flow rate that would otherwise cause an increase in droplet size. It should be noted that the conclusions drawn here are only valid for droplets produced from pulsed electrosprays. Although a pulsed duration study was performed to try and observe the effects of pulse duration on droplet size, more thorough study is needed to determine how the droplets produced from a continuously spraying electrospray source correlate to droplets produced from pulsed electrospray sources. It might be possible to further optimize this method by using dyes with shorter emission wavelengths than rhodamine B to probe below the 200 nm diameter cutoff used here. In the future, one application for this technique is to investigate the extent to which chemical reactions are accelerated in sub-micron sized electrospray droplets.

Conflicts of interest

There are no conflicts to declare.

Acknowledgements

This material is based upon work supported by the United States Department of Energy, Office of Science, Office of Basic Energy Sciences, Separations and Analysis Program, under Award DE-FG02-06ER15807. The authors acknowledge the use of the facilities of the Bindley Bioscience Center, a core facility of the NIH-funded Indiana Clinical and Translational Sciences Institute. Adiv A. Johnson and Adriaan de Feijter from Nikon Instruments are acknowledged for their aid in operating the super resolution microscope's software. James Francis from Photometrics is acknowledged for help in optimizing the CCD camera.

References

- 1 J. Zeleny, *Phys. Rev.*, 1914, **3**, 69–91.
- 2 G. Taylor, *Proc. R. Soc. London, Ser. A*, 1964, **280**, 383.
- 3 M. Wilm, *Mol. Cell. Proteomics*, 2011, **10**, M111.009407.
- 4 S. Banerjee and S. Mazumdar, *Int. J. Anal. Chem.*, 2012, **2012**, 40.
- 5 L. Konermann, E. Ahadi, A. D. Rodriguez and S. Vahidi, *Anal. Chem.*, 2013, **85**, 2–9.
- 6 A. Schmidt, M. Karas and T. Dülcks, *J. Am. Soc. Mass Spectrom.*, 2003, **14**, 492–500.

- 7 A. El-Faramawy, K. W. M. Siu and B. A. Thomson, *J. Am. Soc. Mass Spectrom.*, 2005, **16**, 1702–1707.
- 8 J. T. Cox, I. Marginean, R. D. Smith and K. Tang, *J. Am. Soc. Mass Spectrom.*, 2015, **26**, 55–62.
- 9 R. Juraschek, T. Dülcks and M. Karas, *J. Am. Soc. Mass Spectrom.*, 1999, **10**, 300–308.
- 10 A. C. Susa, Z. Xia and E. R. Williams, *Anal. Chem.*, 2017, **89**, 3116–3122.
- 11 M. S. Wilm and M. Mann, *Int. J. Mass Spectrom. Ion Processes*, 1994, **136**, 167–180.
- 12 M. Wilm and M. Mann, *Anal. Chem.*, 1996, **68**, 1–8.
- 13 I. Marginean, K. Tang, R. D. Smith and R. T. Kelly, *J. Am. Soc. Mass Spectrom.*, 2014, **25**, 30–36.
- 14 T. Müller, A. Badu-Tawiah and R. G. Cooks, *Angew. Chem., Int. Ed.*, 2012, **51**, 11832–11835.
- 15 R. M. Bain, C. J. Pulliam, X. Yan, K. F. Moore, T. Muller and R. G. Cooks, *J. Chem. Educ.*, 2014, **91**, 1985–1989.
- 16 R. M. Bain, C. J. Pulliam and R. G. Cooks, *Chem. Sci.*, 2015, **6**, 397–401.
- 17 R. M. Bain, C. J. Pulliam, S. T. Ayrton, K. Bain and R. G. Cooks, *Rapid Commun. Mass Spectrom.*, 2016, **30**, 1875–1878.
- 18 E. A. Crawford, C. Esen and D. A. Volmer, *Anal. Chem.*, 2016, **88**, 8396–8403.
- 19 R. M. Bain, S. T. Ayrton and R. G. Cooks, *J. Am. Soc. Mass Spectrom.*, 2017, **28**, 1359–1364.
- 20 D. C. Tafflin, T. L. Ward and E. J. Davis, *Langmuir*, 1989, **5**, 376–384.
- 21 E. J. Davis and M. A. Bridges, *J. Aerosol Sci.*, 1994, **25**, 1179–1199.
- 22 A. Hirabayashi and J. Fernández de la Mora, *Int. J. Mass Spectrom. Ion Processes*, 1998, **175**, 277–282.
- 23 B. K. Ku and S. S. Kim, *J. Aerosol Sci.*, 2002, **33**, 1361–1378.
- 24 T. Musapelo and K. K. Murray, *Anal. Chem.*, 2011, **83**, 6601–6608.
- 25 D.-R. Chen, D. Y. H. Pui and S. L. Kaufman, *J. Aerosol Sci.*, 1995, **26**, 963–977.
- 26 F. Cao, F. Donnarumma and K. K. Murray, *Analyst*, 2016, **141**, 183–190.
- 27 K. L. Davidson, D. R. Oberreit, C. J. Hogan Jr. and M. F. Bush, *Int. J. Mass Spectrom.*, 2017, **420**, 35–42.
- 28 Z. Olumee, J. H. Callahan and A. Vertes, *J. Phys. Chem. A*, 1998, **102**, 9154–9160.
- 29 A. Venter, P. E. Sojka and R. G. Cooks, *Anal. Chem.*, 2006, **78**, 8549–8555.
- 30 P. Nemes, I. Marginean and A. Vertes, *Anal. Chem.*, 2007, **79**, 3105–3116.
- 31 A. Wortmann, A. Kistler-Momotova, R. Zenobi, M. C. Heine, O. Wilhelm and S. E. Pratsinis, *J. Am. Soc. Mass Spectrom.*, 2007, **18**, 385–393.
- 32 R. D. Espy, A. R. Muliadi, Z. Ouyang and R. G. Cooks, *Int. J. Mass Spectrom.*, 2012, **325–327**, 167–171.
- 33 R. Wang, A. J. Gröhn, L. Zhu, R. Dietiker, K. Wegner, D. Günther and R. Zenobi, *Anal. Bioanal. Chem.*, 2012, **402**, 2633–2643.
- 34 J. Majewski, *Electr. Rev.*, 2013, **R. 89(3b)**, 300–302.
- 35 F. Onofri, T. Girasole, G. Gréhan, G. Gouesbet, G. Brenn, J. Domnick, T. H. Xu and C. Tropea, *Part. Part. Syst. Charact.*, 1996, **13**, 112–124.
- 36 J. N. Smith, R. C. Flagan and J. L. Beauchamp, *J. Phys. Chem. A*, 2002, **106**, 9957–9967.
- 37 B. K. Ku, S. S. Kim, Y. D. Kim and S. Y. Lee, *J. Aerosol Sci.*, 2001, **32**, 1459–1477.
- 38 M. G. L. Gustafsson, *J. Microsc.*, 2000, **198**, 82–87.